

# POLITECNICO DI TORINO

Corso di Laurea Magistrale in Ingegneria Biomedica

Tesi di Laurea Magistrale

“From biomass to nanomaterials: a green Layer-by-Layer strategy for developing multifunctional silica mesoporous-based nanoparticles with improved antioxidant properties for regenerative medicine”



**Politecnico  
di Torino**

## **Relatori**

Prof.ssa Chiara Tonda-Turo  
Dr. Irene Carmagnola  
Prof. Piergiorgio Gentile

## **Candidato**

Noemi Corbezzolo  
282757

Marzo 2023

## **Abstract**

Posttraumatic stress disorder (PTSD) is a chronic debilitating dysfunction that may occur due to acute stress in the early aftermath of trauma. Not everyone who experiences a traumatic event will go on to develop acute or chronic dysfunction, lifetime prevalence of PTSD is estimated at around 3.9% worldwide. This syndrome is characterized by four symptom clusters, such as, intrusive thoughts, avoidance of reminders, feeling and thinking negatively, as well as arousal and reactive symptoms.

Further biomarker studies found out how these psychobehavioral behaviour and abnormalities in immune indicators are jointly among patients. Results have shown higher levels of proinflammatory cytokines, namely, interleukin IL-1 $\beta$ , IL-6, tumour necrosis factor TNF- $\alpha$ , interferon gamma (IFN- $\gamma$ ), emphasising how inflammation is one potential dysregulated mechanism in PTSD. In particular, the most common underlying mechanisms implicated in PTSD-related inflammatory dysregulation are altered autonomic nervous system (ANS) activity and an impaired reaction of the hypothalamic–pituitary–adrenal (HPA) axis to perceived stress, resulting in a chronic low-grade pro-inflammatory state. In this context, this work aimed at engineering a natural polymer based nanocarrier system for the delivery of antioxidant extracts as an innovative approach to effectively target and reduce inflammation.

To this purpose, layer by layer (LbL) deposition was adopted to build an antioxidant polyelectrolyte multilayer on the surface of spherical silica mesoporous nanoparticles (MNPs) of 200 nm. Pectin (PE) and chitosan (CH) are natural polymer with intrinsic biocompatibility and non-toxicity proprieties. Exploiting their opposite zeta potential, measured using dynamic light scattering (DLS), PE (-39 mV) and CH (+40 mV) were used as polyanion and polycation respectively in the alternated deposition. Due to their negative charge (-28 mV) MNPs were first immersed in CH solution followed by PE solution for a total of 5 layers. To impart the MNPs LbL coating with anti-inflammatory properties for targeting PTSD inflammation, green antioxidants were extracted from cocoa and coffee biowaste and added to the pectin solution. Antioxidants extraction parameters, namely, temperature ( $^{\circ}$ C), time (min) and liquid/solid ratio (mL/mg) were optimized through design of experiments (DOEs) and optimized ultrasound assisted extraction was performed both for cocoa and coffee biowaste using a 50% ethanol solution. Different functional groups were detected in the extracts through FTIR-ATR analysis, total phenolic content (TPC) was valuated using Folin-Ciocalteu reagent and antioxidant performance was evaluated with FRAP colorimetric methods. The highest TPC and antioxidant activity was performed by cocoa extract (3.7 GAE mg/mL and 996.7  $\mu$ M AAE). The morphological and chemical characterization of synthesized MNPs, were carried out performing TEM and FTIR analysis which confirmed all polyelectrolyte presence. Primary neodermal fibroblasts have been used to test the cytocompatibility of the MNPs systems through Live&Dead and AlamarBlue assays, while MNPs antioxidant activity was tested performing ROS test.

## ***Declaration***

This report is submitted as part of the requirements for the Master Degree of Ingegneria Biomedica at the Politecnico di Torino and has not been submitted for any other degree at this or any other University. It is solely the work of Eugenia Crisafulli except where acknowledged in the text or the acknowledgements below. It describes work carried out at the University of Newcastle upon Tyne which is entirely recorded in a Project Logbook which has been made available for examination. I am aware of the penalties for plagiarism, fabrication and unacknowledged syndication and declare that this report is free of these.

## ***Acknowledgements***

Vorrei ringraziare la Prof.ssa Chiara Tonda-Turo e la Dr.ssa Irene Carmagnola per la possibilità che mi hanno dato.

Ringrazio il mio supervisor Piergiorgio Gentile che si è dimostrato per tutto questo tempo un punto di riferimento su cui poter sempre contare, senza farmi sentire mai troppo lontana da casa.



# Content

Abstract	1
Declaration	2
Acknowledgements	2
1.Introduction	6
1.1 Post-traumatic stress disorder	6
1.2 Reactive oxygen species	7
1.3 Oxidative stress and neuroinflammation	7
1.4 Conventional treatment and their limitation	8
1.5 Alternative strategies	9
1.6 Natural antioxidant	9
1.6.1 Coffee and cocoa as natural antioxidants	10
1.7 Innovative extraction techniques and optimization methods for bioactive compounds recovery	11
1.8 Nanocarrier-mediated antioxidant delivery	12
1.9 Layer-by-Layer nanoparticles assembly coating technique	14
1.9.1 Polyelectrolyte solutions	14
1.9.2 Biomass source	15
2. Aim and Objectivities	16
3. Materials and Methods	18
3.1 Reagents	18
3.2 Methods	19
3.2.1 Ultrasound assisted extraction of antioxidants from cocoa and coffee biomass	19
3.2.2 Chemical characterization of antioxidant extracts	21
3.2.2.1 Determination surface functional groups by FTIR-ATR analysis	21
3.2.2.2. Determination of total phenolic compounds by Folin-Ciocalteu method	21
3.2.3. Determination of antioxidant activities by Ferric Reducing Antioxidant Power method	21
3.2.4 LbL nanoparticles preparation	22
3.2.4.1 Polyelectrolyte solutions preparation	22
3.2.4.2 Polyelectrolyte solutions analysis	22
3.2.4.3 Layer-by-Layer deposition	22
3.2.5 Nanoparticles Characterization	24
3.2.5.1 Determination of $\zeta$ -potential through dynamic light scattering	24
3.2.5.2 Morphology characterization through transmission electron microscope	24
3.2.5.3 Chemical characterization	24
3.2.5.3.1 Fourier Transformed Infrared spectroscopy analysis(FTIR-ATR)	24
3.2.5.3.2 X-ray photoelectron spectroscopy analysis (XPS)	24
3.2.6 Cell Culture	25
3.2.7 Cellular test	25
3.2.8 Cytotoxicity Evaluation	25
3.2.8.1 Live/Dead assay	25

3.2.8.2 PrestoBlue assay	26
3.2.9 Nanoparticles antioxidant activity evaluation through fluorescence assay for Intracellular ROS generation	26
3.2.10 Statistical Analysis	27
4. Results and discussions	28
4.1 Ultrasound Assisted Extraction (UAE) optimization through design of experiment	28
4.2 Chemical characterization of antioxidant extracts	38
4.3 Total phenolic content (TPC) and antioxidant activity evaluation	40
4.4 Nanoparticles Characterization	41
4.4.1 Polyelectrolyte solution analysis	41
4.4.2 $\zeta$ -potential measurement	45
4.4.3 Morphology analysis	47
4.4.4 Chemical composition	49
4.5 Cytotoxicity Evaluation	56
4.5.1 Live and Dead assay	56
4.5.2 PrestoBlue assay	63
4.6 Fluorescence assay for Intracellular ROS generation	65
5. Conclusions and Future perspective	71
6. References	73
Appendix	76





## **1. Introduction**

### **1.1 Post-traumatic stress disorder**

Acute stress in the early aftermath of trauma can have acute adverse effects on cognitive and affective function linked to later development of chronic debilitating dysfunction in the form of posttraumatic stress disorder (PTSD). Not everyone who experiences a traumatic event will go on to develop acute or chronic dysfunction, lifetime prevalence of PTSD is estimated at around 3.9% worldwide. Identifying the underlying neural basis for variability in stress susceptibility may provide targets for early intervention and treatment of chronic stress-related disorders [1]. PTSD is a debilitating psychiatric condition that develops in a subset of individuals after a major traumatic event characterized by four symptom clusters, namely, intrusive thoughts, avoidance of reminders (i.e. avoiding places or activities that can bring back intrusive memories), feeling and thinking negatively (i.e. ongoing fear, anger, guilt), as well as arousal and reactive symptoms (issues with concentration, sleep, or angry outbursts). Oftentimes, it is comorbid with anxiety, depression, or substance-use disorder. [2-3]

While psychobehavioral symptoms are the major factors, a growing number of studies have investigated the immunological alterations in PTSD as to understand the immunological alterations that occur in tandem with these symptoms. Biomarker studies have analyzed various immunological indicators among patients with traumatic stress disorder, especially those with PTSD, showing abnormalities in immune indicators among patients [4]. Patients with PTSD show significantly higher levels of common proinflammatory cytokines relative to non-PTSD trauma-exposed or healthy individuals, including interleukin IL-1 $\beta$ , IL-6, tumor necrosis factor TNF- $\alpha$ , interferon gamma (IFN- $\gamma$ ), as well as the inflammation-stimulated acute phase protein, C-reactive protein (CRP) [5-6]. The most common underlying mechanisms implicated in PTSD-related inflammatory dysregulation are altered autonomic nervous system (ANS) activity and an impaired reaction of the hypothalamic–pituitary–adrenal (HPA) axis to perceived stress, resulting in a chronic low-grade pro-inflammatory state. This condition is evidenced by a dominant sympathetic nervous system (SNS) and delayed reactivation of the parasympathetic nervous system (PNS), which, in turn, can increase inflammation [7-8].

Despite the growing evidence for dysregulated inflammation and cognitive function in PTSD, it is important to note that inflammation is only one potential mechanism dysregulated in PTSD. Additional highly developed research on the bidirectional interplay of these pathways will advance a deeper understanding of the progression and maintenance of this disorder, to develop innovative pharmacological approaches and behavioral interventions that effectively target inflammation and cognitive function and reduce PTSD symptomatology. [9]

Moreover, it is important to recognize that the COVID-19 pandemic added an extra layer of stress to people's lives, with many individuals facing new challenges such as social isolation, economic uncertainty, and fear of infection. As a result, some people may experience higher levels of stress, leading to a greater risk of mental health problems. Although the current evidence is scarce concerning direct effects of COVID-19 on mental health, there are indications of increased levels of post-traumatic stress symptoms and depression following the COVID-19 infection [10].

## 1.2 *Reactive oxygen species*

Reactive oxygen species (ROS), including radicals such as superoxide, nitric oxide, and hydroxyl radicals and nonradical species such as hydrogen peroxide, ozone, and peroxy nitrates, are reactive intermediates of molecular oxygen generated as byproducts of cellular metabolism.

At physiological concentrations, ROS play a crucial role as second messengers in the transduction of intracellular and extracellular signals involved in different biological processes, like the progression of many inflammatory diseases. When cellular production of ROS overwhelms the buffering capacity of the antioxidant defense systems, or when antioxidant enzymes are defective, oxidative stress occurs and initiates destructive oxidative processes such as lipid peroxidation, chlorophyll and betalain bleaching, and protein oxidation. This condition has been identified as the root cause of the pathogenesis of several human diseases. Depending on the source of ROS, cell type, and tissue environment, ROS signaling may contribute to a maladaptive response that leads to metabolic dysfunction and inflammatory signaling including neurodegenerative disorders, cancer, renal diseases, pulmonary diseases, metabolic diseases and aging [11-12]. Understanding the role of ROS signaling in the regulation of metabolic activity and inflammatory activation, has become a challenge for researchers to find novel therapies to treat these disorders.

## 1.3 *Oxidative stress and neuroinflammation*

All multicellular organisms depend on highly complex networks of both extracellular and intracellular signals to orchestrate cell-cell communication in diverse physiological processes. Molecular oxygen (dioxygen;  $O_2$ ) is essential for the survival of all aerobic organisms. Aerobic energy metabolism is dependent on oxidative phosphorylation, a process by which the oxidoreduction energy of mitochondrial electron transport (via a multicomponent NADH dehydrogenase enzymatic complex) is converted to the high-energy phosphate bond of ATP.  $O_2$  serves as the final electron acceptor for the terminal enzymatic component of this mitochondrial enzymatic complex, that catalyzes the four-electron reduction of  $O_2$  to  $H_2O$ . Partially reduced and highly reactive metabolites of  $O_2$  may be formed during these electron transfer reactions. These  $O_2$  metabolites include superoxide anion ( $O_2^{\cdot-}$ ) and hydrogen peroxide ( $H_2O_2$ ), formed by one- and two-electron

reductions of O<sub>2</sub>, respectively and are often referred to as reactive oxygen species ROS due to their higher reactivities relative to molecular O<sub>2</sub>. [13]

The protective mechanisms our body has developed against these molecules are sometimes insufficient to counteract the huge damages produced. Recently, natural antioxidants such as vitamins, polyphenols and plant-derived bioactive compounds are being studied to introduce them as preventive agents and potential therapeutic drugs [14]. Vitamins, alkaloids, flavonoids, carotenoids, curcumin, berberine, quercetin and many other compounds have been screened in vitro and tested in vivo, displaying antiinflammatory and antioxidant properties, and have been introduced as complementary therapies for several diseases associated with metabolic dysfunction.

#### *1.4 Conventional treatment and their limitation*

Conventional treatments for PTSD include psychotherapy and medications such as antidepressants and anti-anxiety medications, where the psychotherapy strategies may include cognitive-behavioral therapy (CBT), interpersonal psychotherapy (IPT), accelerated resolution therapy (ART) [15]. For example, cognitive-behavioral therapy (CBT) involves identifying and challenging negative thoughts and behaviors related to the traumatic event. Strategies used in CBT generally include imaginal or in vivo exposure to trauma-related and fear-provoking stimuli to gradually reduce the distress associated with those triggers [16]. Considering that exposure therapy can be difficult to tolerate for many individuals, not everyone responds to this approach, especially if the trauma was particularly severe or if the individual has other mental health conditions.

On the other hand, Benzodiazepines and Selective Serotonin Reuptake Inhibitors (SSRI) are the most antidepressants and anti-anxiety medications used for PTSD treatment [17]. For example, benzodiazepines are a class of psychoactive drugs that act as central nervous system (CNS) depressants enhancing the activity of a neurotransmitter called gamma-aminobutyric acid (GABA) in the brain, which reduces the activity of the central nervous system. The problem with this type of medications is that prolonged benzodiazepine use may also lead to abuse, dependence, and tolerance, leading to misuse, dose escalations, and withdrawal reactions [18]. In September 2020, the US Food and Drug Administration (FDA) announced an anticipated update to the boxed warning on all benzodiazepines to explicitly “address the serious risks of abuse, addiction, physical dependence, and withdrawal reactions” among this class of medications [19]. The widespread prevalence of the disorder and limitations of current treatments led to innovative approaches and new strategies for the treatment of PTSD.

## 1.5 *Alternative strategies*

Since, oxidative stress and neuroinflammation attract increasing attention as important mechanisms in PTSD, ongoing research are focusing into the use of antioxidants as innovative potential treatment strategy. Johannes de Munter et al., investigated the effects of a standardized herbal cocktail (SHC), an extract of clove, bell pepper, basil, pomegranate, nettle, and other plants, that was designed as an antioxidant treatment, resulted in an effective and safe supplement to current medications of PTSD [20]. Moreover, *Withania somnifera* (WS) traditionally as "Ashwaghandha" show its effect as antioxidant, anti-inflammatory, anti-stressor, anti-anxiety, and memory enhancer in many studies. Karem H. Alzoubi et al., founded that WS protects against PTSD induced impairment of short- and long-term memory possibly through antagonizing hippocampal oxidative stress [21].

While more research is needed to fully understand the potential benefits of antioxidants in the treatment of PTSD, these findings suggest that antioxidants may be a promising avenue for further investigation. It's important to note, however, that the use of antioxidants alone is unlikely to be sufficient for treating PTSD, and should be used in conjunction with other treatments such as therapy and medication for the best possible outcomes.

## 1.6 *Natural antioxidant*

Antioxidants are well-known compounds extract from plants, fruits, vegetables, oil, red wine, fungi, algae, and bacteria, able to eliminate harmful ROS excess, and inhibit or delay molecular oxidation. The activity of an antioxidant is determined by: i) its reactivity as a hydrogen or electron donating agent, which relates to its reduction potential, ii) the fate of the resulting antioxidant derived radical, which is governed by its ability to stabilize and delocalize the unpaired electron, iii) its reactivity with other antioxidants, iv) the transition metal-chelating potential [22].

Over the last decade, significant research has focused on the potential use of these extracts against metabolic and inflammatory disorders, due to their capacity to quench free radical species and promote endogenous antioxidant capacity. In this sense, antioxidant biomaterials come from natural sources have been developed and used in drug delivery systems, soft tissue regeneration, chronic wound healing, and cosmetical applications [23].

Between all the natural antioxidants, phenolic and flavonoid compounds have recently attracted a lot of interest because they are potent antioxidants and exhibit various physiological activities like anti-inflammatory, antimicrobial, antiallergic, anticarcinogenic and antihypertensive activities. Flavonoids, thanks to their chemical structure, are able to chelate both free radicals immediately, by donating a hydrogen atom or by single-electron transfer, and trace metal ions such as  $Fe^{2+}$  and  $Cu^{+}$  that play a vital role in oxygen metabolism and free radical formation [24-25].

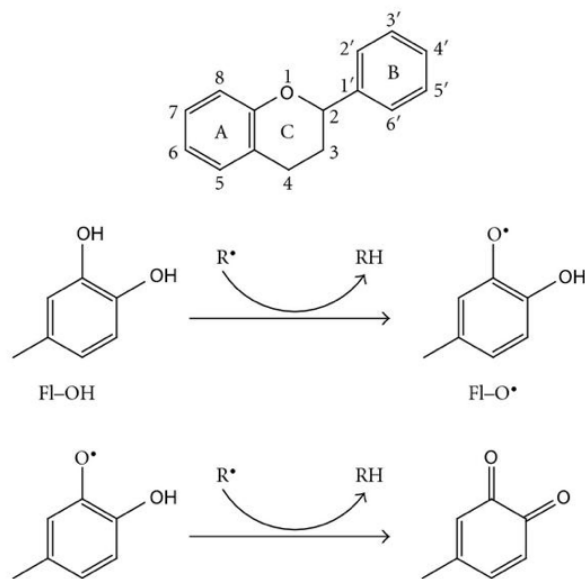


Figure 1 (a) Basic structure of a flavonoid, a C15-skeleton showing the A, B, and C ring (b) Scavenging of ROS ( $R^\bullet$ ) by flavonoids [26]

### 1.6.1 Coffee and cocoa as natural antioxidants

Many different plants have been studied for their potential benefits in a range of health conditions, including mental health issues like anxiety and depression, as well as other health conditions associated with oxidative stress and inflammation. In this study cocoa and coffee biomass was investigated as natural antioxidants sources contain since that have been shown to have potent antioxidant and anti-inflammatory effects.

Coffee is one of the most common consumed beverages in the world, and it has always been of great scientific interest because of its potential benefits on health as a good source of bioactive compounds, particularly chlorogenic, ferulic, caffeic, and n-coumaric acids contained which may play an important role against oxidative stress [27-28]. Moreover, studies on cocoa have shown its greater antioxidant capacity related to very high levels of polyphenols such as flavonoids, proanthocyanidins, anthocyanins and lyphenolic acids [29]. These characteristics have led to the use of cocoa and coffee as sources of natural antioxidants.

## *1.7 Innovative extraction techniques and optimization methods for bioactive compounds recovery*

Researchers have been investigated not only the antioxidant power of several types of fruit and vegetables; various optimization techniques to maximize phenolics recovery from biowaste have been developed. These techniques include supercritical, microwave-assisted, ultrasound-assisted, high voltage electric discharge, high pressure, infrared radiation-deep eutectic solvent, solid-state fermentation, hydrophobic interaction chromatography, ball milling, cellulase magnetic nanobiocatalyst, and encapsulation. However, each technique has its own advantages and limitations [30].

For example, supercritical fluid extraction is a method that uses a supercritical fluid, such as carbon dioxide, as the solvent. This method has several advantages, including high selectivity, high efficiency, and minimal solvent residue. However, it requires specialized equipment and can be more expensive than other extraction methods.

Microwave-assisted extraction exploits microwave energy to heat the sample and the solvent, facilitating the extraction of antioxidant compounds. This method is relatively fast and efficient and has been shown to yield high levels of phenolic compounds from cocoa and coffee [31]. Moreover, in ultrasonic-assisted extraction high-frequency sound waves are used to break down the cell walls of the cocoa or coffee sample, facilitating the release of antioxidant compounds into the solvent. This method is relatively fast and efficient and has been shown to yield high levels of antioxidant compounds [32].

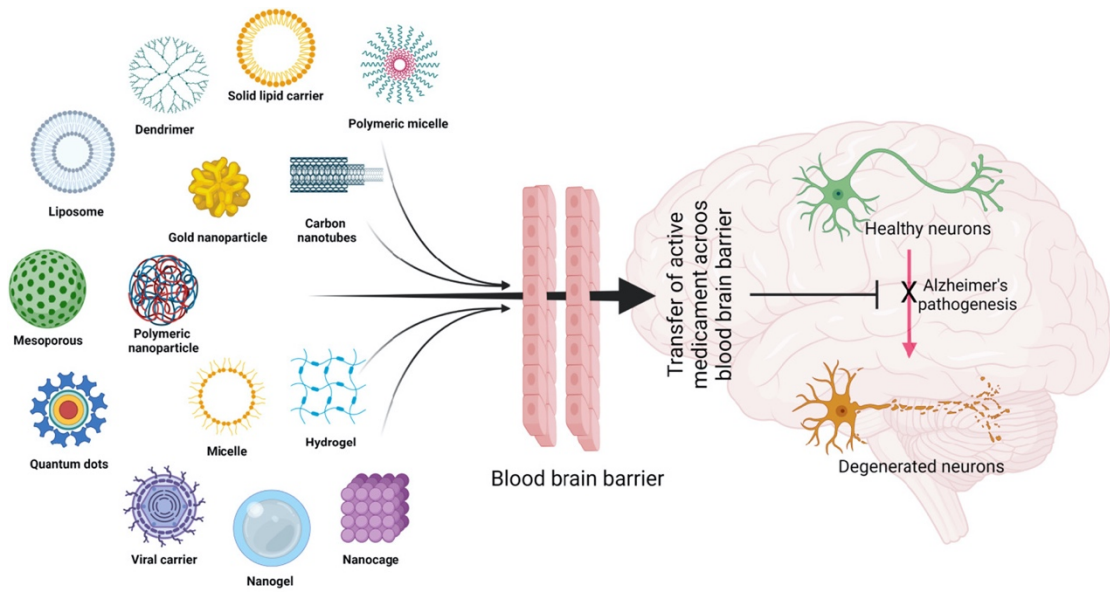
Furthermore, according to the specific characteristics of the extraction process, such as the type of extract being produced, the solvent system being used, and the processing equipment available, many optimization methods can be used to improve the efficiency, quality, and cost-effectiveness of the extraction process. Sushma Chakraborty et al., used response surface methodology (RSM) to optimize the extraction process of antioxidant compounds from bitter melon, which enabled better understanding of the combined effect of the various control variables on the system response [33]. RSM is a statistical approach that uses a series of designed experiments to model the relationship between input variables (such as solvent type, temperature, and extraction time) and output variables (such as yield and purity), to optimize the extraction process by identifying the optimal combination of input variables that maximizes the output variables.

## 1.8 *Nanocarrier-mediated antioxidant delivery*

Encapsulation technology, as a promising approach, has been employed for the protection and controlled release of different bioactive compounds including natural antioxidants [34]. Nanocarrier-mediated antioxidant delivery is a strategy to deliver antioxidants using nanocarriers, such as liposomes, nanoparticles, and micelles, to target cells or tissues for the prevention or treatment of oxidative stress-related diseases.

This technique offers several advantages for antioxidant delivery, including increased bioavailability, targeted delivery, and controlled release of antioxidants, protecting natural compounds from degradation, and improving their solubility and stability, which can enhance their therapeutic efficacy. Additionally, nanocarriers can be functionalized with targeting ligands or responsive moieties to increase their specificity and selectivity for diseased cells or tissues. For example, Christofori Nastiti et al., successfully developed self-assembling, stable, and physically suitable resveratrol (RSV) nanoformulations to enhance the penetration and permeation of RSV into and through the skin in order to potentially exert an antioxidant effect in the skin [35].

Considering, some of recent studies focused on using nanomaterials having antioxidant properties to attenuate oxidative stress in the brain. One of the major challenges in drug delivery is getting treatment across the blood-brain barrier (BBB), which is a protective barrier that prevents many drugs and other substances from entering the brain. The encapsulation of these compounds in nanocarriers like lipid-based or polymeric nanostructures seems to be able to overcome the limitations connected to the use of plain drugs [36]. Anthony Cunha et al [37]. engineered PLGA nanoparticles, which being both biocompatible and biodegradable, allow drug protection, enhance their bioavailability, and possess active targeting capabilities facilitating and delivering directly into the brain without losing their neuroprotective properties. Overall, the development of nanocarriers that can effectively cross the BBB is an active area of research, and new strategies are being explored to help overcome this important barrier to drug delivery in the brain.



Various Nanocarrier systems

Figure 2: Schematic representation of different nanocarriers to attenuate oxidative stress in the brain. [38]

## 1.9 *Layer-by-Layer nanoparticles assembly coating technique*

Layer-by-layer (LbL) technique is a versatile and widely used approach for the functionalization of nanoparticles. In this technique, layers of materials are deposited onto a substrate one at a time, typically using methods such as chemical vapor deposition, physical vapor deposition, or solution-based techniques. Each layer can be designed to have specific chemical, physical, or electronic properties, and the thickness and composition of each layer can be precisely controlled. This strategy can be used to introduce a variety of functional groups onto the nanoparticle surface, including targeting ligands, imaging agents, and therapeutic molecules. In action, LbL method can also be used to tune the surface charge and hydrophilicity of the nanoparticle, which can affect its pharmacokinetic properties and cellular uptake. Overall, the layer-by-layer technique is a powerful tool for designing and fabricating thin films and nanostructures with tailored properties, and its widespread use in both academic and industrial research reflects its versatility and effectiveness.

### 1.9.1 *Polyelectrolyte solutions*

Chitosan, is a cationic, meaning that it carries a positive charge due to the presence of amino groups in its chemical structure, and biocompatible polyelectrolyte derived from chitin, regarded as a promising compound in medical and pharmaceutical technology [39]. When chitosan is dissolved in water, the amino groups can become protonated, resulting in a net positive charge on the molecule.

Pectin is a complex carbohydrate (polysaccharide) found in the cell walls of plants, particularly in fruits such as apples, oranges, and berries. It is used as a gelling agent and thickener in a variety of food products, such as jams, jellies, and fruit-based desserts. Beyond its use in food products, pectin has also been studied for its potential health benefits since is one of the few polysaccharides with biomedical activity [40].

Pectin has a complex structure (Fig.3) composed of its sub-domains, rhamnogalacturonan I (RGI), rhamnogalacturonan II (RGII), and xylogalacturonan (XG), attached to the homogalacturonan (HG) skeleton. According to the US Pharmacopeia, the structure of pectin must contain  $\geq 65\%$  galacturonic acid (GalA) and the relation between the units of GalA esterified with methyl and the total units of GalA in the HG skeleton represents the degree of esterification (DE). The ubiquitous presence of hydroxyl and carboxyl groups in pectin contribute to their hydrophilicity and, hence, to the favorable biocompatibility, low toxicity, and biodegradability [41-42]. In line with sustainable development goals, studies have been undertaken to assess the efficiency of non-conventional green extraction methods, such as microwave-assisted extraction, ultrasound-assisted extraction, and enzyme-assisted extraction, on the yield and characteristics of pectin extracted from tropical and sub-tropical fruits [43].

When pectin and chitosan are mixed in water, they can form polyelectrolyte complexes due to the electrostatic interactions between the anionic pectin and cationic chitosan. These complexes can form a variety of structures, including nanoparticles, films, and hydrogels, which have potential applications in drug delivery, food packaging, and tissue engineering.

### *1.9.2 Biomass source*

It was chosen to use a non-commercial pectin and particularly to extract it from cocoa biomass, that refers to the solid material that remains after cocoa beans have been processed into chocolate or cocoa powder. This material is composed of the pod husk of the cocoa beans, as well as the pulp and other plant materials and considered for that waste product of chocolate and cocoa production. However, it has several potential uses, including as a source of bioenergy, animal feed, and fertilizer. By finding new ways to utilize this material, we can reduce waste and improve the sustainability of the chocolate and cocoa industry.

## 2. Aim and Objectivities

Aim of this work was to optimize a green extraction method for the recovery of antioxidants compounds reducing the use of harmful solvents, energy consumption, and minimize waste generation. To fulfil this aim coffee and cocoa biomass pod husk were chosen as natural source of antioxidants compounds (Fig.3), and the Design of Experiments through box-Behnken design was used to determine the optimal extraction conditions.

Briefly, using Minitab, 20 different combination of extraction process parameters were generated. Once all the experiments were carried out, obtained extracts were tested to assess their total phenolic content. Then, system responses were used as inputs to the RSM to find the optimal condition for the system. In particular, extraction time (min), temperature (°C) and ratio (mL/mg) were selected as extraction parameters combination to optimize in order to maximize the total phenolic content of each extract.

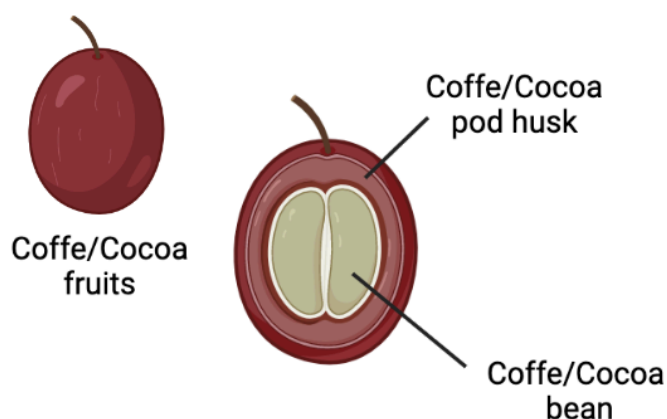


Figure 3: Cocoa and coffee biomass.

Optimized cocoa and coffee extracts were then used to reach the second goal of the project. In the context of the PTSD, Layer-by-Layer assembly coating technique was used to functionalized silica mesoporous nanoparticles to give them antioxidant behavior. To fulfil this goal chitosan and pectin was used as polycation and polyanion solution and antioxidant extract were loaded into the negative solution, according to their  $\zeta$ -potential measurement. Once the layer deposition control was established, two different systems were engineered, one for coffee and the other for cocoa extract. Figure 4 showed a schematical representation of each deposited layer and the final MNPs functionalized.

The manufactured MNPs were tested on Neo-dermal fibroblast cells in a bidimensional culture model. Cell viability, metabolic activity and morphology were analysed before and after the treatment with both the manufactured MNPs and free extracts. Last step was to qualitatively characterize H<sub>2</sub>O<sub>2</sub>-induced intracellular ROS generation, to evaluate coffee and cocoa extracts and MNPs functionalized antioxidant behaviour.

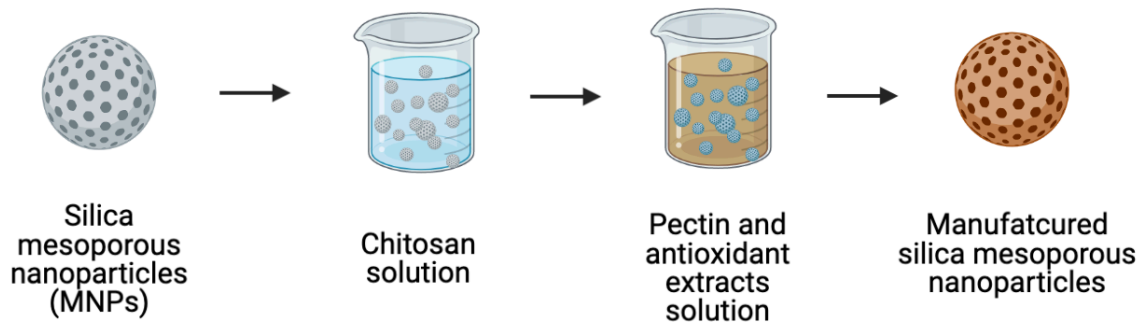


Figure 4: Silica mesoporous nanoparticles functionalization process through Layer-by-Layer technique.

### **3. Materials and Methods**

#### **3.1 Reagents**

Cocoa and coffee fruits were harvested in Neiva, Huila (Colombia) from producing farms. After the multiple washing steps with clean water, cocoa and coffee beans were removed to collect fruits pod husk (PH). The first step in processing involved cutting PH obtained into thin slices (~2 cm) and letting them dry under the sun light until constant weight. Once dried, cocoa and coffee PH samples were prepared through mechanical grinding process, by using an analytical mill (IKA A11 basic Analytical mill, IKA Germany), until powder reach a particle size of ~200  $\mu\text{m}$ . Powder was then stored in a plastic bag until further extraction.

Extraction process was carried out using Distilled water (Milli-Q® water system) and Ethanol (99.8%, Sigma-Aldrich) as solvents. For layer-by-layer deposition silica mesoporous nanoparticles (200 nm particle size, pore size 4nm), Chitosan (Low Mw, Deacetylation Degree 75%) and Acetic acid (glacial, ReagentPlus®,  $\geq 99\%$ ) were purchased by sigma Aldrich. Antioxidant characterization was performed on extracts using Folin & Ciocalteu's phenol reagent and sodium carbonate ( $\text{Na}_2\text{CO}_3$ ), purchased by sigma Aldrich, and Invitrogen™ assay kit (Thermo Fisher Scientific, Inc.).

Other materials used included Hydrochloric acid (HCl) (reagent grade 37%), (Sigma-Aldrich, UK), Gallic Acid (97.5-102.5% (titration)), (Sigma-Aldrich, UK). For cell culture tests, Fetal Bovine Serum (FBS, ThermoFisher Scientific, Inc), penicillin/streptomycin (P/S, Sigma-Aldrich), Human Fibroblast Growth Factor (hFGF-2, Sigma-Aldrich), L-Glutamine (LG, 5 mM, Sigma-Aldrich), Phosphate Buffered Saline (PBS Sigma-Aldrich), Trypsin/EDTA (Sigma-Aldrich), Dulbecco's Modified Eagles Medium (DMEM, Sigma-Aldrich, Gibco high glucose 4500 mg/L) were used.

## 3.2 Methods

### 3.2.1 Ultrasound assisted extraction of antioxidants from cocoa and coffee biomass

Different samples of cocoa and coffee powdered biomass were prepared, and two different solvents were tested as extraction solvent: ultrapure water at different pH, 6 and 12, and a 50% ethanol solution. Ultrasound-assisted extraction (UAE), shown in Figure 5, was performed on a VWR ultrasonic cleaner bath at 45kHz using 10 mL of 50% ethanol solution as final extraction solvent.

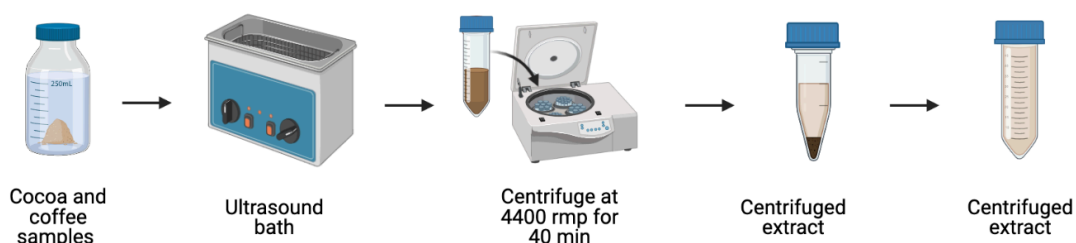


Figure 5: Ultrasound assisted extraction process.

The extraction process was carried out according to the Design of Experiments, through Box-Behnken design, to evaluate the effect of Temperature ( $^{\circ}\text{C}$ ), Extraction Time (min) and Liquid/Solid Ratio (mL/g) on the total phenolic content of coffee and cocoa samples. Minitab Statistical software was used to generate 20 combinations of extraction variables, reported in Table 1, resulting that temperature was set from  $23^{\circ}\text{C}$  to  $57^{\circ}\text{C}$ , liquid/solid ratio at 10 to 35 mL/g, and the extraction time from 16 to 59 minutes. Six of these combination (Temperature of  $40^{\circ}\text{C}$ , Ultrasonic bath time of 37.5 mins and Ratio of 22.5 mL/g) were the central points.

After each extraction, mixtures were poured into centrifuge tubes and centrifuged at 4400rpm for 40 minutes into Thermo Scientific™ Megafuge 16R TX-200 Centrifuge. The resulting supernatant solution was then collected into 20 mL flask for ethanol evaporation performed in a rotary evaporator RV-8-Flex (IKA) at 130 rpm and  $48^{\circ}\text{C}$  until the initial volume was half reduced.

To analyse the DoE of cocoa and coffee antioxidant extract response surface methodology (RSM) was used. In particular, exploiting Pareto charts, Surface plots and Contour plots, statistical analysis of extraction parameters (Temperature (°C), Extraction Time (min) and Liquid/Solid Ratio (mL/g)) was carried out to evaluate their effects on the final extracts gallic acid concentration (GAE (mg/mL)). Therefore, Response Optimization was performed to find the optimal extraction parameters for maximize gallic acid concentration.

# Run	Temperature (°C)	Time (min)	Ratio (mL/mg)
1	30	50	15
2	40	37.5	22.5
3	40	37.5	22.5
4	30	50	30
5	30	25	30
6	40	37.5	35.1
7	50	25	30
8	56.8	37.5	22.5
9	50	25	15
10	30	25	15
11	50	50	15
12	40	16.5	22.5
13	23.2	37.5	22.5
14	40	37.5	22.5
15	50	50	30
16	40	37.5	22.5
17	40	37.5	22.5
18	40	58.5	22.5
19	40	37.5	9.8
20	37.5	40	22.5

Table 1: The Design of Experiment (DoE) for antioxidants extraction.

### *3.2.2 Chemical characterization of antioxidant extracts*

#### *3.2.2.1 Determination surface functional groups by FTIR-ATR analysis*

Surface functional groups of cocoa and coffee extracts were detected performing FTIR-ATR analysis on the samples. Analysis was performed with a Spectrum Two PE instrument equipped with a horizontal attenuated total reflectance (ATR) crystal (ZnSe) (PerkinElmer Inc., US). Cocoa and coffee samples were previously freeze-dried to obtain powders and placed directly on the ATR crystal. The spectra were collected in absorbance mode and recorded in the wavelength range 4000-550  $\text{cm}^{-1}$ . Each spectrum was the result of averaging 16 scans with a resolution of 2  $\text{cm}^{-1}$ .

#### *3.2.2.2. Determination of total phenolic compounds by Folin-Ciocalteu method*

The extracts total phenol content (TPC) was determined according to the Folin-Ciocalteu method [44] using a UV-Vis spectrophotometer (FLUOstar Omega, BMG Labtech, Germany). Folin-Ciocalteu reacts with the phenolic compounds in the sample to form a blue colour that is proportional to the number of phenolic compounds present. Hence, 50  $\mu\text{L}$  of the extracts were mixed with 430  $\mu\text{L}$  of distilled water and 20  $\mu\text{L}$  of the Folin-Ciocalteu reagent. After stirring, a 20% w/v  $\text{Na}_2\text{CO}_3$  solution was added and left 10 min to rest. The mixture was finally diluted with 450  $\mu\text{L}$  of distilled water and its absorbance was recorded at a wavelength of 680 nm, measured against the blank prepared with 50  $\mu\text{L}$  of ultrapure water. For this, a calibration curve was prepared by dissolving gallic acid in distilled water in 7 known concentrations ranging from 0.05 mg/mL to 5 mg/mL ( $R^2=0.997$ ). The TPC was expressed as gram equivalents of gallic acid per mL of samples (GAE (mg/mL)). All measurements were recorded in triplicate and the mean values were calculated.

#### *3.2.3. Determination of antioxidant activities by Ferric Reducing Antioxidant Power method*

The Ferric Reducing Antioxidant Power (FRAP) assay was carried out to evaluate the total antioxidant activity of cocoa and coffee extracts. To this purpose Invitrogen™ assay kit was used (Thermo Fisher Scientific, Inc.). After 30 min of incubation at room temperature, the absorbance of the coloured product was measured at a wavelength of 560 nm using a UV-Vis spectrophotometer (FLUOstar Omega, BMG Labtech, Germany). The results were expressed as ascorbic acid equivalent (AAE  $\mu\text{M}$ ), which was used as positive control. All measurements were recorded in triplicate and the mean values were calculated.

### 3.2.4 LbL nanoparticles preparation

#### 3.2.4.1 Polyelectrolyte solutions preparation

Chitosan (CH) and pectin (PE) were used as polyelectrolytes in the LbL deposition due to their opposite charge. Two different solution (1 mg/mL) were prepared dissolving PE in a H<sub>2</sub>O buffer solution (pH=6) and CH in a 1% v/v glacial acetic acid and H<sub>2</sub>O buffer solution (pH=6). According to  $\zeta$ -potential measurement antioxidant extracts have negative charge therefore were add to PE solution 1:4. Final pH of both polyanion and polycation solution was adjusted using NaOH (0.25M) and HCl (0.1 M) at pH=6.

#### 3.2.4.2 Polyelectrolyte solutions analysis

Surface functional groups of pectin and chitosan polyelectrolyte solution were detected performing FTIR-ATR analysis on the samples. Samples were were previously freeze-dried in order to obtain powders and analysis was performed with a Spectrum Two PE instrument equipped with a horizontal attenuated total reflectance (ATR) crystal (ZnSe) (PerkinElmer Inc., USA). The spectra were collected in absorbance mode and recorded in the wavelength range 4000-550 cm<sup>-1</sup>. Each spectrum was the result of averaging 16 scans with a resolution of 2 cm<sup>-1</sup>.

Furthermore, in order to established Layer-by-Layer deposition sequences, dynamic light scattering was used to measure polyelectrolyte solution  $\zeta$ -potential usinf a Zetasizer Nano-S90 (Malvern Instruments, Malvern, UK). An aliquot (100  $\mu$ L) of each solution was gently mixed with 900  $\mu$ L of buffer solution and added to the Zetasizer cuvette. All measurements were recorded in triplicate and the mean values were calculated and results were expressed then as the mean  $\pm$  standard deviation.

#### 3.2.4.3 Layer-by-Layer deposition

LbL deposition, shown in Figure 6, started by dipping the silica mesoporous nanoparticles into the polycation CH solution to maximize electrostatic interaction between MNPs negative charge and CH positive charge. Two different vials were prepared to functionalize MNPs with cocoa and coffee extracts separately.

Briefly, 10 mL of CH solution were added to 20 mg of MNPs, then sonicated until the solution become homogenous. After 15 min of shaking at 95 rpm by Orbital shaker SSM1 (Cole Parmer/Stuart), MNPs solution was centrifugate for 5 minutes at 4400 rpm. Afterwards, two washing step in H<sub>2</sub>O buffer solution was performed to remove the excess polyelectrolyte.

Therefore, supernatant was replaced by 5 mL of buffer solution, sonicated until the solution become homogenous and centrifugated (5 min at 4400 rpm)

after 10 minutes shaking at 95 rpm. This step was repeated using 3 mL of H<sub>2</sub>O buffer solution and reducing shaking time at 3 minutes. Before the last centrifuge, 100  $\mu$ L of functionalized MNPs were taken for  $\zeta$ -potential analysis. In the final step the MNPs were centrifuged (15 min at 4400 rpm), supernatant was moved and the deposition of polyanion PE solution was carried out following the same protocol. This process was repeated until 5 opposite charged layers were deposited consecutively. Final MNPs functionalized systems were freeze-dried and then kept in vacuum desiccator for further test.

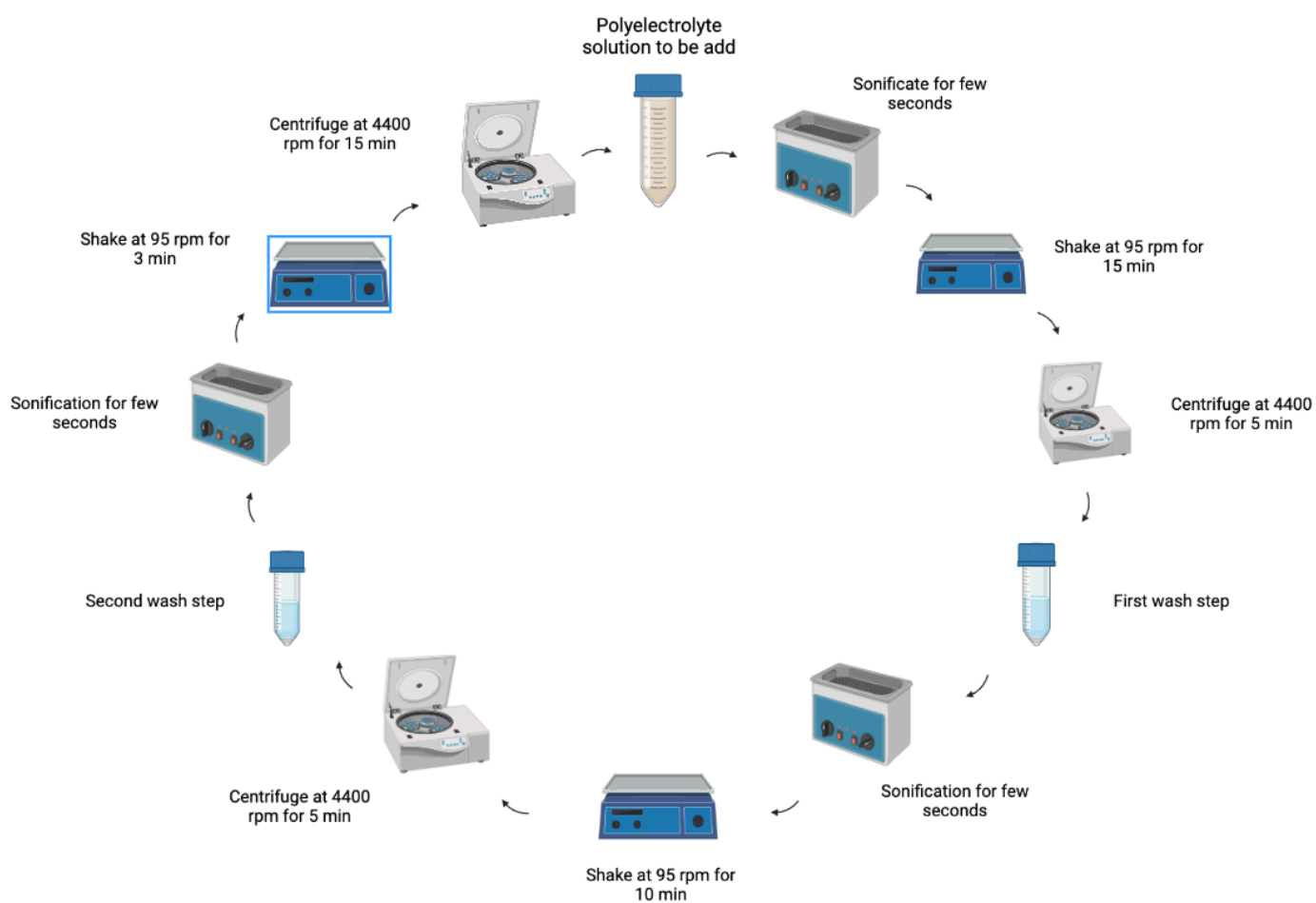


Figure 6: LbL deposition protocol

### *3.2.5 Nanoparticles Characterization*

#### *3.2.5.1 Determination of $\zeta$ -potential through dynamic light scattering*

Dynamic light scattering was used to measure MNPs  $\zeta$ -potential expressed then as the mean  $\pm$  standard deviation. Analysis was performed as previously describe in section 3.2.4.2.

#### *3.2.5.2 Morphology characterization through transmission electron microscope*

Transmission electron microscope was used to determine MNPs morphology (TEM) (Philips CM 100 Compustage FEI) at 100kV. For TEM sample preparation the supernatant aliquot (10  $\mu$ L), removed before the last centrifuge, was directly added to the TEM grid and placed in the middle of the specialized chamber of the microscope. On the high magnified images obtained, precise diameter measurement was carried using ImageJ software.

#### *3.2.5.3 Chemical characterization*

##### *3.2.5.3.1 Fourier Transformed Infrared spectroscopy analysis (FTIR-ATR)*

Surface functional groups of engineered silica nanoparticles were detected performing FTIR analysis on the samples, which were previously freeze-dried in order to obtain powders. Analysis was performed as previously describe in section 3.2.4.2.

In order to verify the correct LbL deposition also mesoporous nanoparticles purchased from sigma was tested in order to compare their spectra with MNPs obtained from cocoa and coffee one.

##### *3.2.5.3.2 X-ray photoelectron spectroscopy analysis (XPS)*

Freeze-dried nanoparticles were analyzed through XPS to quantitatively assess the elemental composition of the surface of the biomaterials. Samples were examined by a scanning microprobe Kratos Axis UltraDLD XPS spectrometer (EPSRC Harwell XPS Service Cardiff, UK), equipped with a monochromatised AlK $\alpha$  X-ray radiation source. The base pressure in analysis chamber was 10<sup>-9</sup> mbar. Samples were analysed in High 96 Power mode with an X-ray take-off angle of 45° (scanned size~1400  $\times$  200  $\mu$ m). For each specimen, survey scans (Fixed Analyser Transmission mode, binding energy (BE) range 0–1200 eV, pass energy 117.4 eV) and high-resolution spectra (FAT mode, pass energy 29.35 eV) were acquired of C1s and O1s. Atomic concentration (At.%) on the survey scan was performed using the built-in CasaXPS software package and in order to detect the Binding Energy (BE)

representing the chemical binding states of the each elements within the films, the XPS spectra for the chemical elements detected from the films were subjected to peak deconvolution using the same software

### 3.2.6 Cell Culture

Neo-dermal fibroblast cells were grown in Dulbecco's Modified Eagle's Medium (DMEM), with 10% fetal bovine serum (FBS) and 5000 U/mL penicillin/streptomycin and maintained at 37 °C with 5 % CO<sub>2</sub> in a humidified incubator. All culture materials were purchased from Sigma Life Science.

### 3.2.7 Cellular test

2D cells model was created for Neo-dermal fibroblast in order to test cell behaviour after incubation with manufactured nanoparticles. To the aim, Greiner CELLSTAR® 96 well-plates with a density of 10000cells/well was used, as shown in Figure 7.

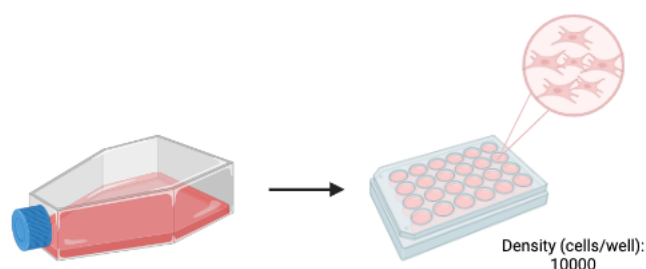


Figure 7: 2D cells culture model for extracts and MNPs treatment.

### 3.2.8 Cytotoxicity Evaluation

#### 3.2.8.1 Live/Dead assay

To evaluate cell viability, a two-colour fluorescence test was used: Live/Dead assay (LIVE/DEAD® Cell Imaging Kit, Life Technologies, Thermo Fisher Scientific, UK). With this method we are able to simultaneously determines the population of live cells (green staining) and dead cells population (red staining). In particular, live cells were determined by green fluorescence (ex/em ~495 nm/~515 nm) obtained by enzymatic conversion of non-fluorescent calcein AM to intensely fluorescent calcein. On the other hand, dead cells were indicated by red fluorescence (ex/em ~495 nm/~635 nm) of ethidium homodimer (EthD-1), able to bind nucleic acids entering cells through damaged membranes. Several samples were prepared dissolving different

quantities of free cocoa and coffee antioxidant extracts, MNPs from sigma and functionalized MNPs systems into DMEM, to test the effects of different concentrations (from 10 ( $\mu\text{g}/\text{mL}$ ) to 100 ( $\mu\text{g}/\text{mL}$ )). Therefore, Live/Dead assay was carried out according to the manufacturer's instructions. Briefly, L/D staining solution was realized by mixing 1  $\mu\text{l}$  of Calcein with 4  $\mu\text{l}$  of Ethidium in 2ml of PBS. Cells were incubated for 48h with antioxidants and MNPs different concentrations; when incubation time ran out, all wells were washed twice with PBS and incubated with 100  $\mu\text{L}$  of L/D staining solution for 30 min at 37°C. Finally, samples were imaged using EVOS M5000 fluorescence microscope from Thermo Fisher Scientific.

### 3.2.8.2 *PrestoBlue assay*

To evaluate cell metabolic activity of Neo-dermal fibroblast PrestoBlue assay was performed using PrestoBlue™ Cell Viability Reagent, (Thermo Scientific, USA). Briefly, cells were seeded in a 96-well plate (10000 cells/well) with different concentration of nanoparticles and extracts to be tested (100, 250, 500, 1000  $\mu\text{g}/\text{mL}$ ). After 48h of incubation, culture medium was removed, and samples were washed with pre-warmed PBS at 37 °C to assess the metabolic activity of cells using PrestoBlue solution.

PrestoBlue™ reagent (Thermo Scientific, USA), pre-warmed at 37 °C, was diluted in DMEM (1:10). Vial containing the reagent was covered with aluminum to protected from light the solution. Then, 200  $\mu\text{L}$  of reagent solution was added to each well and incubated for 1h at 37°C, 5% CO<sub>2</sub>. After the incubation, 100  $\mu\text{L}$  of each well solution was transferred to a white bottom 96-well plate and a FLUOstar Omega MicroPlate Reader (BMG Labtech) was used to measure the fluorescence (560 nm excitation and 590 nm emission). The obtained values were corrected subtracting the average fluorescence of control wells with only PrestoBlue solution. Results are shown in viability (%) obtained by relating the value in fluorescence of each sample with the average fluorescence value of the control cells (which was incubating with only DMEM).

### 3.2.9 *Nanoparticles antioxidant activity evaluation through fluorescence assay for Intracellular ROS generation*

To qualitatively characterize H<sub>2</sub>O<sub>2</sub>-induced intracellular ROS generation and evaluate antioxidant behaviour of extracts and functionalized nanoparticles, the 2',7'-dichlorofluorescein diacetate (DCFDA) fluorescence assay was used. To the aim, several samples of extracts and engineered MNPs were prepared at different concentration (10, 50, 100, 500  $\mu\text{M}$ ), including MNPs purchased from sigma and a solution of resveratrol. Then, Neo-dermal fibroblast cells were seeded in a 96-well plate (10000 cells/well) and incubated with 100  $\mu\text{L}$  of each sample for 24h at 37°C, 5% CO<sub>2</sub>. When incubation time ran out, media was removed and each well was washed with PBS, pre-warmed at 37 °C. 50  $\mu\text{L}$  of a 150  $\mu\text{M}$  solution of H<sub>2</sub>O<sub>2</sub> were added to each well and left in the incubator for 1h at 37°C, 5% CO<sub>2</sub>. Final step was

added 50  $\mu\text{L}$  of a 10  $\mu\text{M}$  DCFDA solution to each well and incubated for 30 min 1h at 37°C, 5%  $\text{CO}_2$ . After the incubation, 100  $\mu\text{L}$  of each well solution was transferred to a white bottom 96-well plate and a FLUOstar Omega MicroPlate Reader (BMG Labtech) was used to measure the fluorescence (488 nm excitation wavelength and 520 nm emission). Results are shown in ROS generation (%) obtained by relating the value in fluorescence of each sample with the average fluorescence value of the control cells (which was incubating with only DMEM and treated with the  $\text{H}_2\text{O}_2$  solution). Moreover, 96-well plate was imaged using EVOS M5000 fluorescence microscope from Thermo Fisher Scientific.

### *3.2.10 Statistical Analysis*

Tests were performed in triplicate for each sample. Results are presented as means  $\pm$  standard deviations. Statistical significance was evaluated using GraphPad software by analysis of variance (ANOVA), followed by Turkey's multiple comparison test using levels of statistical significance of  $p < 0.05$  (\*),  $p < 0.01$  (\*\*),  $p < 0.001$  (\*\*\*), and  $p < 0.0001$  (\*\*\*\*).

## 4. Results and discussions

### 4.1 Ultrasound Assisted Extraction (UAE) optimization through design of experiment

According to the Design of Experiments, UAE conditions were optimized to evaluate the effect of extraction parameters on the total phenolic content (TPC). Hence, 20 different combination of extraction parameters were generated through Minitab and system responses are shown in Table 2.

# Run	Temperature (°C)	Time (min)	Ratio (mL/mg)	Coffee TPC(mg/mL)	Cocoa TPC(mg/mL)
1	30	50	15	2.3	2.9
2	40	37.5	22.5	1.9	2.4
3	40	37.5	22.5	2.03	2.5
4	30	50	30	1.8	2.8
5	30	25	30	1.9	2.7
6	40	37.5	35.1	1.4	2.8
7	50	25	30	1.6	3.0
8	56.8	37.5	22.5	1.9	2.7
9	50	25	15	1.8	2.5
10	30	25	15	1.8	2.1
11	50	50	15	2.2	2.4
12	40	16.5	22.5	1.9	2.4
13	23.2	37.5	22.5	2.1	2.8
14	40	37.5	22.5	1.9	2.5
15	50	50	30	1.4	2.3
16	40	37.5	22.5	2.0	2.5
17	40	37.5	22.5	1.9	2.4
18	40	58.5	22.5	2.2	2.6
19	40	37.5	9.8	1.8	2.3
20	37.5	40	22.5	1.9	2.6

Table 2: Combination of extraction parameters and system responses expressed through total phenolic content (TPC).

Response surface methodology (RSM) was then used to express TPC, respectively for cocoa and coffee, as a function of the independent variables exploiting a second-order polynomial equation:

$$TPC = -0.698 - 0.008 \text{ Temp} + 0.115 \text{ Time} + 0.089 \text{ Ratio} + 0.001 \text{ Temp}^2 - 0.002 \text{ Temp} \cdot \text{Time} - 0.002 \text{ Time} \cdot \text{Ratio} \quad (\text{Eq.1})$$

$$TPC = -0.121 - 0.009 \text{ Temp} + 0.043 \text{ Time} + 0.157 \text{ Ratio} - 0.002 \text{ Ratio}^2 - 0.002 \text{ Time} \cdot \text{Ratio} \quad (\text{Eq.2})$$

Moreover, Pareto charts, contour, and surface plots of the system responses against extraction parameters were used to evaluate the reliability of the fitted models.

In cocoa Pareto charts of the TPC (Figure 8), Temperature ( $^{\circ}\text{C}$ ), Ratio (mL/mg) and extraction Time (min) exceeded the alpha value ( $\alpha = 0.05$ ) demonstrating that significantly influenced the TPC of final extracts. In particular, the most influencing parameter on final TPC is the combination of Temperature and Time ( $p < 0.0001$ ).

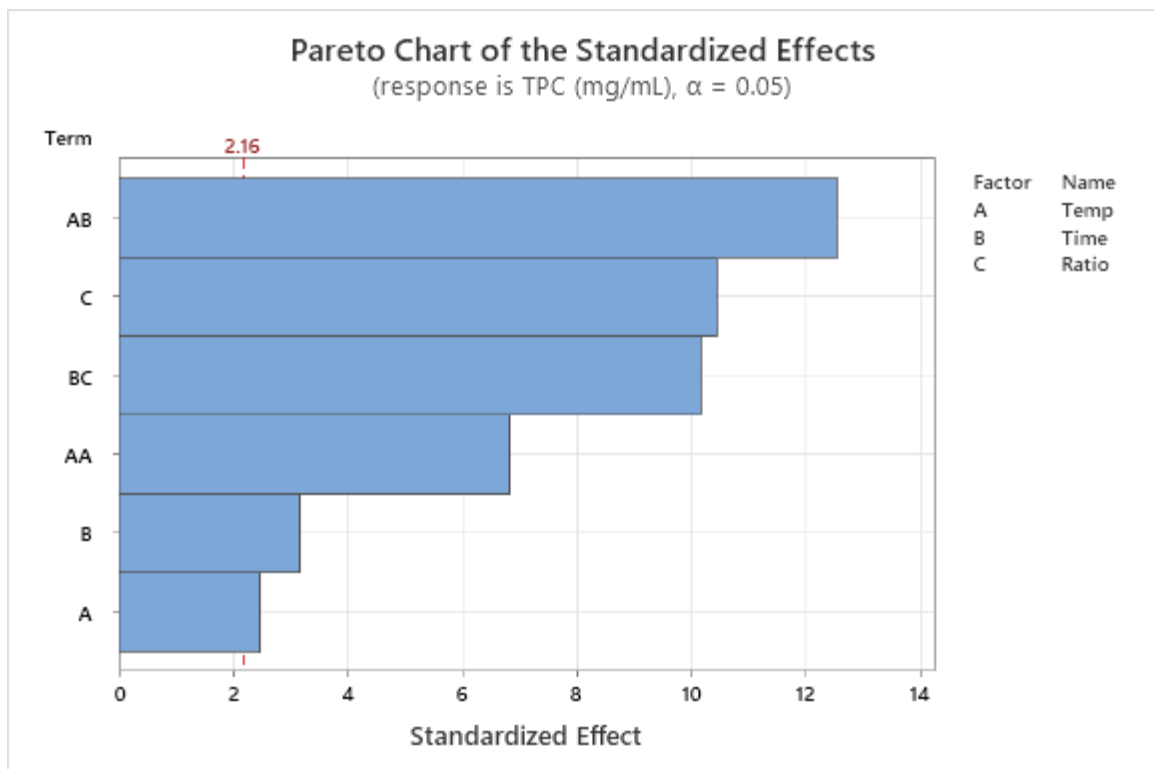
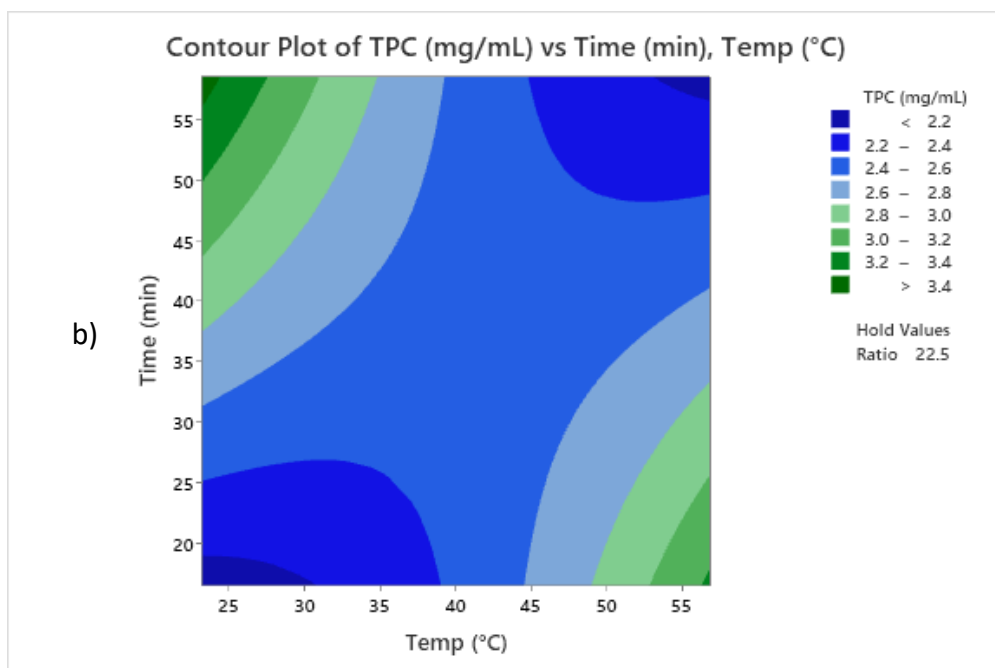
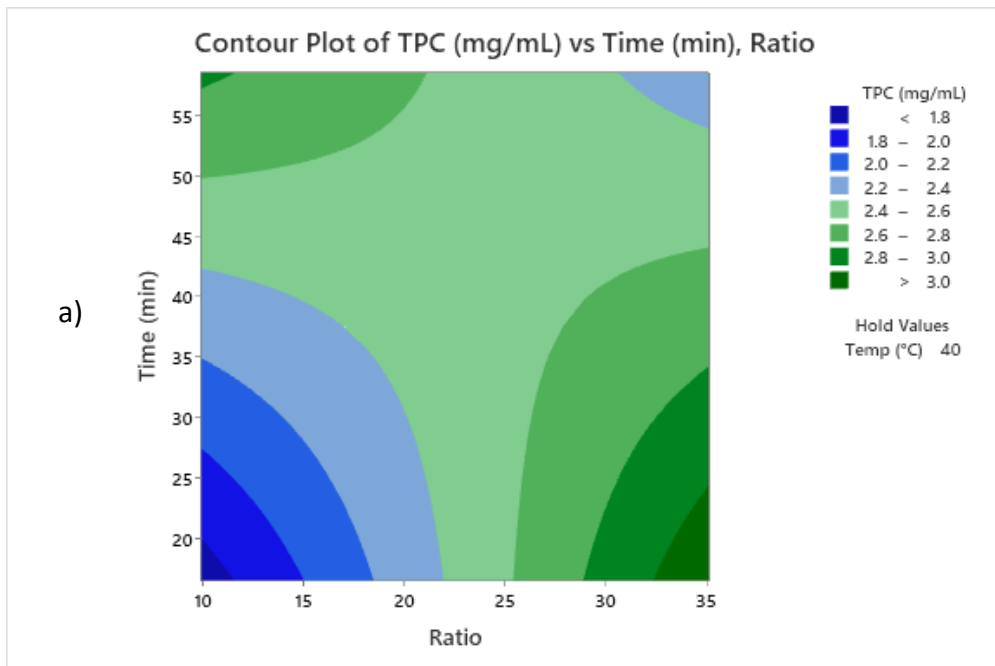


Fig 8: Pareto charts for TPC (mg/mL), showing the alpha value and the standardized effect of each parameter on the resulting size of the particle.

Hence, looking at cocoa contour and surface plot (Figure 9-10) higher value of extraction time combined with lower value of ratio and lowest value of ratio seemed to produce the most consistent results in terms of TPC.



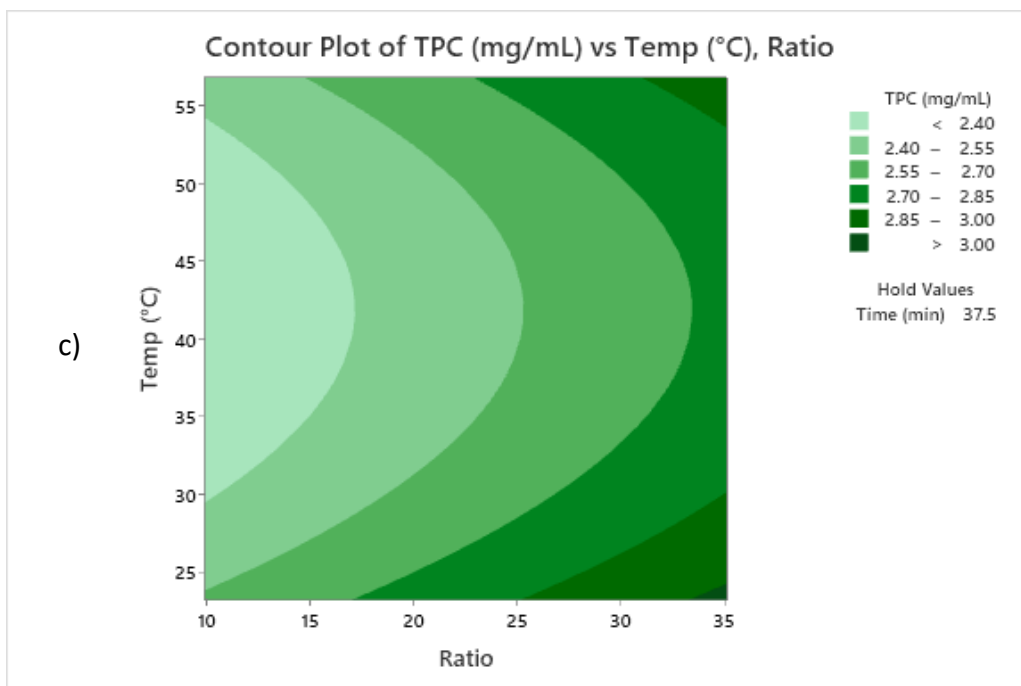
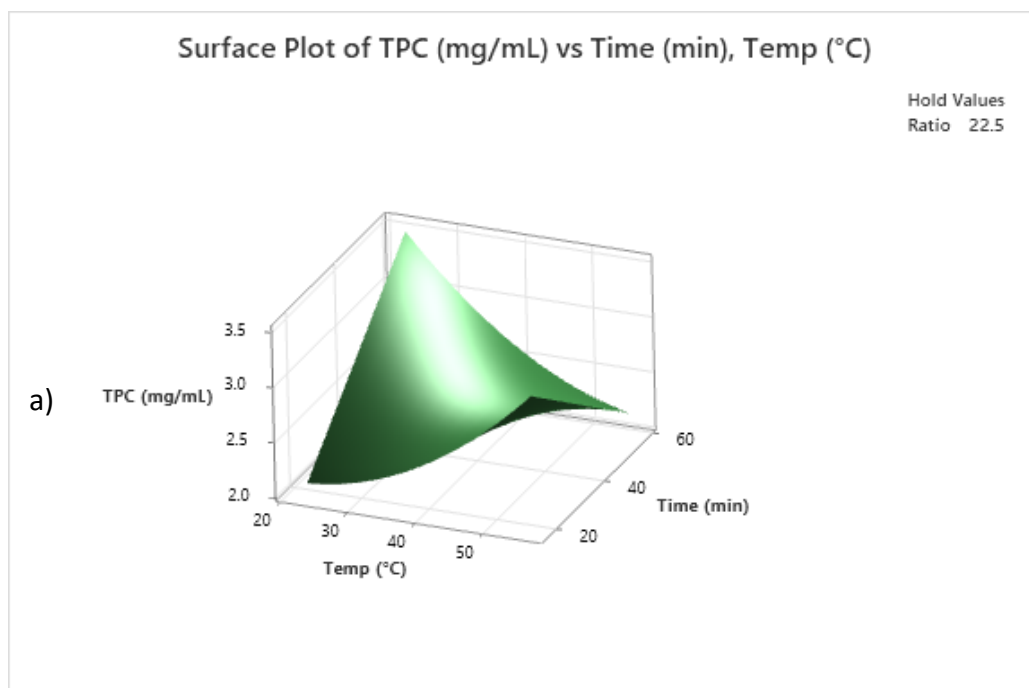


Fig. 9: a) Contour Plot of TPC (mg/mL) against Time (min) and Temperature (°C), b) Contour Plot of TPC (mg/mL) against Time (min) and Ratio (mL/mg), c) Contour Plot of TPC (mg/mL) against Temperature (°C) and Ratio (mL/mg).



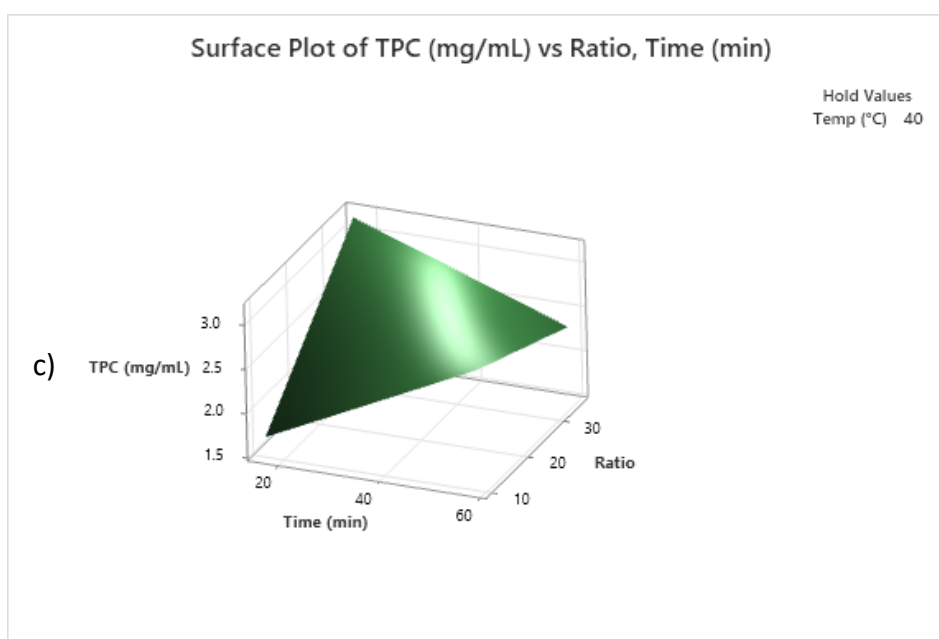
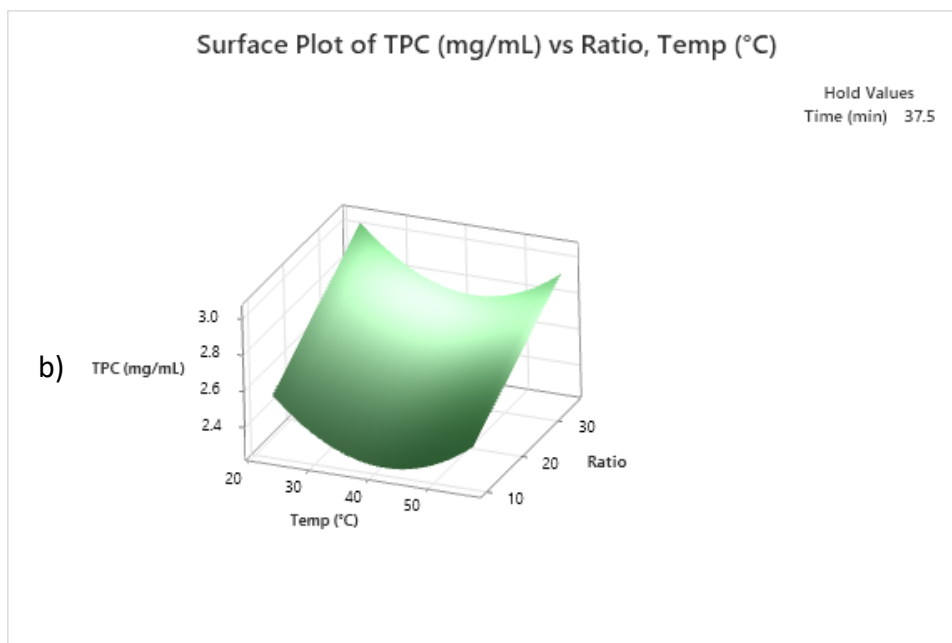


Fig. 10: a) Surface Plot of TPC (mg/mL) against Time (min) and Temperature (°C), b) Surface Plot of TPC (mg/mL) against Temperature (°C) and Ratio (mL/mg), c) Contour Plot of TPC against Time (min) and Ratio (mL/mg).

In coffee Pareto charts (Figure 11), Temperature ( $^{\circ}\text{C}$ ), Ratio (mL/mg) and extraction Time (min) exceeded the alpha value ( $\alpha = 0.05$ ) as cocoa extracts, but in this case the most influencing parameter on final TPC is the ratio ( $p < 0.0001$ ).

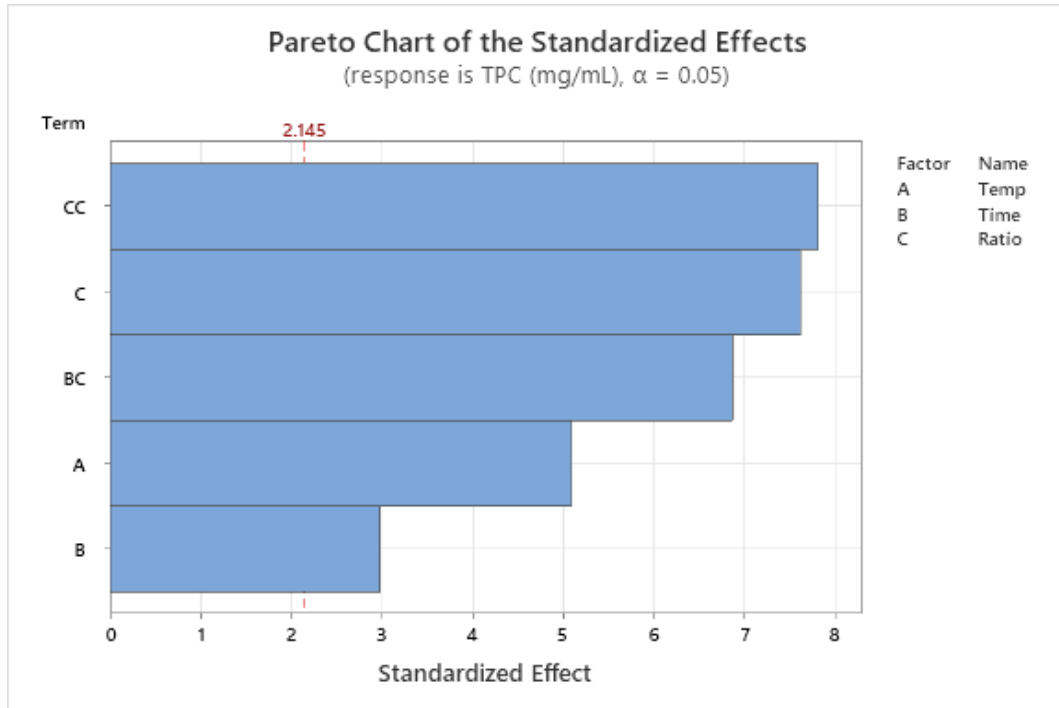
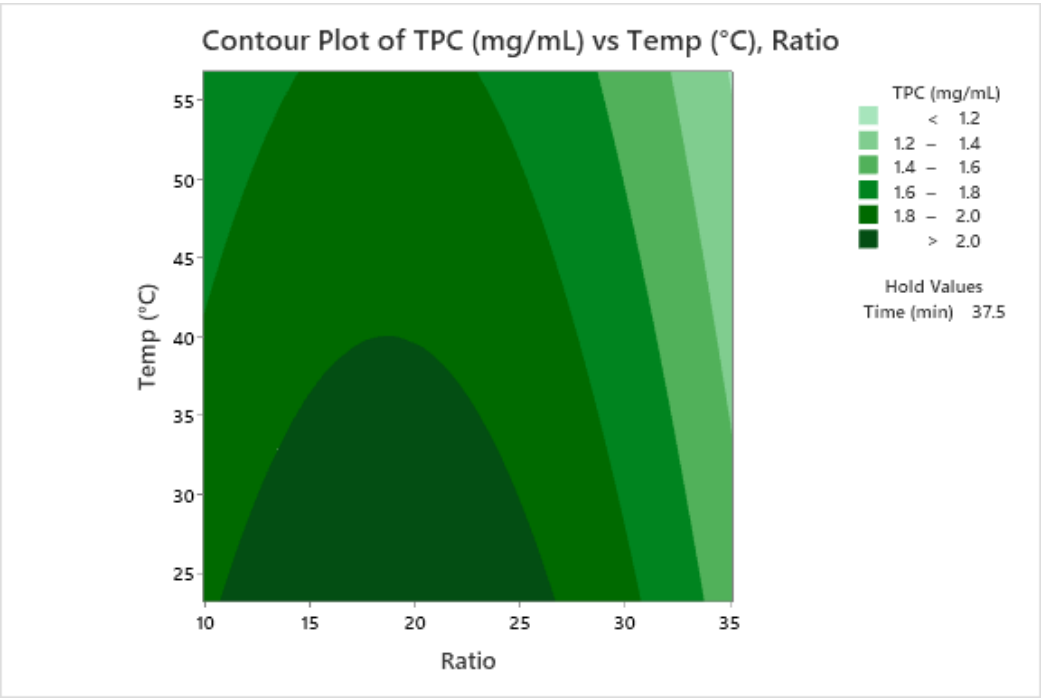
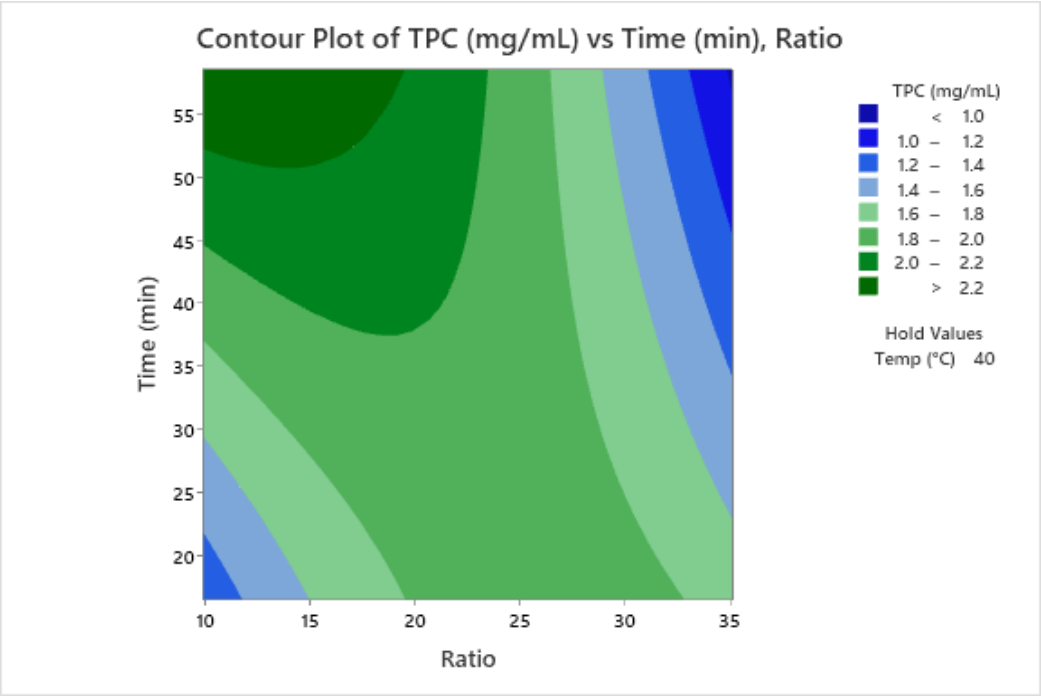


Fig 11: Pareto charts for TPC (mg/mL), showing the alpha value and the standardized effect of each parameter on the resulting size of the particle.

Looking at coffee contour and surface plot (Figure 12-13) indeed higher value of extraction time combined with lower value of ratio and temperature seemed to produce the most consistent results in terms of TPC.



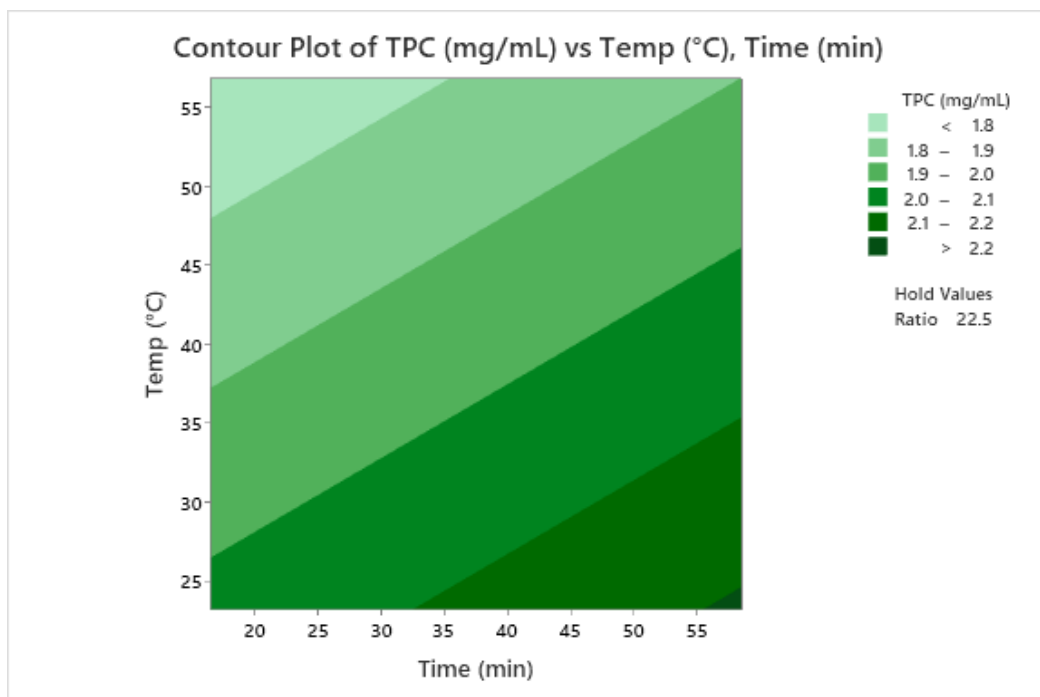
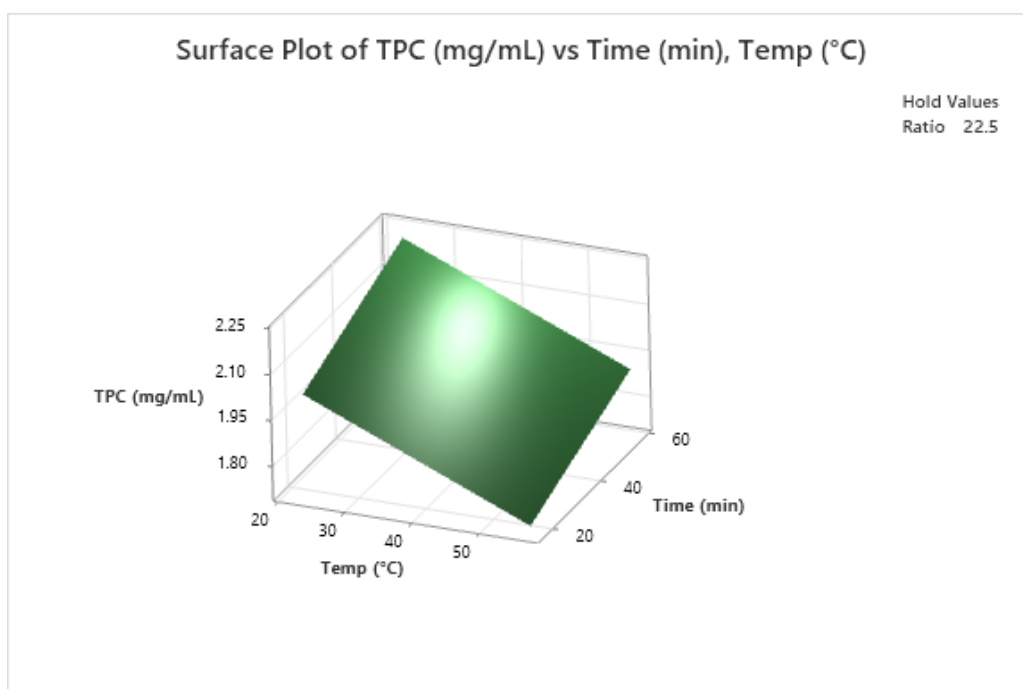


Fig 12: a) Contour Plot of TPC (mg/mL) against Time (min) and Ratio (mL/mg),  
 b) Contour Plot of TPC (mg/mL) against Temperature (°C) and Ratio (mL/mg),  
 c) Contour Plot of TPC (mg/mL) against Time (min) and Temperature (°C).



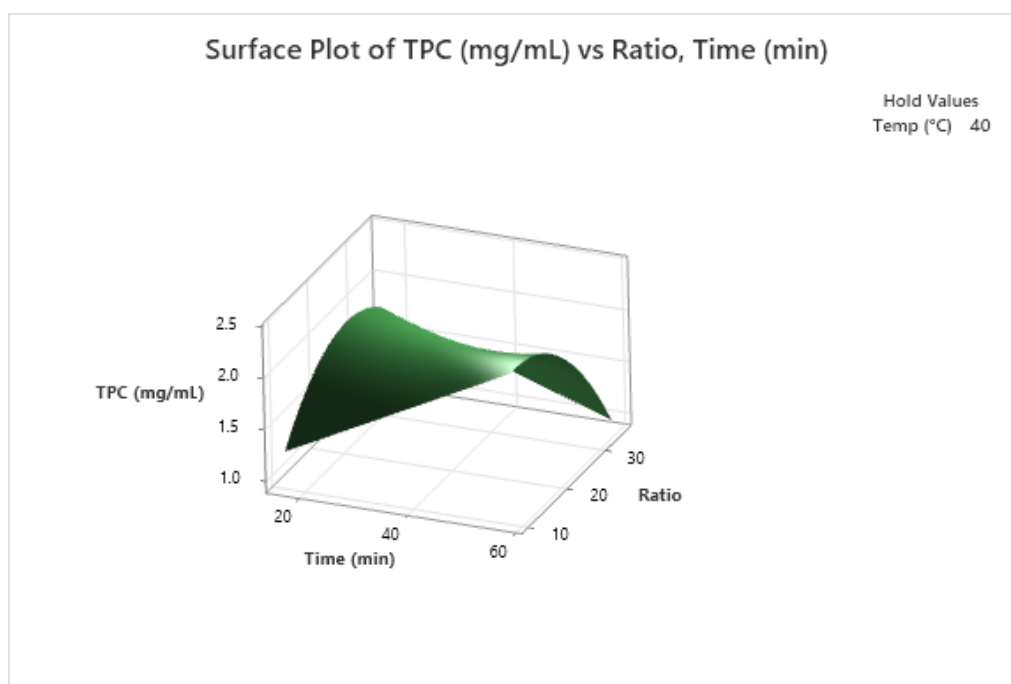
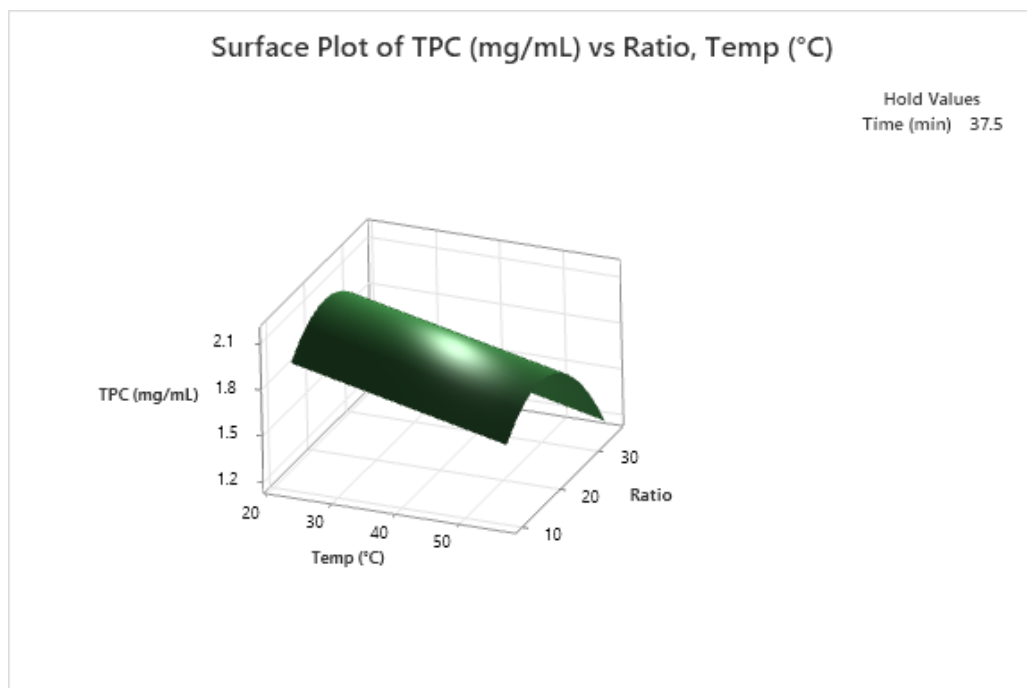


Fig 13: a) Surface Plot of TPC (mg/mL) against Time (min) and Temperature (°C), b) Surface Plot of TPC (mg/mL) against Temperature (°C) and Ratio (mL/mg), c) Contour Plot of TPC against Time (min) and Ratio (mL/mg).

R-squared (R-sq) value obtained from the analysis was approx. 97% for both cocoa biomass and coffee biomass, resulting in an optimal correlation between the resulting values and the regression model. Adjusted R-squared (R-sq(adj)) and Predicted R-squared (R-sq(pred)) are also calculated in addition to R-sq resulting and showed in Table 3 e Table 4 for cocoa and coffee respectively.

R-sq	R-sq(adj)	R-sq(pred)
97.1 %	95.7 %	94.20 %

Table 3: Model Summary for cocoa optimized extraction

R-sq	R-sq(adj)	R-sq(pred)
96.8 %	94.9 %	91.1 %

Table 4: Model Summary for coffee optimized extraction

Final step included the Response Optimization of extraction process using Response Optimizer on Minitab. Response Optimization was performed to determine the optime combination of extraction parameters able to maximize the final TPC.

Response prediction of TPC in coffee antioxidants extract should be reached the maximum value (TPC= 2.6 (mg/mL)) when ratio is of 11.16 (mL/mg) and the extraction was performed at 23.18°C for 58.5 min. On the contrary, in cocoa extraction the highest total phenolic content (TPC=3.8 (mg/mL)) should be obtained when the process is carried out at the same temperature of coffee for 16.5 min and the ratio is of 35.1 (mL/mg). Subsequent extraction performed with optimized parameters confirmed model prediction. Optimized coffee antioxidants extract presented a final TPC concentration of 2.35 (mg/mL), while for cocoa sample higher value of 3.71 (mg/mL) was reached.

The full statistical results, including variance analysis can be found in the appendix, section *Appendix*.

## 4.2 Chemical characterization of antioxidant extracts

FTIR-ATR analyses were conducted on coffee and cocoa extract, which were previously freeze dried, to analyse their bioactive composition. Cocoa spectrum, in Figure 14, is characterized by the presence of absorption peaks in the 3200-3600  $\text{cm}^{-1}$  range, indicating the presence of hydroxyl (-OH) groups, and 2800-3000  $\text{cm}^{-1}$  range, corresponding to C-H stretching vibrations of polysaccharides CH<sub>2</sub> groups. Phenolic compounds can be identified by their characteristic absorption bands in the 1500-1600  $\text{cm}^{-1}$  range, which correspond to C=C stretching vibrations of aromatic rings. Moreover, cocoa biomass contains significant amounts of carbohydrates such as cellulose and hemicellulose; these compounds can be identified by their characteristic absorption bands in the 1000-1200  $\text{cm}^{-1}$  range, corresponding to C=O stretching vibrations [45]. Final characteristic absorption bands appeared between 900–600  $\text{cm}^{-1}$  due to the stretching vibrations of the entire anhydroglucose ring [46].

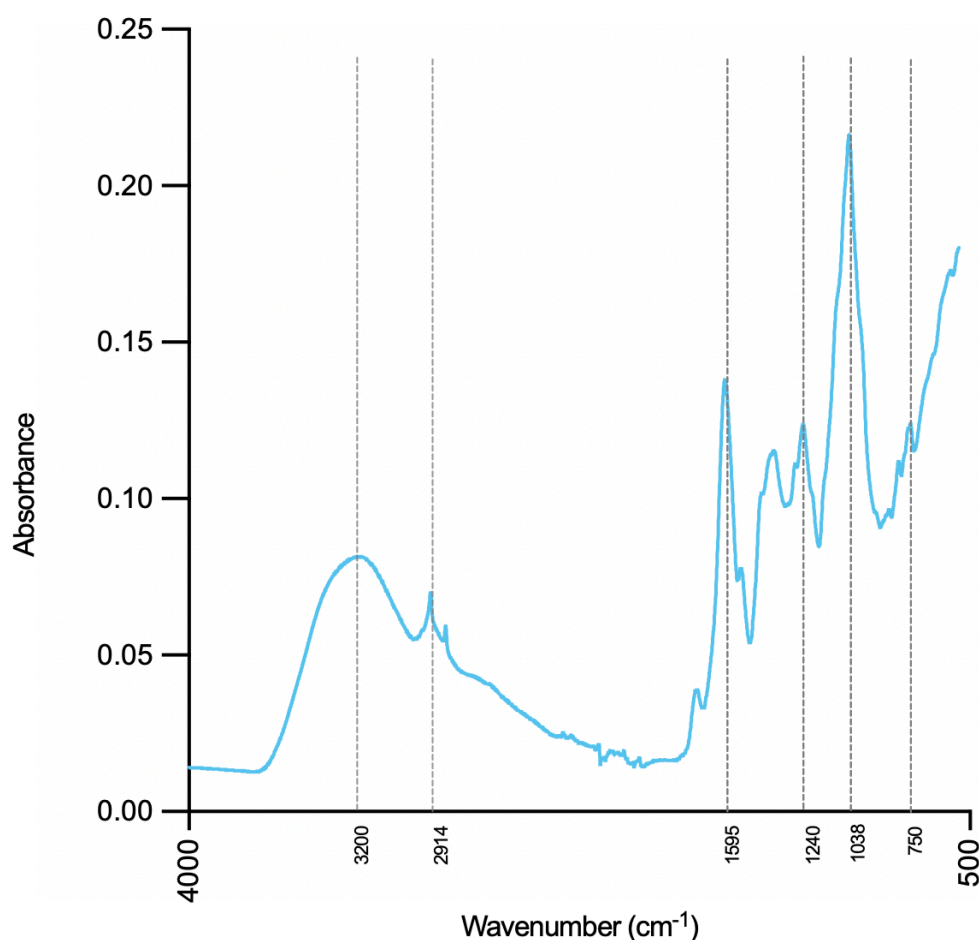


Fig 14: FTIR spectra of cocoa biowaste antioxidant extract.

Figure 15 shows FTIR spectrum of coffee extract in which characteristic peaks are very similar to cocoa. Briefly, the presence of absorption peaks in the 3200-3600  $\text{cm}^{-1}$  range, indicate the presence of hydroxyl (-OH) groups, while 2800-3000  $\text{cm}^{-1}$  range, correspond to C-H stretching vibrations of polysaccharides  $\text{CH}_2$  groups. Absorption bands in the 1500-1600  $\text{cm}^{-1}$  range correspond to C=C stretching vibrations of aromatic rings due to phenolic compounds presence, while carbohydrates can be identified by their characteristic absorption bands in the 1000-1200  $\text{cm}^{-1}$  range, corresponding to C-O and C-C stretching vibrations. Final characteristic absorption bands appeared between 900–600  $\text{cm}^{-1}$  due to the stretching vibrations of the entire anhydroglucose ring.

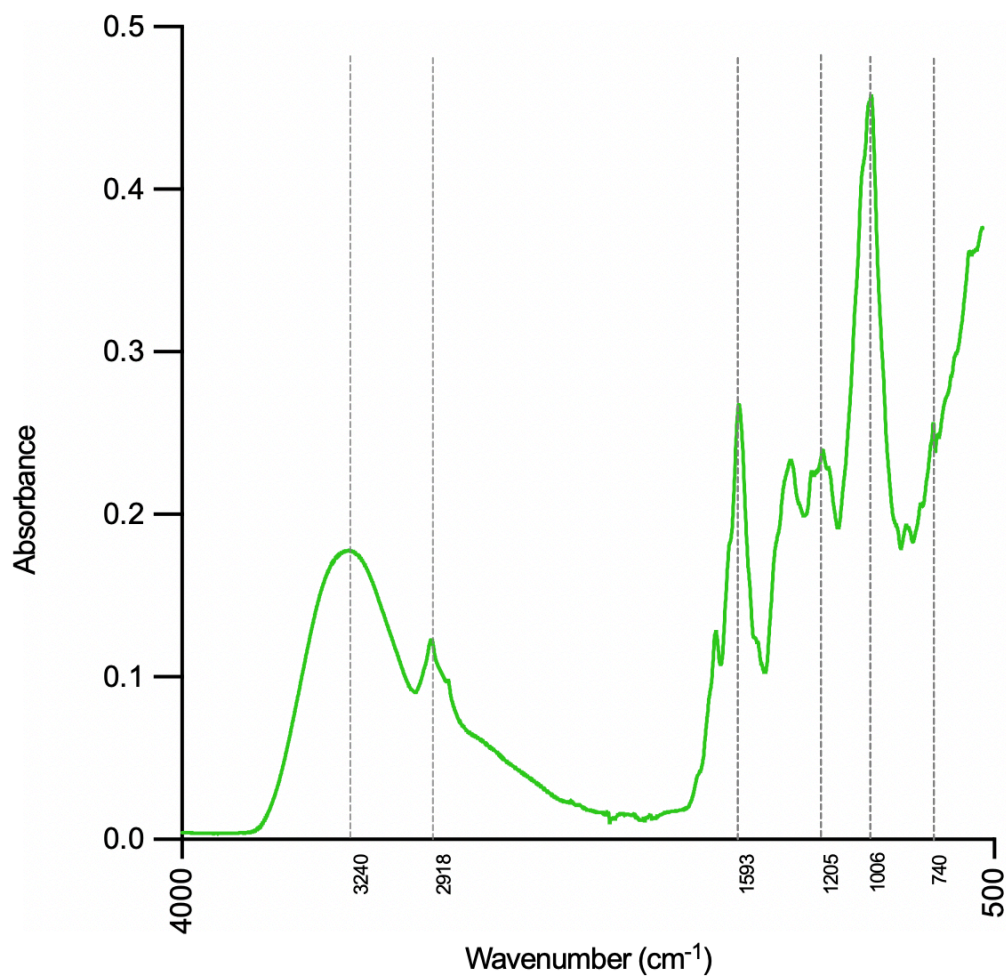


Fig 15: FTIR spectra of coffee biowaste antioxidant extract.

### 4.3 Total phenolic content (TPC) and antioxidant activity evaluation

Total phenolic content (TPC) was reported as the equivalent amount of gallic acid (GAE (mg/mL)) present in the sample. The test was carried out on all the cocoa and coffee extracts obtained with the 20 several combinations of extraction parameters and the results were presented in previously Table 2. The highest gallic acid concentration, 3.04 GAE (mg/mL), was obtained for cocoa extracts when the extraction was carried out at 50°C for 25 min and the amount of sample was of 0.67 g. On the other hand, antioxidants extraction performed at the same temperature for 50 min with 0.34 g of coffee resulted in a lower amount of gallic acid, 1.39 GAE (mg/mL). In general, cocoa extracts were characterized by a higher average concentration of gallic acid, with a rate of  $2.56 \pm 0.24$  GAE (mg/mL) compared to coffee extracts, characterized by  $1.39 \pm 0.23$  GAE (mg/mL).

Once the ultrasound extraction parameters were optimized, final coffee and cocoa antioxidant extracts were obtained, and their total antioxidant activity was evaluated through FRAP method. Results are grouped in Table 5 show how in cocoa extracts a higher antioxidant activity is detected.

Cocoa extract	Coffee extract
996.7 AAE ( $\mu$ M)	980.0 AAE ( $\mu$ M)

Table 5: FRAP assay results in AAE ( $\mu$ M)

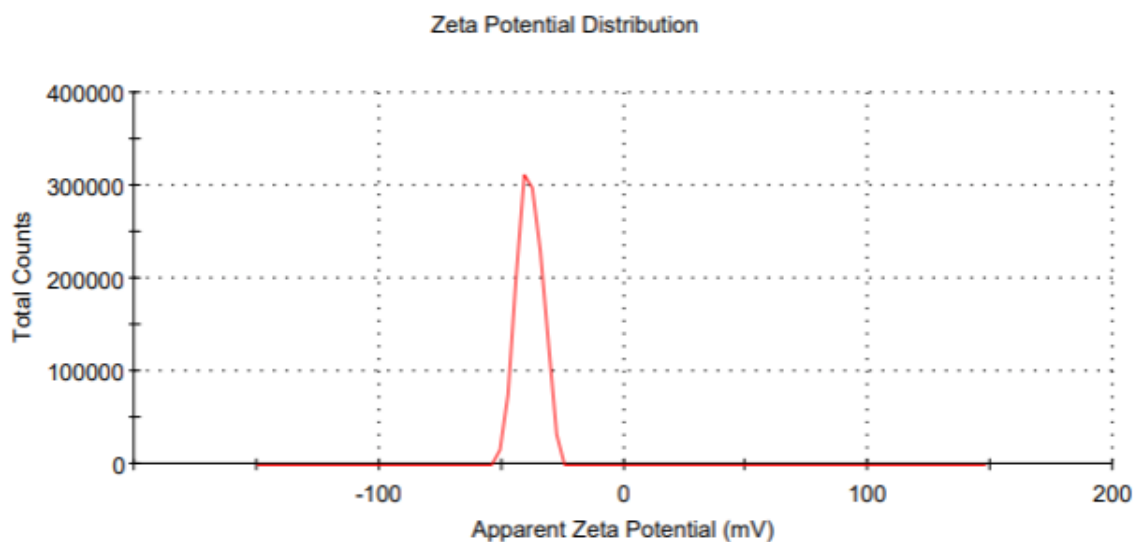
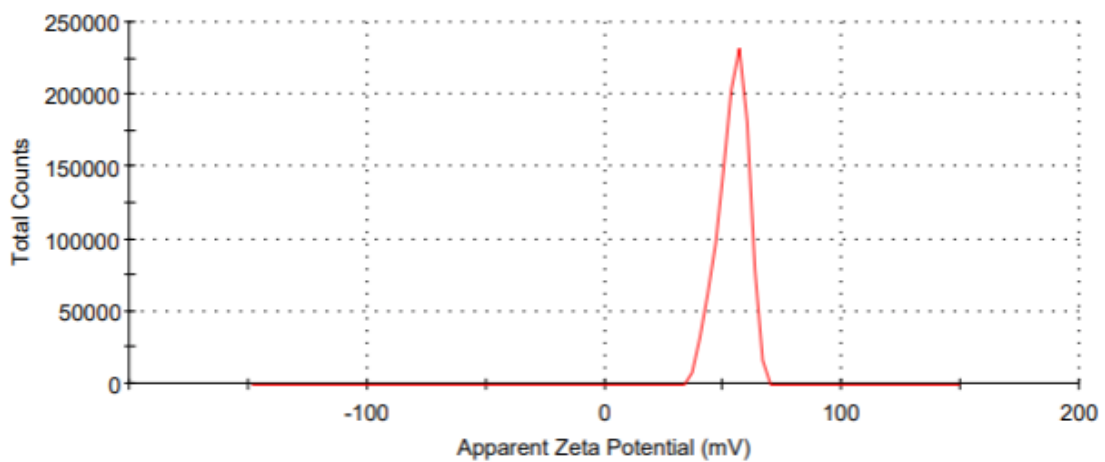
In general, in all previously test conducted on biomass extractions cocoa once exhibited greater antioxidant proprieties then coffee extract. These results confirmed what several studies had founded in literature. For example, Toung at al. reported that both coffee and cocoa had high levels of phenolic compounds, which are known to have antioxidant properties. However, the antioxidant activity of cocoa was found to be higher than that of coffee in most of the assays used [47]. Furthermore, C. Martínez-Cano et al., comparing these two natural materials, showed how both coffee and cocoa extracts increased the antioxidant capacity of plasma, but cocoa may have a more beneficial effect on oxidative stress in the body than coffee [48].

## 4.4 Nanoparticles Characterization

### 4.4.1 Polyelectrolyte solution analysis

Dynamic light scattering (DLS) investigations were performed on pectin, chitosan and antioxidant extracts solutions (Fig x) in order to evaluate the order in layer-by-layer (LBL) deposition.

Results confirm a positive charge for chitosan ( $+40.0 \pm 4.0$  mV) and a negative  $\zeta$ -potential value for pectin solution ( $-39.2 \pm 3.0$  mV). DLS also shown negative charge of both cocoa ( $-20.2 \pm 4.9$  mV) and coffee ( $-13.5 \pm 5.1$  mV) extracts, which were added to pectin solution for that reason.



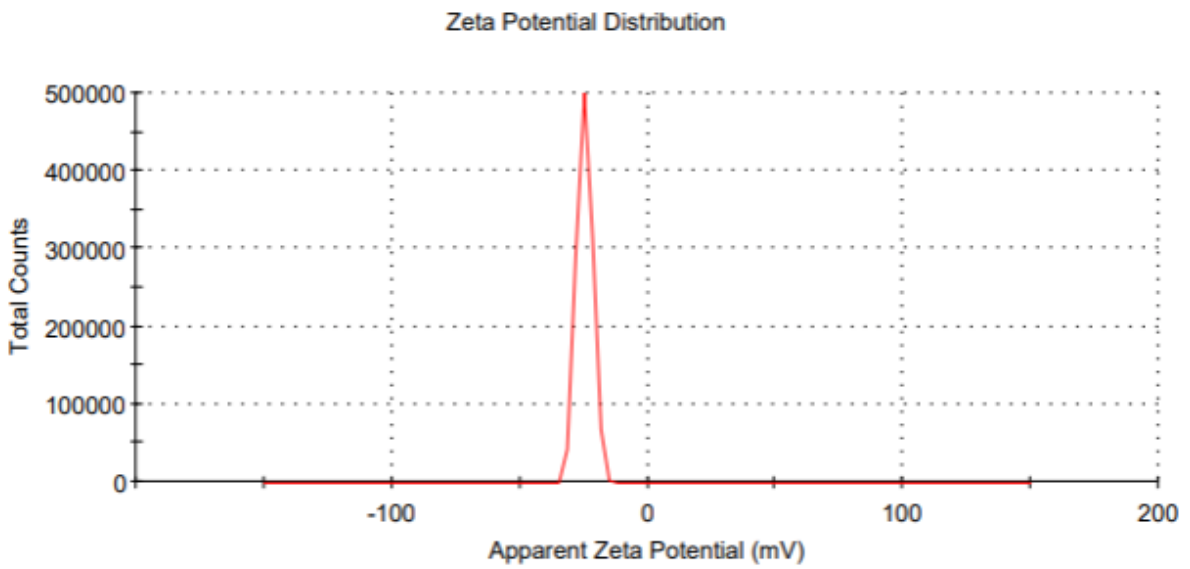
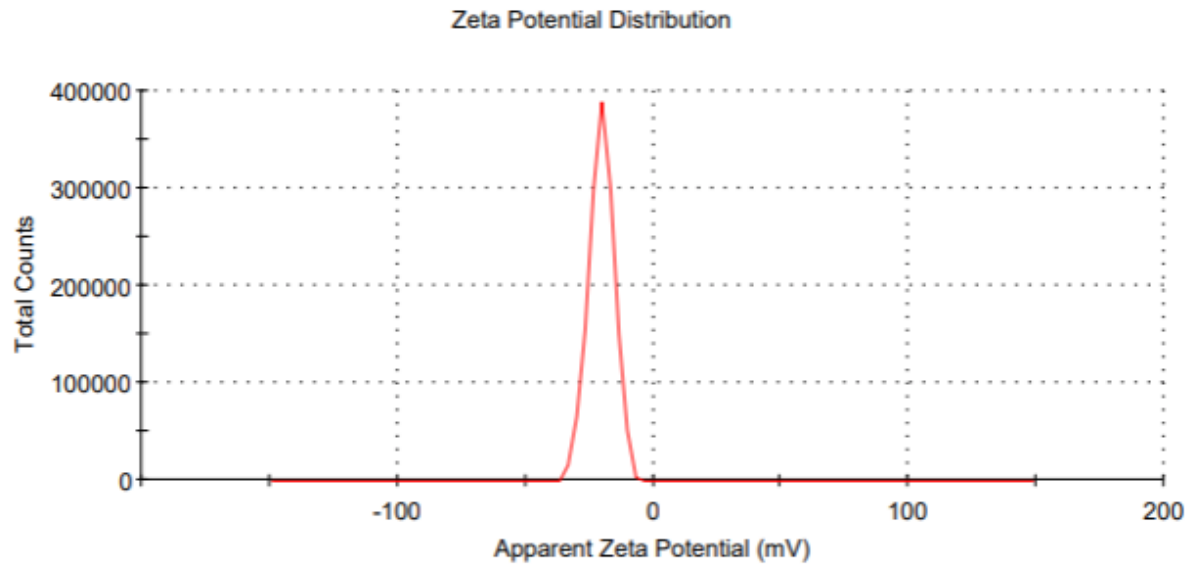


Fig 16: DLS analysis for  $\zeta$ -potential evaluation of polyelectrolyte solutions. a) Chitosan solution, b) Pectin solution, c) Cocoa biowaste antioxidant extract, d) Coffee biowaste antioxidant extract.

Moreover, FTIR-ATR spectra of chitosan and pectin solution was analysed to compare polyelectrolyte chemical composition with molecular structure and composition of final MNPs system.

Chitosan spectrum (Fig.17) present peak around  $3300\text{cm}^{-1}$ , due to the -OH vibration of the hydroxyl groups, and between  $3000\text{-}2850\text{ cm}^{-1}$ , due to C-H stretching. The peak around  $1650\text{ cm}^{-1}$  corresponds to the C=O stretching vibration of the amide carbonyl group, while a similar one at  $1540\text{ cm}^{-1}$  is produced by N-H bending vibration of the amine group. Absorption bands around  $1400\text{ cm}^{-1}$  correspond to  $\text{-CH}_2$  bending vibration, whereas  $\text{CH}_3$  symmetrical deformation produced a peak around  $1370\text{ cm}^{-1}$ . The peak around  $1120\text{ cm}^{-1}$  corresponds to antisymmetric stretch of C-O-C and C-N. Skeletal vibration of C-O stretching usually produced strong bands around  $1000\text{ cm}^{-1}$ [49].

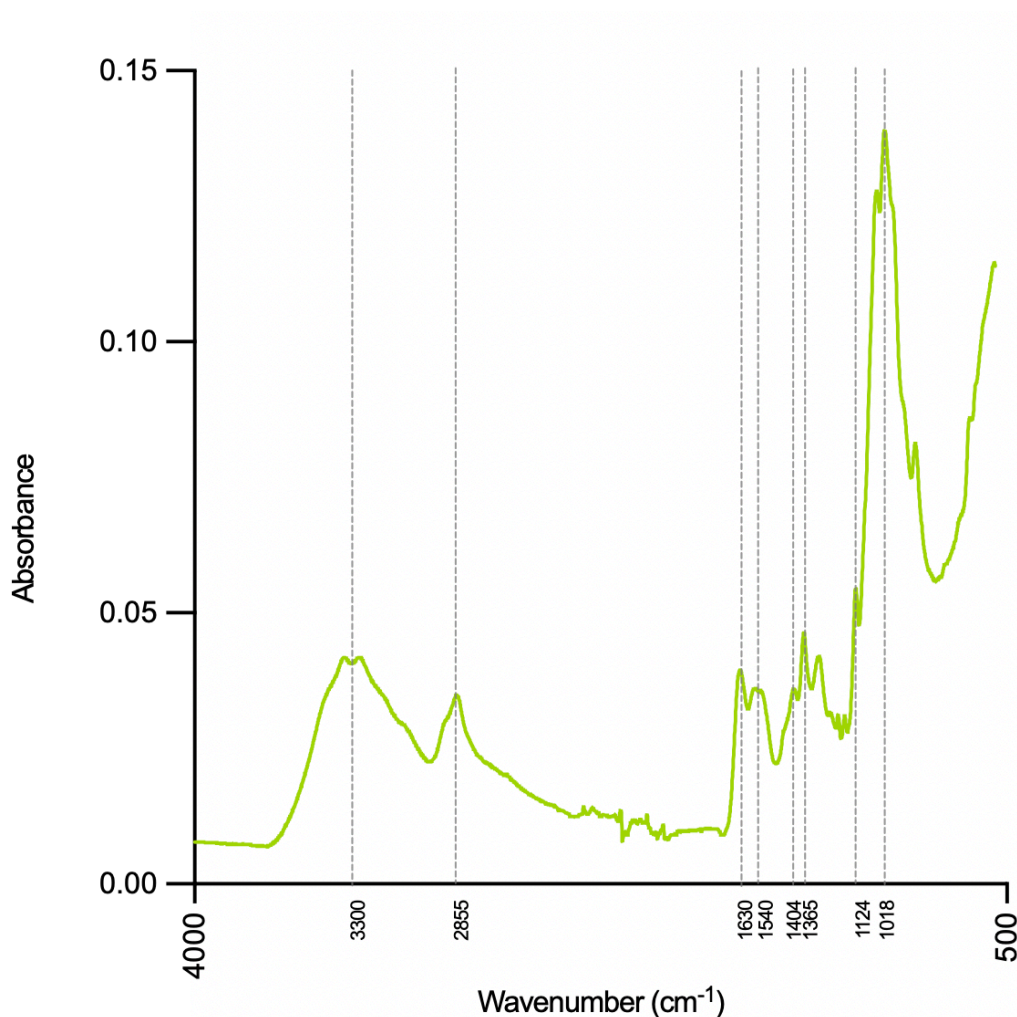


Fig.17: FTIR spectra of Chitosan.

Individual spectral bands for pectin, including the backbone and side group vibration bands, are identified in Fig. x. Pectin spectra shows several peaks around  $3200\text{ cm}^{-1}$  and between  $2900\text{-}2800\text{ cm}^{-1}$ , corresponding, respectively to  $\text{-OH}$  and  $\text{C-H}$  stretching [50]. The bands around  $1500\text{ cm}^{-1}$  correspond to the non-esterified carboxyl groups ( $\text{COO-}$ ) of pectin, while peaks related to the stretching of the  $\text{C-O}$  bond were observed between  $1300$  and  $1000\text{ cm}^{-1}$ . Peak at  $1270\text{ cm}^{-1}$  was due to the cyclic  $\text{C-C}$  bond in the ring structure of pectin. Finally, the region between  $1100\text{-}950\text{ cm}^{-1}$  has been reported for the spectral identification of galacturonic acid in peptide polysaccharides.

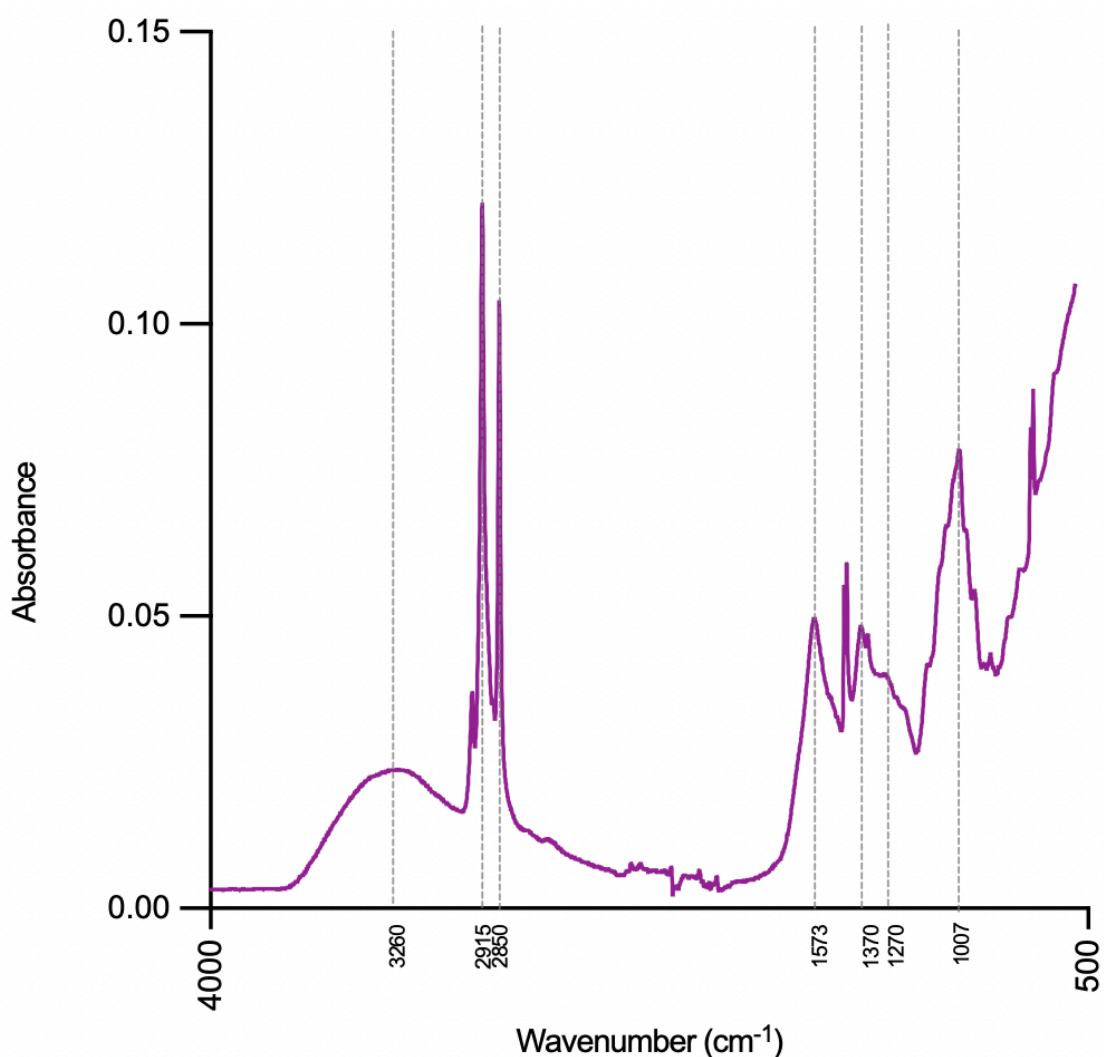


Fig 18: FTIR spectra of Pectin extracted from cocoa biowaste.

#### 4.4.2 $\zeta$ -potential measurement

DLS was then performed on silica mesopores nanoparticles (MNPs) to evaluate which polyelectrolyte solution had to be deposited first. Since MNPs shown a negative charge ( $-30.3 \pm 2.4$  mV) (Fig 19), polycation CH solution was used for the first layer deposition. Zeta potential measurements were also used to confirm appropriate charge of each deposited layer as shown in Figure 20.

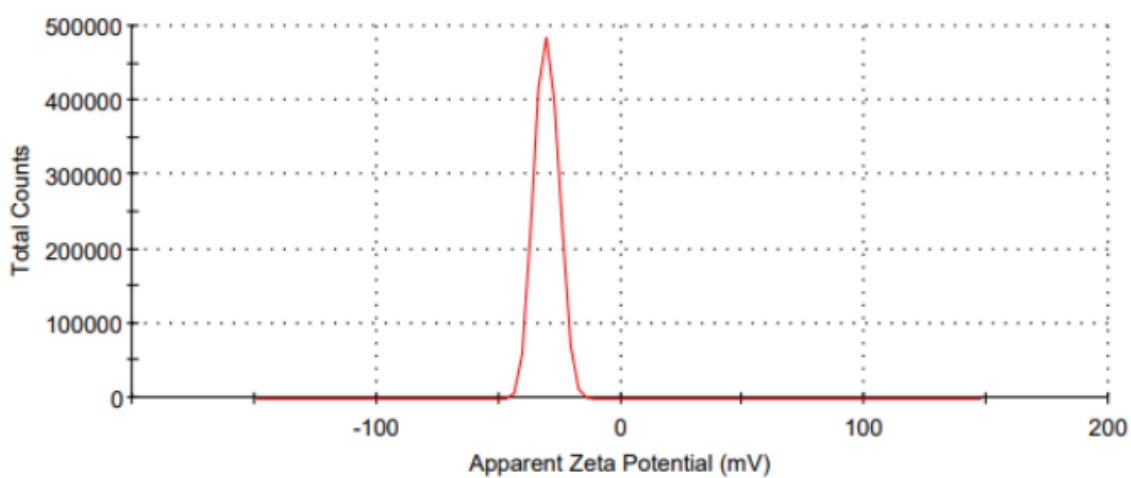
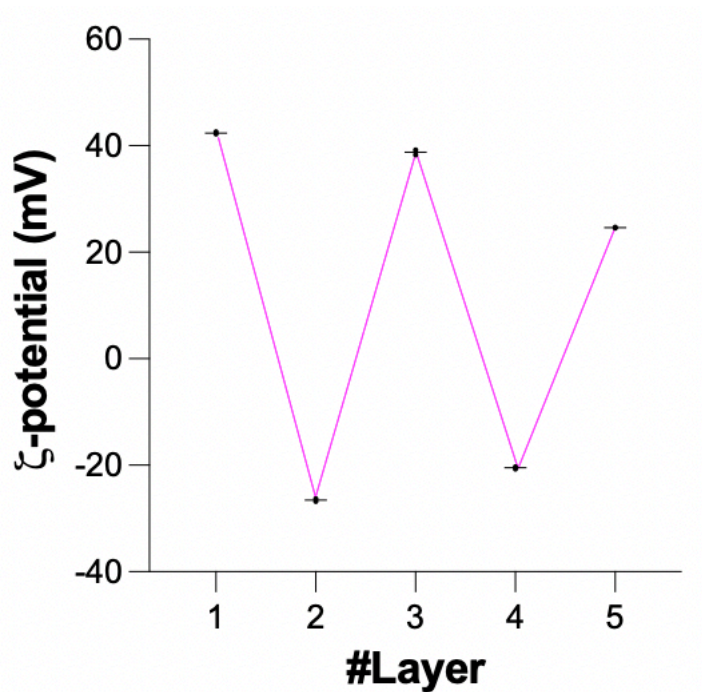


Fig 19. DLS analysis for  $\zeta$ -potential evaluation of MNPs purchased from sigma.

a)



b)

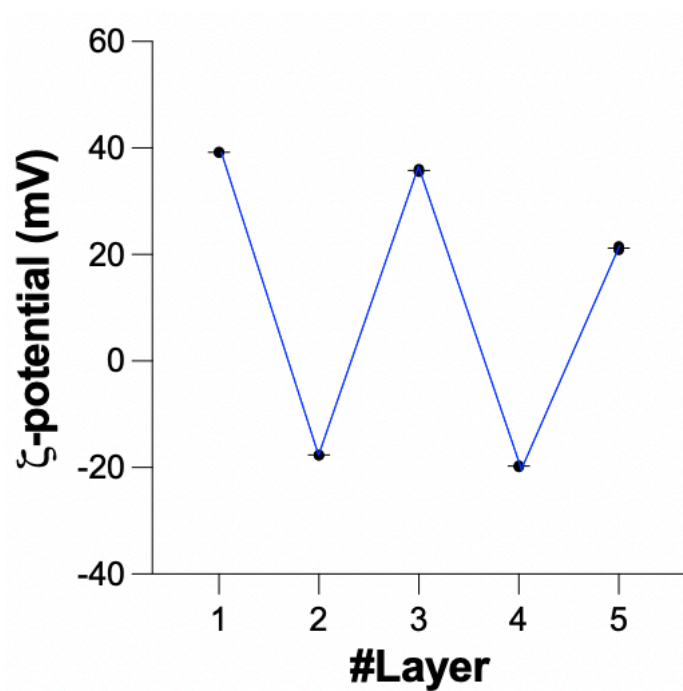
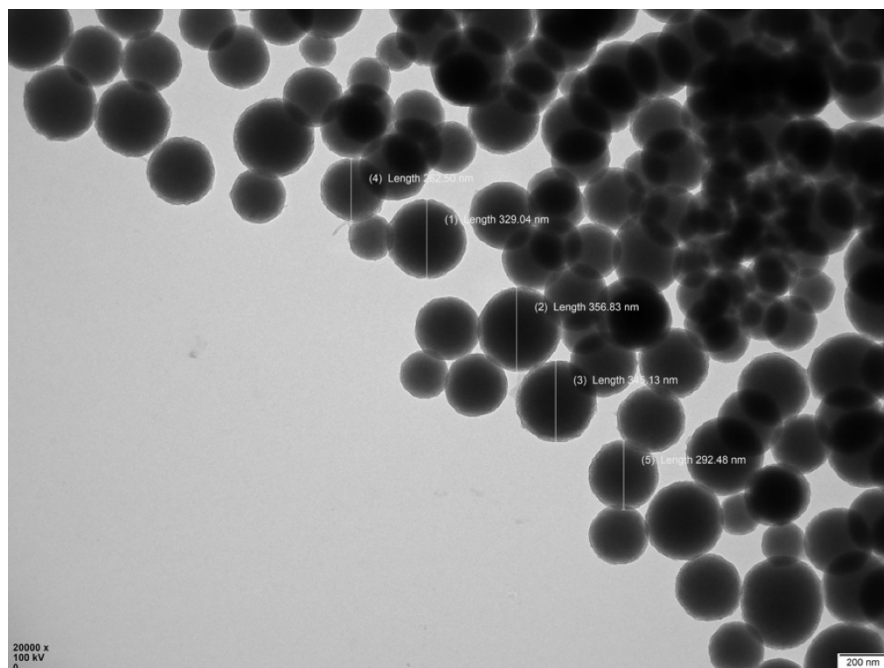
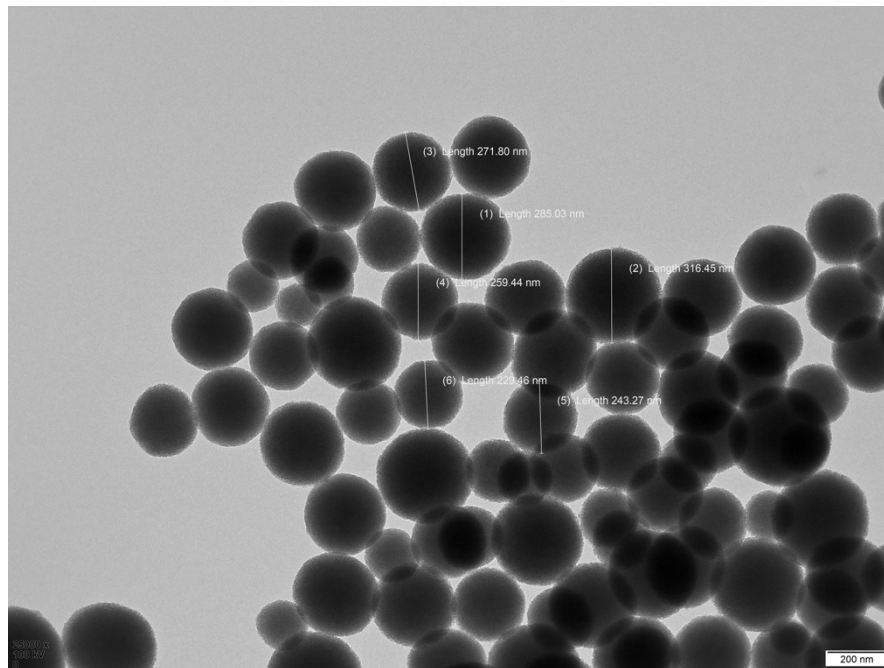


Fig 19: DLS analysis for  $\zeta$ -potential evaluation of each deposited layers. a) Layer-by-Layer functionalized MNPs with cocoa extract, b) Layer-by-Layer functionalized MNPs with coffee extract.

### 4.4.3 Morphology analysis

High-resolution TEM images performed on nanoparticles purchased from sigma and functionalized MNPs after each layer deposition are reported in Fig. 21(a-d). Results confirm that spherical shape is preserved after LbL deposition and show an increase in functionalized nanoparticles diameter compared to silica one.



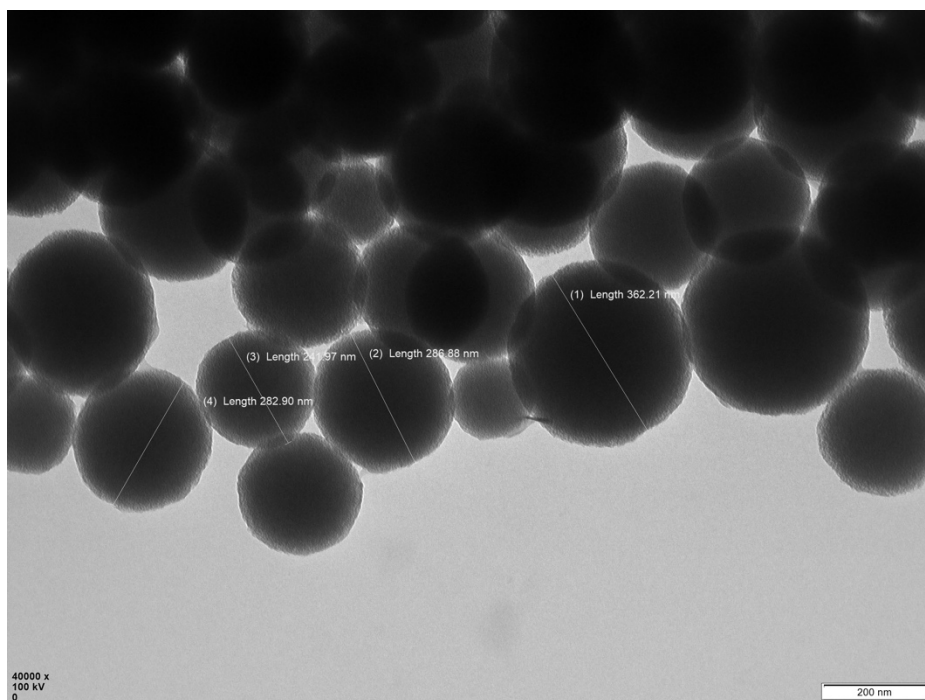
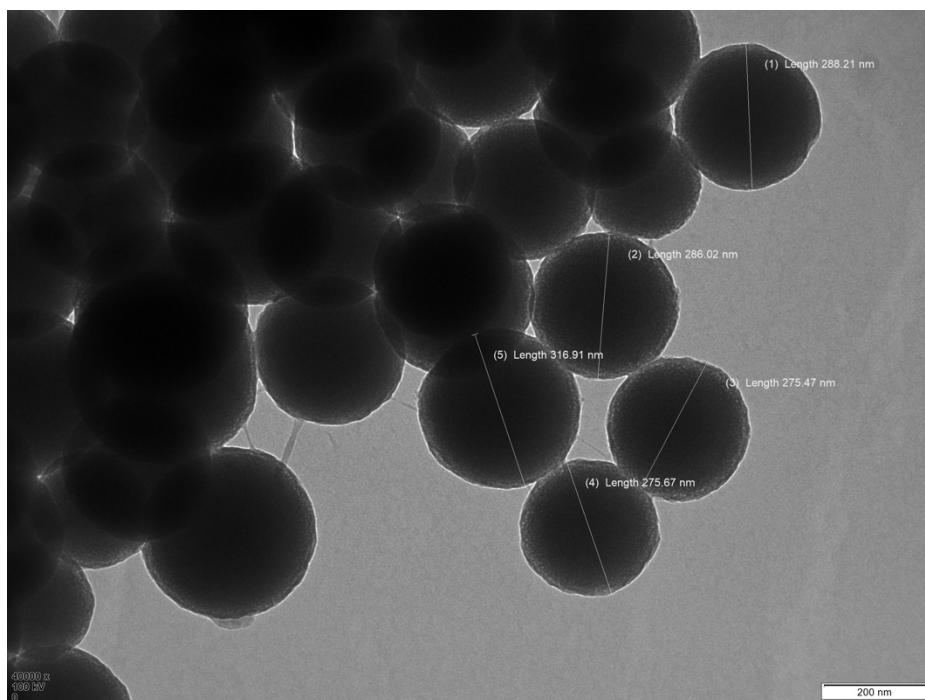


Fig.20: TEM analysis for morphological characterization of silica nanoparticles. a) MNPs purchased from sigma, b) MNPs control system without the use of cocoa and coffee extracts in polyelectrolyte solutions, c) Layer-by-Layer cocoa functionalized MNPs, d) Layer-by-Layer coffee functionalized MNPs.

#### 4.4.4 Chemical composition

FTIR\_ATR analyses were conducted on MNPs and after each layer deposition to evaluate the correct ongoing of LbL technique. Analysis was conducted also on a control system in which antioxidant extracts were not loaded onto pectin solution.

The specific spectrum of silica mesoporous nanoparticles may vary depending on the synthesis method used, the size and shape of the nanoparticles, in this case (Fig 21) one of the most prominent peaks is the stretching vibration of the Si-O bond in the region of 1000-1200  $\text{cm}^{-1}$ . The peaks at 3005  $\text{cm}^{-1}$  were assigned to the stretching and bending vibration of hydroxyl and water. Additional peaks in the range of 500-800  $\text{cm}^{-1}$  corresponding to the bending and stretching modes of the Si-OH bonds on the surface of the mesoporous silica nanoparticles, in particular symmetric stretching and bending vibration of Si-O-Si. On the contrary, bond in the range of 950-1100  $\text{cm}^{-1}$  corresponding to asymmetric stretching of Si-O-Si and symmetric stretching of Si-OH. [50]

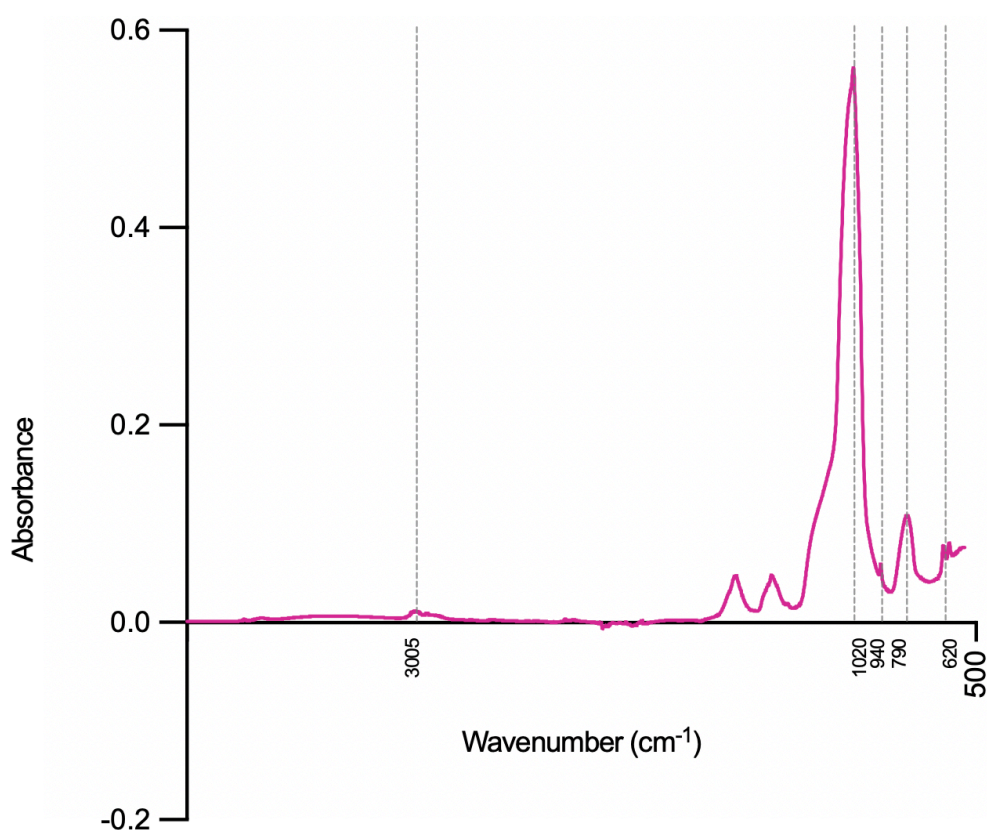


Fig 21: FTIR spectra of silica mesoporous nanoparticles purchased from sigma.

MNPs control system spectrum is report in Fig 22. and compared with silica nanoparticles from sigma, chitosan and pectin one. MNPs control FTIR-ATR spectrum presented a peak (1) around  $3330\text{ cm}^{-1}$ , corresponding to -OH stretching, as chitosan and pectin, while the bands (2) around  $3005\text{ cm}^{-1}$ , correspond to the stretching and bending vibration of hydroxyl and water in MNPs system. Moreover, peaks at (3)  $1630\text{ cm}^{-1}$  and (4)  $1370\text{ cm}^{-1}$  are related to C=O stretching vibration of the chitosan amide carbonyl group, and to the stretching of the pectin C-O bond. The specific spectrum of silica mesoporous nanoparticles, also show a peak (5) around  $1020\text{ cm}^{-1}$  and (6)  $790\text{ cm}^{-1}$  as MNPs control sample, that confirmed the presence of silica in the LbL system.

Furthermore, MNPs systems obtained from cocoa and coffee were analyzed through FTIR-ATR in order to directly compare their spectra with MNPs system control one (Fig 23).

MNPs coffee spectra shows a peak (1) around  $1205\text{ cm}^{-1}$  and between  $900\text{--}600\text{ cm}^{-1}$  (3) which confirm the presence of coffee. On the other hand, MNPs cocoa spectra presents bands at (2)  $\text{cm}^{-1}$  and around (4)  $900\text{--}600\text{ cm}^{-1}$  which confirm the presence of coffee in the sample.

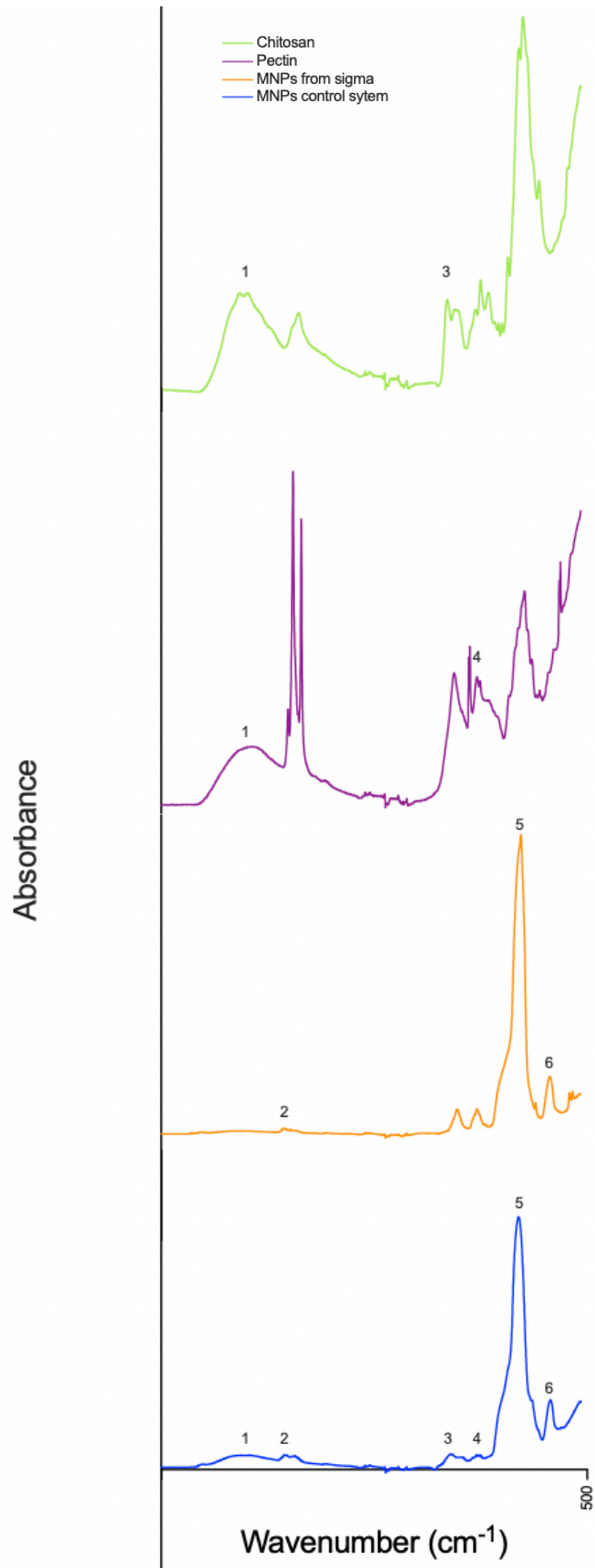


Fig 22: FTIR spectra comparison between chitosan, pectin, MNPs and MNPs control system.

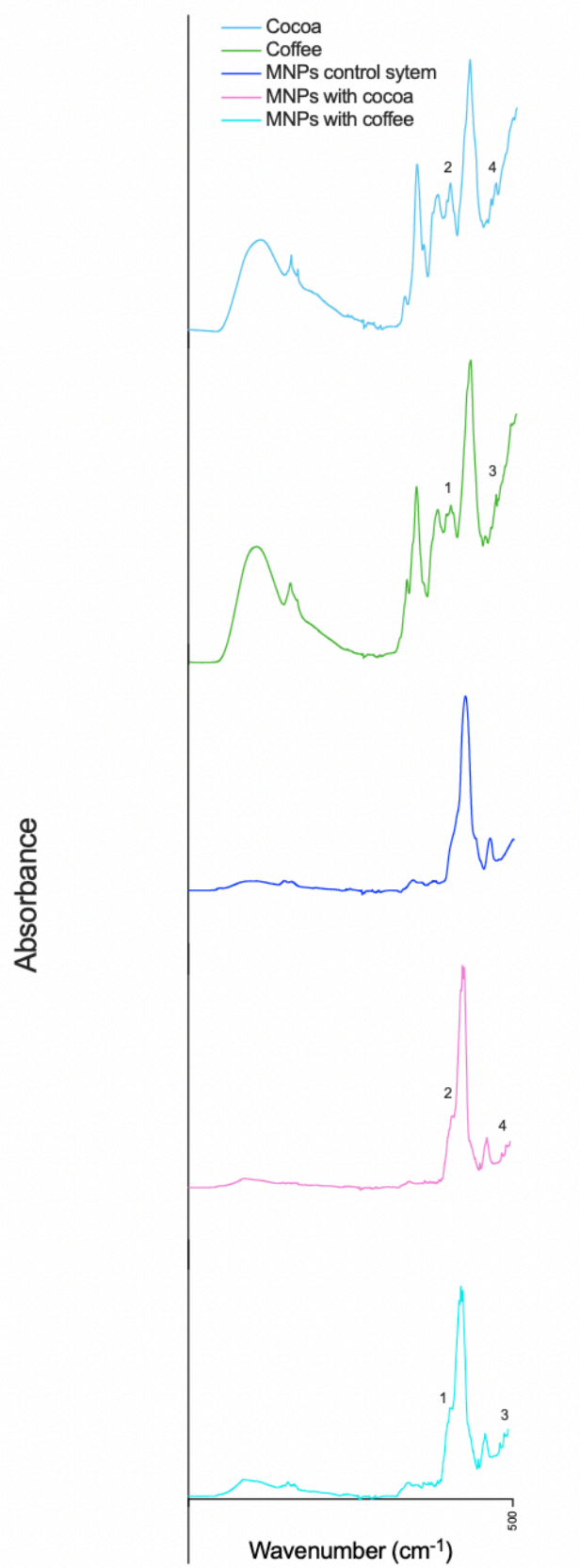


Fig 23: FTIR spectra comparison between biowaste extracts, MNPs control system and engineered MNPs

Nanoparticles from Sigma-Aldrich (Fig 24) and MNPs control samples were directly compared with XPS readings to validate the composition of these structures obtained by FTIR-ATR.

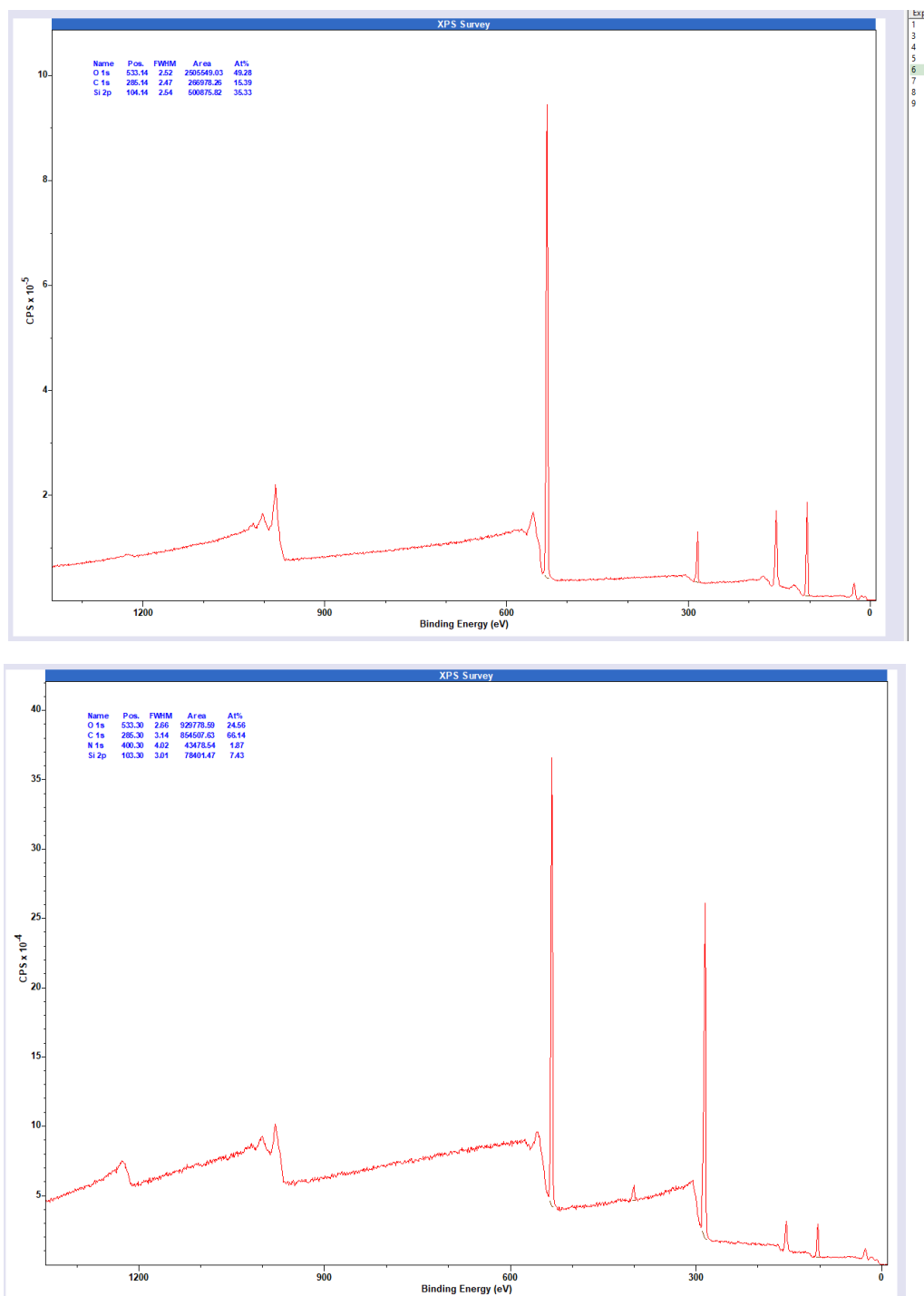


Fig 24: XPS spectra. a) MNPs purchased from sigma, b) MNPs control system.

XPS spectra of both samples show a peak around 103 eV corresponding to the Si2p signal, confirming the presence of silica in both systems. In addition peaks corresponding to carbon and oxygen are present around 285 eV and 533 eV, respectively, in both samples. In particular, in MNPs control system (Fig 25) investigating C1s peak, the presence of C-C and C-O peaks confirmed the presence of pectin in the functionalized system. Moreover, MNPs control XPS spectra presents N1s peak around 400 eV, confirming the presence of chitosan.

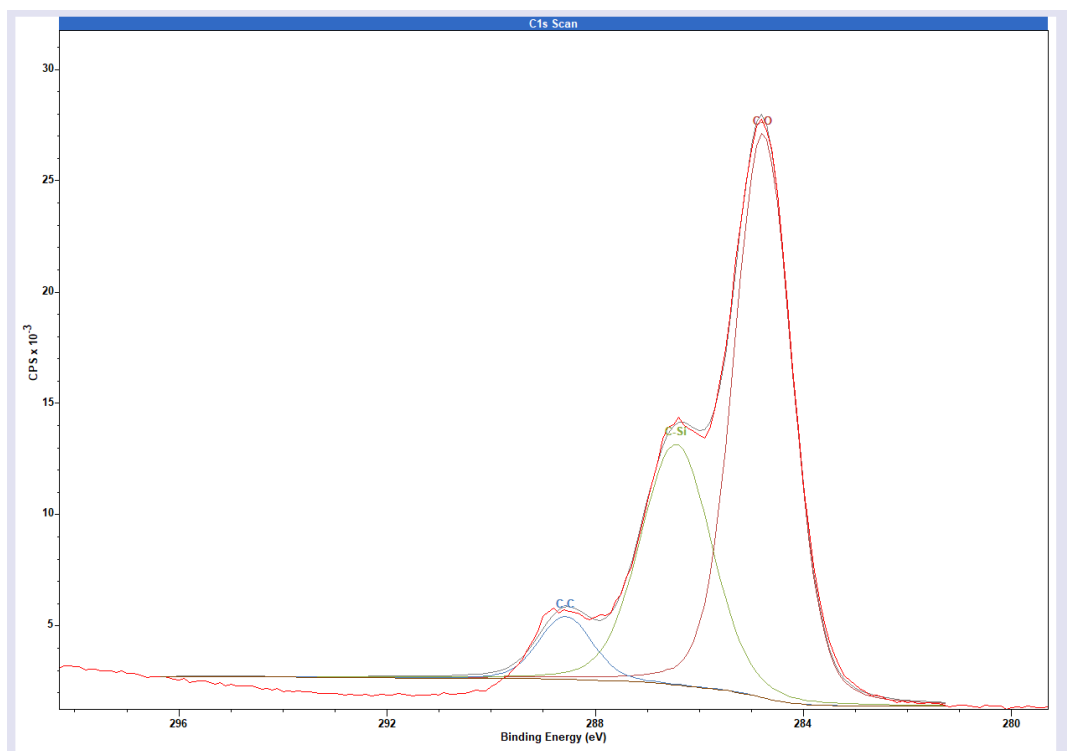


Fig 25: XPS spectra of deconvoluted C1s peak of MNPs control system.

Moreover, MNPs from cocoa and coffee extracts were analyzed at XPS and results, reported in Fig 26, show same spectra for both samples. In particular, peaks corresponding to O1s, C1s, N1s and Si2p are present respectively around 533 eV, 286 eV, 400 eV and 103 eV, confirming FTIR-ATR results.

Focusing on C1s peak, in both samples the presence of C-C and C-O peaks confirmed the presence of pectin and antioxidants extract in the functionalized system.

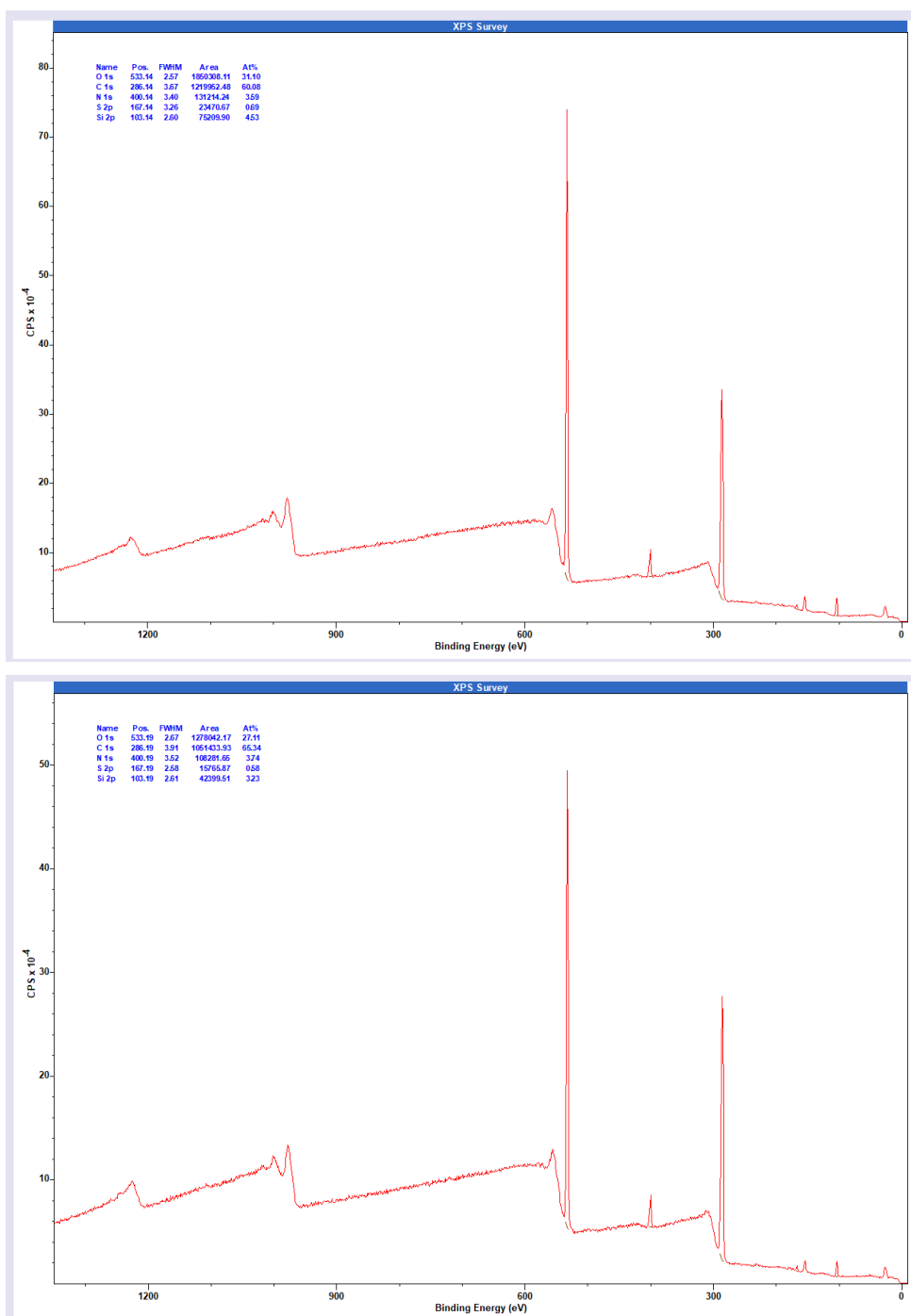


Fig 26: XPS spectra. a) MNPs functionalized with cocoa extract, b) MNPs functionalized with coffee extract.

## 4.5 Cytotoxicity Evaluation

### 4.5.1 Live and Dead assay

Live and dead assay was conducted on cells in the two-dimensional model to evaluate cells viability at different concentrations of antioxidant extracts and MNPs (100, 250, 500, 1000  $\mu\text{g/mL}$ ). Neo-dermal fibroblast cells without any treatment were used as a control. All the samples were incubated for 48h. Results are represented in fig. 27-.

In Fig. 27, live and dead images of Neo-dermal fibroblast after 48h of incubation without treatment were reported, showing proliferated and elongated cells.

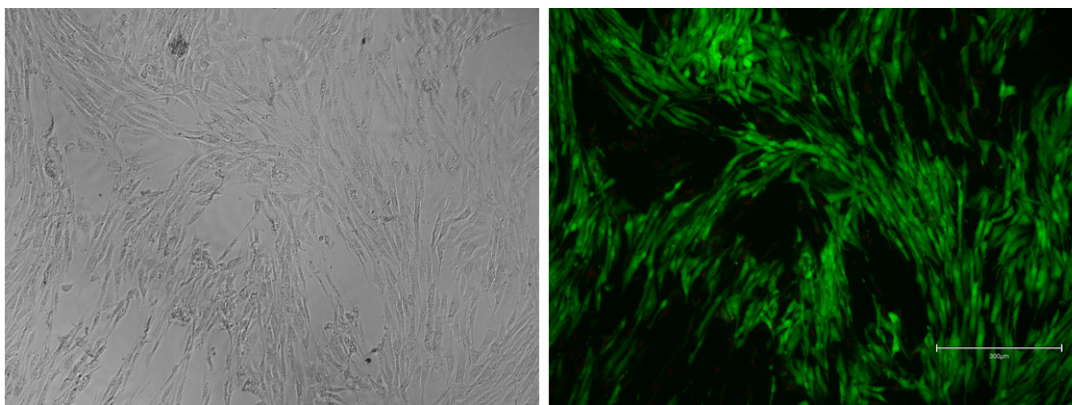


Fig 27. Live and Dead assay conducted on Neo-dermal fibroblast without any treatment. Bar=300 $\mu\text{m}$

Four different concentrations of cocoa extract were incubated, and results reported in Figure 28.

Marked cell death for all the samples resulted in a very inconsistent number, compared to the alive ones, indicating low apoptotic activity of cocoa extract. Considering the number of cells and their morphology, it seemed that they remained constant for all the concentrations tested, with a little variation in the last sample. The observed change resulted, indeed, in a few numbers and less elongated fibroblast where cells were incubated with the highest concentration of antioxidant extract.

Antioxidant coffee extract was tested at the same time and concentrations of cocoa one. Results, reported in Fig 29, were shown a very small number of red cells indicating low apoptotic activity of coffee extract, as reported for cocoa case. Comparing coffee samples with cocoa ones, they showed the same trend.

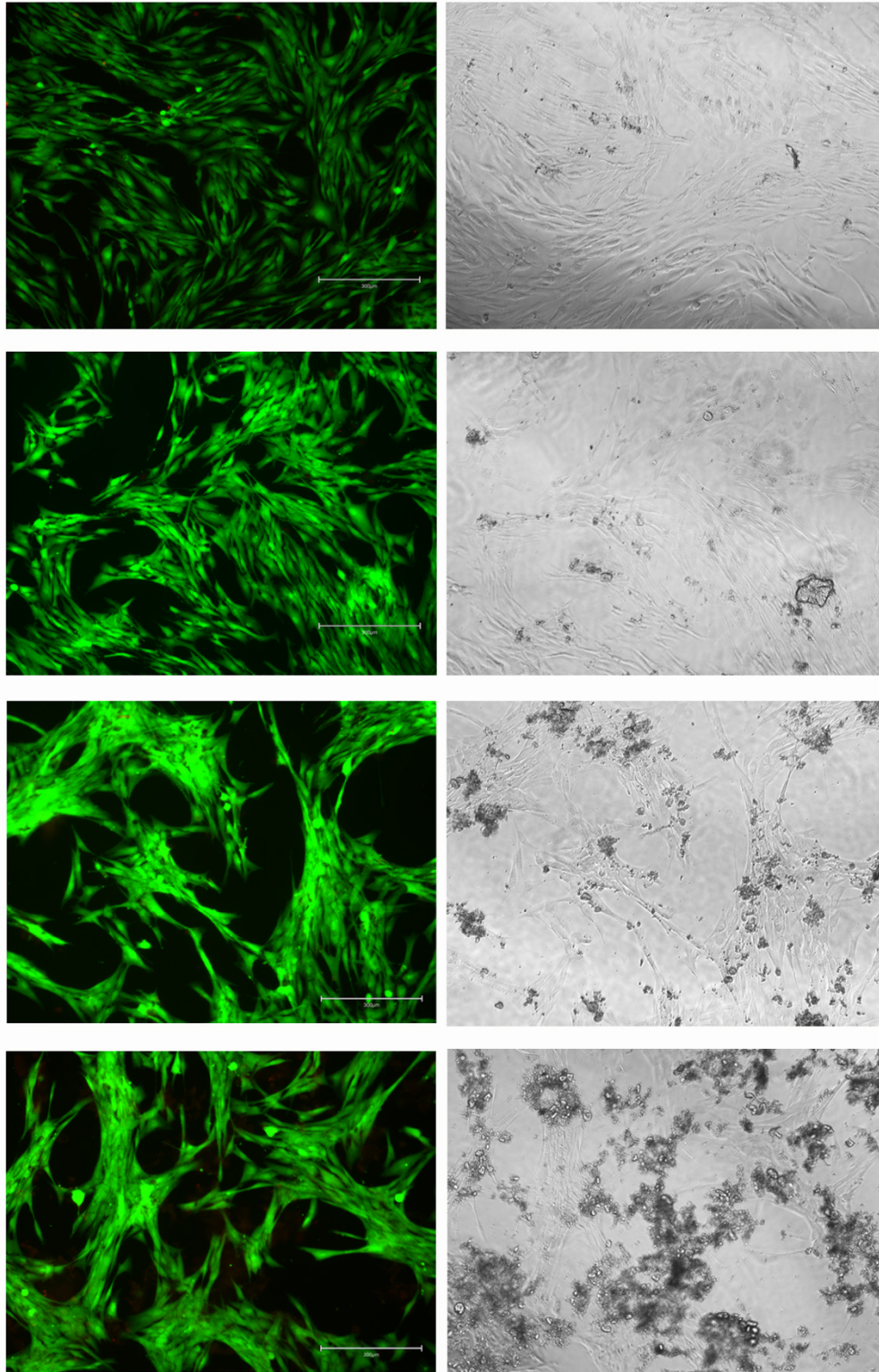


Fig 28: Live and Dead assay with four different concentrations of cocoa extract: a) 100 µg/mL, b) 250 µg/mL, c) 500 µg/mL, d) 1000 µg/mL. Bar=300µm

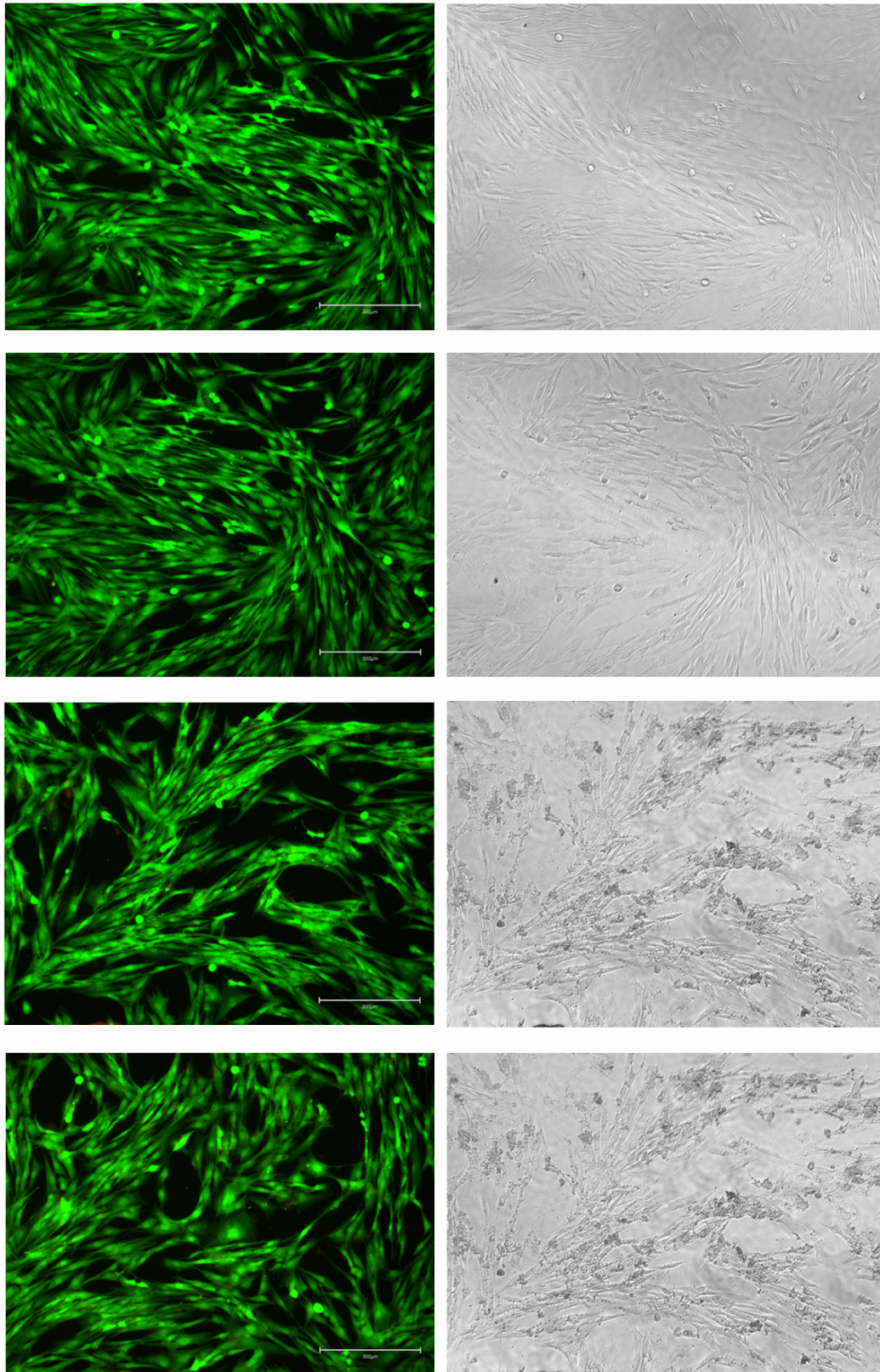


Fig 29: Live and Dead assay with four different concentrations of coffee extract: a) 100 µg/mL, b) 250 µg/mL, c) 500 µg/mL, d) 1000 µg/mL. Bar=300µm

Live and dead assay was then performed on MNPs samples, including nanoparticles from sigma and mesoporous LbL functionalized systems.

Figure 30 show live and dead results in MNPs from Sigma- Aldrich samples where marked cell death resulted in a very inconsistent number, compared to the alive ones, indicating low apoptotic activity of mesoporous nanoparticles purchased from Sigma- Aldrich. Considering the number of cells and their morphology, it seemed that they remained constant for all the concentrations tested, with a little reduction in the total number of fibroblasts where the sample in much concentrated.

MNPs functionalized with cocoa extract were tested and results reported in Fig 31. This LbL system exhibited a very low apoptotic activity against cells as the inconsistent number of death cells marked as showed in all the samples. Total amount of cells and their morphological shape seemed that remained constant for all different concentrations of samples, even if comparing the lowest concentrated well with the highest one, resulting in a reduced number of fibroblasts.

Live and dead results of MNPs obtained from coffee extract were grouped in Fig 32. and showed the same general trend of other samples.

Comparing all the previously results it seemed that cells incubated with free cocoa and coffee extract resulted in a higher number then samples with nanoparticles purchased from sigma and LbL functionalized MNPs. No significant difference in the fluorescence intensity and in cells morphological shape were detected evaluating the results.

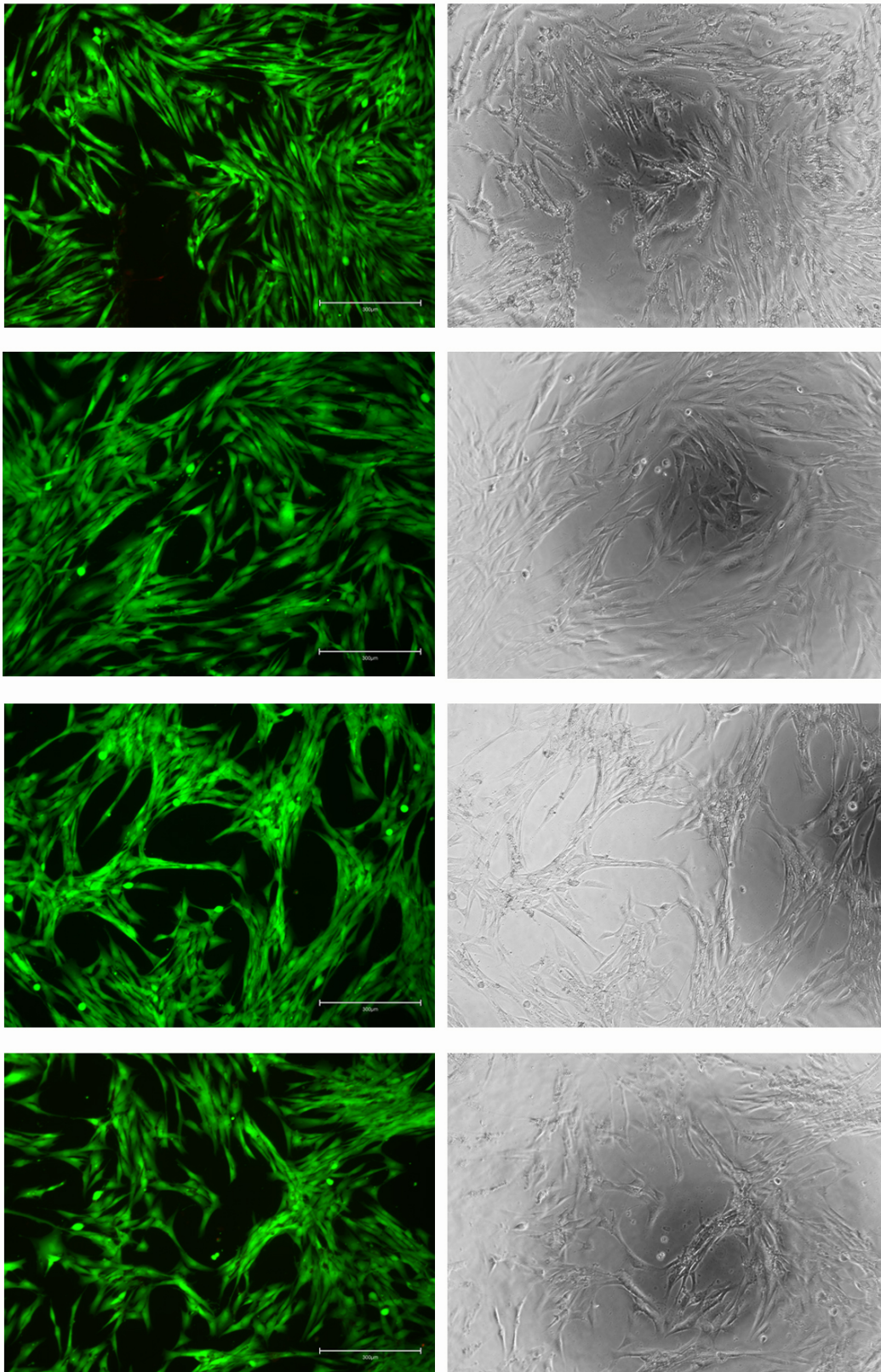


Fig 30: Live and Dead assay with four different concentrations of MNPs purchased from sigma: a) 100 µg/mL, b) 250 µg/mL, c) 500 µg/mL, d) 1000 µg/mL. Bar=300µm

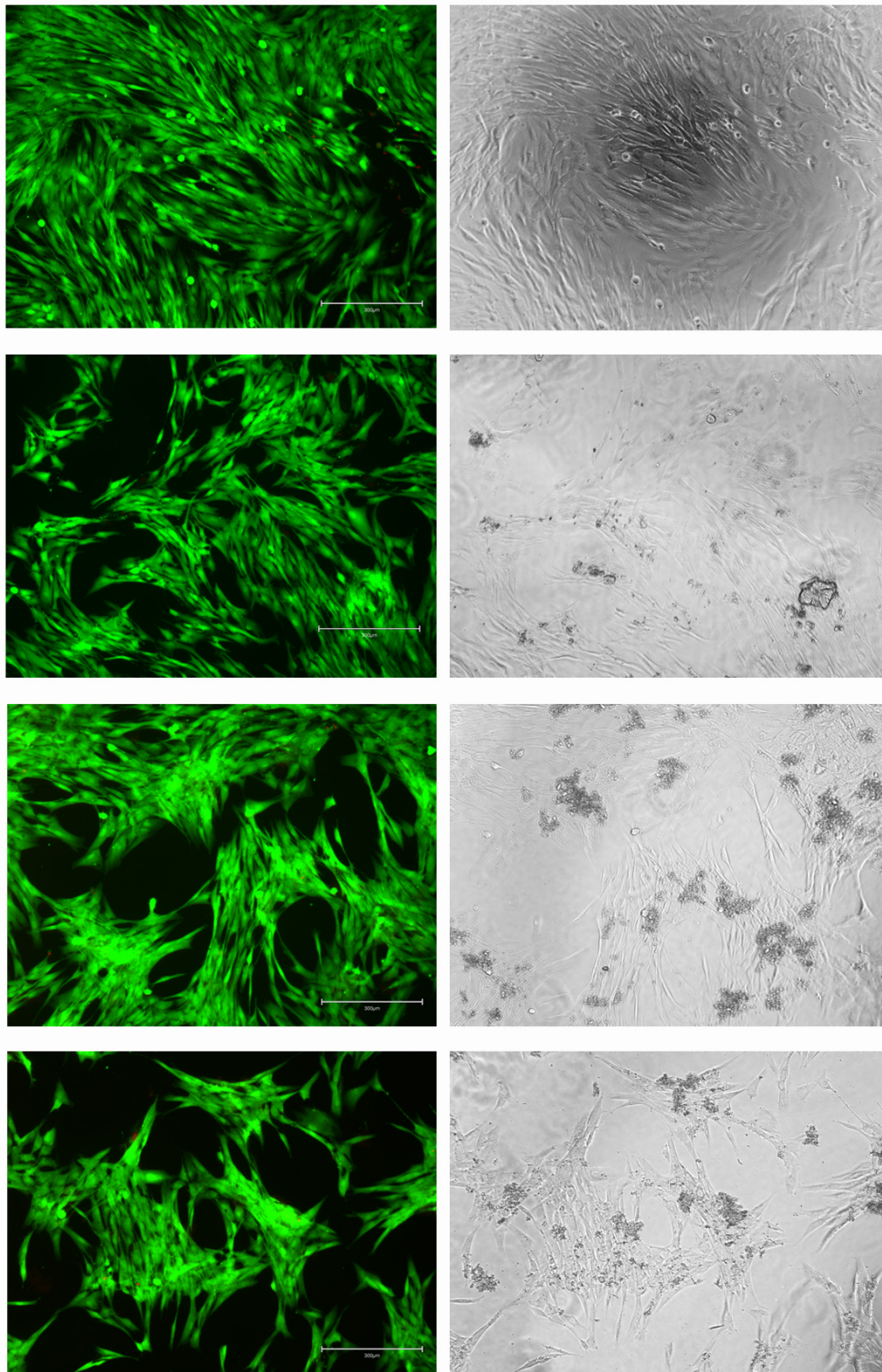


Fig 31: Live and Dead assay with four different concentrations of MNPs functionalized with cocoa extract: a) 100  $\mu\text{g/mL}$ , b) 250  $\mu\text{g/mL}$ , c) 500  $\mu\text{g/mL}$ , d) 1000  $\mu\text{g/mL}$ . Bar=300 $\mu\text{m}$

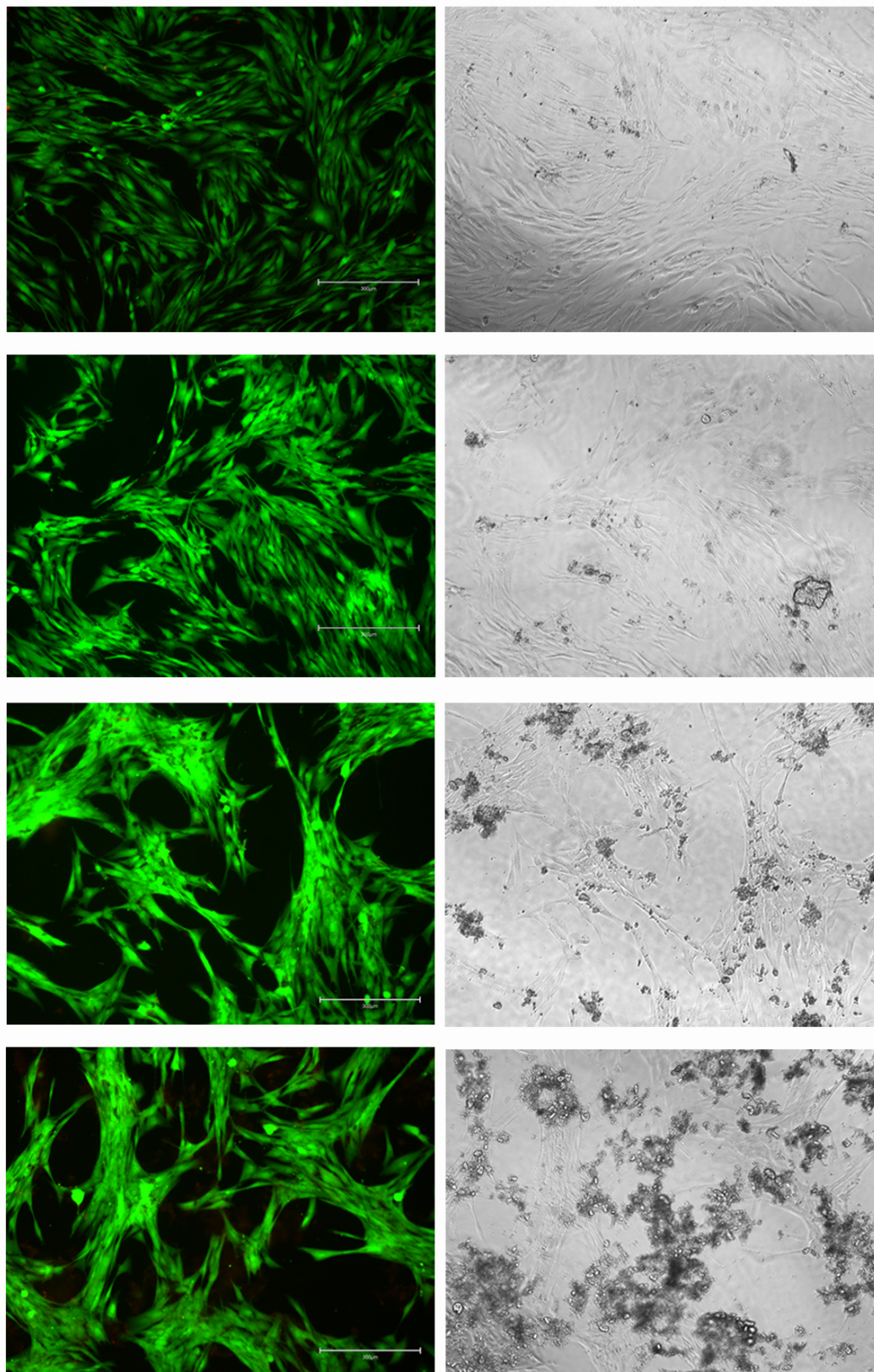


Fig 32. Live and Dead assay with four different concentrations of MNPs functionalized with coffee extract: a) 100 µg/mL, b) 250 µg/mL, c) 500 µg/mL, d) 1000 µg/mL. Bar=300µm

#### 4.5.2 PrestoBlue assay

PrestoBlue assay was conducted to evaluate cell metabolic activity after treatment with different concentrations of antioxidant extracts and MNPs (100, 250, 500, 1000 µg/mL). Following 48h of incubation, metabolic activity was reported in terms of fluorescence values of PrestoBlue solution and normalized considering the negative control (i.e., fibroblast cultured in DMEM). Results were reported in Figure 33.

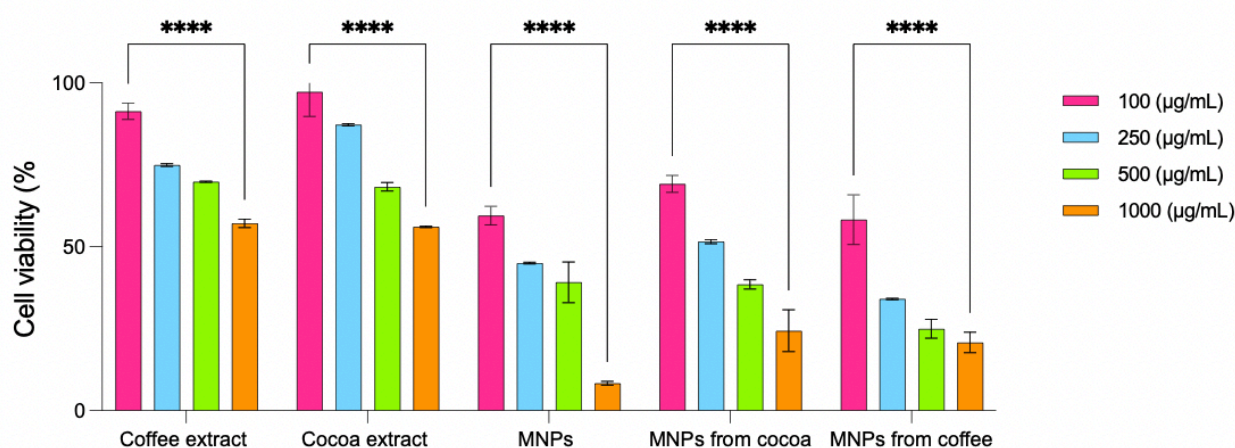


Fig 33. Cell viability results obtained by incubating Neo-dermal fibroblast with different MNPs, cocoa and coffee extract samples concentration.

Results in Fig. 33, had demonstrated that lower samples concentration resulted in a higher fibroblast viability independently from the type of engineered systems considered, confirming previously live and dead analysis. In particular, highest cell viability was obtained in lower concentrated samples incubated with free cocoa and coffee extracts, 96% and 90 % respectively; while exposure of fibroblast cells to highest concentrated silica nanoparticles samples, resulted in the lowest cell metabolic activity, around 60%.

It is important to note that the relationship between cell viability and samples type and concentration is complex and can depend on many factors. Numerous studies had confirmed that it is difficult to make broad statements about the relationship between silica nanoparticle and cytotoxicity without considering multiple factors as their size, charge and concentration. In-Yong Kim et al., studied the effects of silica nanoparticle exposure on NIH/3T3 fibroblasts, founding that cell showed size and dose dependent reductions in viability at doses  $\geq 50$  µg/mL. In particular, 100-200 nm silica nanoparticles were more toxic than the same dose of smaller diameter particles after 24h exposure [51]. Moreover, according to Shengchang et al., high dosages of silica nanoparticles were more toxic to normal human fibroblast cells than to

cancer cells and their cytotoxic effects were significantly reduced by synthesizing the nanoparticles with chitosan [52]. In general, samples incubated with lower concentration of manufactured MNPs resulted in a good compatibility, 69% for cocoa extract and 58% for coffee case, due to their LbL functionalization with antioxidant compounds.

#### 4.6 Fluorescence assay for Intracellular ROS generation

The 2',7'-dichlorofluorescein diacetate (DCFDA) fluorescence assay was used to qualitatively characterize H<sub>2</sub>O<sub>2</sub>-induced intracellular ROS generation, to evaluate coffee and cocoa extracts antioxidant behavior. Fibroblast cells were incubated for 24 h with different concentrations of antioxidant extracts, then a 150 μM H<sub>2</sub>O<sub>2</sub> solution was added to each well. As positive control cells incubated with DMEM was used, while fibroblast cells without any treatment were used as negative control. To evaluate extracts and LbL antioxidant behavior also resveratrol was used as control. Intracellular ROS generation was both examined under a fluorescence microscope and measured on a microplate reader.

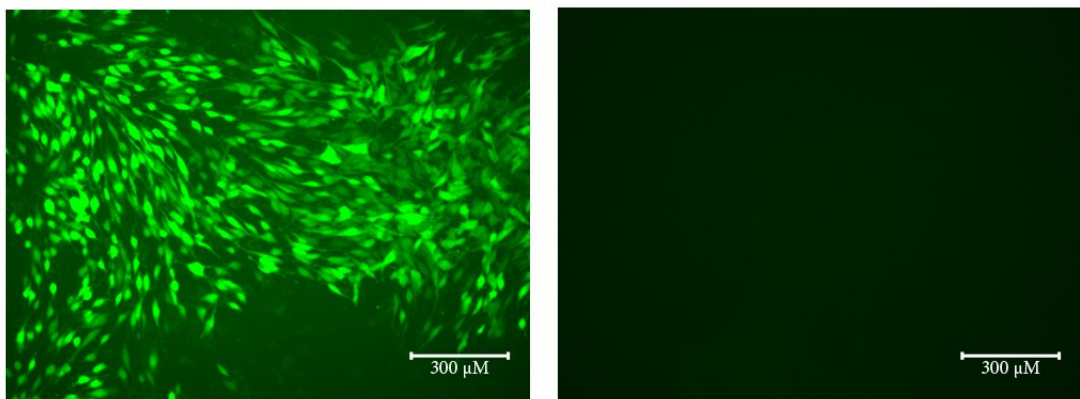


Fig 34: Repressive effect of antioxidant extracts and manufactured MNPs on H<sub>2</sub>O<sub>2</sub>-induced intracellular oxidative stress Neo-dermal fibroblast. a) negative control, b) positive control. Bar=300μm

As shown in Fig. 34a-b, ROS levels were markedly higher in H<sub>2</sub>O<sub>2</sub>-exposed fibroblasts than in positive control cell. In Fig. 35(1-4) H<sub>2</sub>O<sub>2</sub>-exposed fibroblasts were treated with different concentration of resveratrol solution (10, 50, 100, 500 μM, respectively). Images had shown a clearly weaker fluorescence intensity in sample where resveratrol is more concentrated, confirming its repressive effect on H<sub>2</sub>O<sub>2</sub>-induced intracellular oxidative stress.

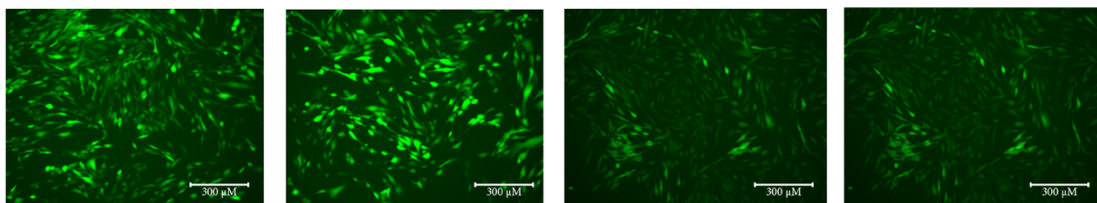


Fig 35: Repressive effect of antioxidant extracts and manufactured MNPs on H<sub>2</sub>O<sub>2</sub>-induced intracellular oxidative stress Neo-dermal fibroblast. c) treatment with resveratrol solution: c1- 10μM, c2- 50μM, c3- 100μM, c4- 550μM. Bar=300μm

Fig. 36-37(1-4) reported H<sub>2</sub>O<sub>2</sub>- induced intracellular oxidative stress levels in cells treated with cocoa and coffee extract, respectively. Fluorescence intensity resulted in the same trend of resveratrol case, confirming antioxidant activity of biowaste extract.

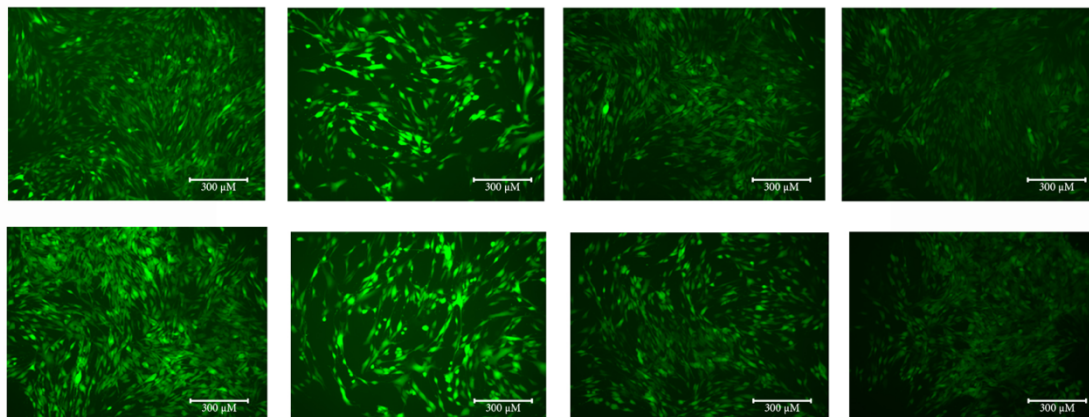


Fig 36-37. Repressive effect of antioxidant extracts and manufactured MNPs on H<sub>2</sub>O<sub>2</sub>-induced intracellular oxidative stress Neo-dermal fibroblast. d) treatment with cocoa extract solution, e) treatment with coffee extract solution. Bar=300μm

ROS immunostaining assay was also performed on MNPs purchased from sigma and LbL functionalized silica nanoparticles. Microscope images of MNPs were reported in Fig. 38(1-4). In this case, results were in contrast with previously investigations, resulting in a higher fluorescence intensity which seemed to remain constant for all the samples concentration tested.

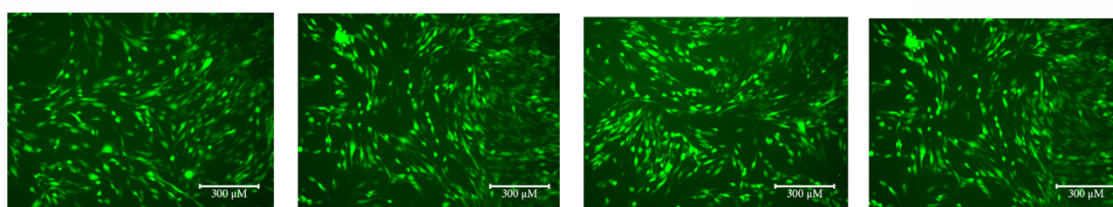


Fig 38. Repressive effect of antioxidant extracts and manufactured MNPs on H<sub>2</sub>O<sub>2</sub>-induced intracellular oxidative stress Neo-dermal fibroblast. f) treatment with MNPs purchased from sigma solution: f1- 10μM, f2- 50μM, f3- 100μM, f4- 550μM.

On the contrary, microscope images of cocoa and coffee functionalized MNPs Fig. 39-40(1-4) resulted in a lower fluorescence intensity where samples were much concentrated, confirming repressive effect on H<sub>2</sub>O<sub>2</sub>-induced intracellular oxidative stress of engineered nanoparticles.

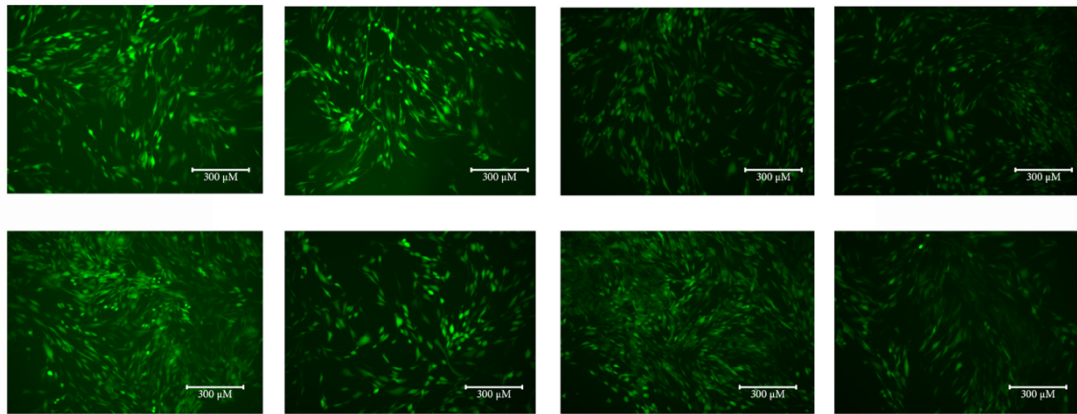


Fig 39-40: Repressive effect of antioxidant extracts and manufactured MNPs on  $H_2O_2$ -induced intracellular oxidative stress Neo-dermal fibroblast. g) treatment with coffee functionalized MNPs solution, h) treatment with cocoa functionalized MNPs solution. Bar=300 $\mu$ m

To perform better quantitative comparisons, all images taken were grouped in Figure 41.

Highest fluorescence intensity was reached in negative control and in samples treated with MNPs purchased from sigma, confirming the absence of antioxidant activity in each well. On the other hand, lowest level of ROS production was detected in positive control where  $H_2O_2$  treatment wasn't performed.

It is important to note that comparing resveratrol, cocoa and coffee antioxidant extracts with functionalized MNPs, it seemed that fluorescence signal was higher in free formulation than engineered nanoparticles. On the contrary, results not had shown any significant differences between cocoa and coffee case, and between MNPs functionalized with both extracts.

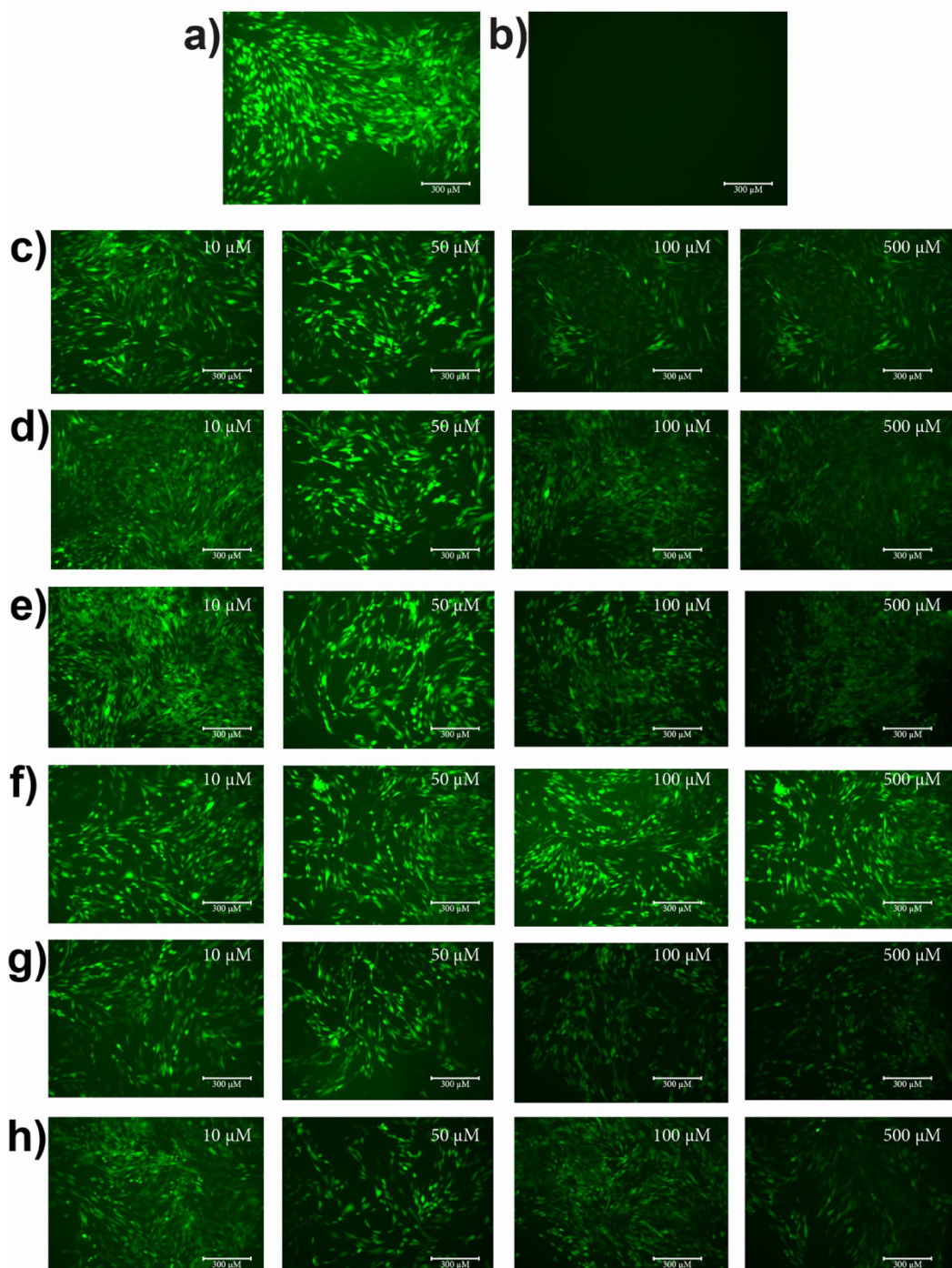


Fig 41: Repressive effect of antioxidant extracts and manufactured MNPs on  $H_2O_2$ -induced intracellular oxidative stress on Neo-dermal fibroblast. Treatment with a) negative control, b) positive control, c) resveratrol, d) cocoa extract, e) coffee extract, f) MNPs purchased from sigma, g) coffee functionalized MNPs, h) treatment with cocoa functionalized MNPs. Bar=300μm.

Fluorescence was then measured on a microplate reader and results were reported in Figure 42.

ROS generation in H<sub>2</sub>O<sub>2</sub> - exposed fibroblasts was reported in terms of fluorescence values of 2',7'-dichlorofluorescein diacetate and normalized considering the negative control.

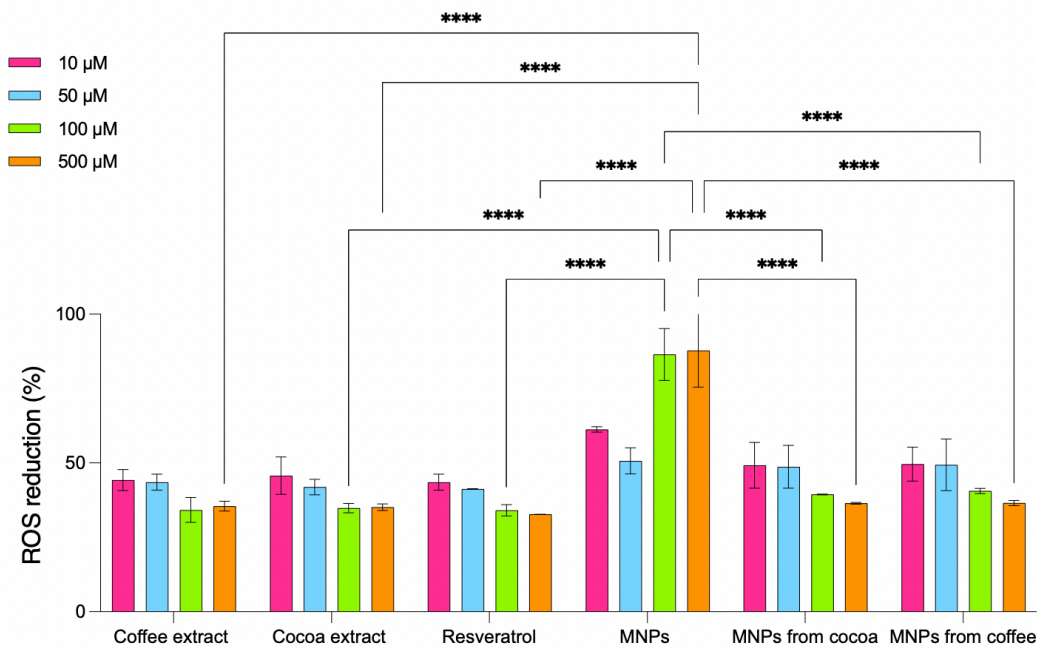


Fig 42: ROS reduction results obtained by incubating Neo-dermal fibroblast with different MNPs, cocoa and coffee extract samples concentration.

Results had demonstrated that ROS levels were markedly higher in MNPs from the commercial samples, when concentration of silica nanoparticles was the highest, resulting in a ROS reduction activity of 87%. On the contrary, highest repressive effect on H<sub>2</sub>O<sub>2</sub>- induced intracellular oxidative stress was performed by free resveratrol, coffee and cocoa extract solutions, resulting in ROS reduction activity of 42%, 44 % and 45% respectively. In general, also functionalized MNPs showed a great repressive effect on H<sub>2</sub>O<sub>2</sub>- induced intracellular oxidative stress on neo-dermal fibroblasts, when their concentration in the samples were higher.

It is important to note that, as for cell viability, the relationship between ROS reduction activity and the type of sample and its concentration can depend on many factors. Numerous studies had confirmed that the cytotoxicity induced by silica nanoparticles is closely correlated to increased oxidative stress [53]. Petrache Voicu et al. founded that a significant increase in ROS production after silica nanoparticles exposure was reported in several cell types [54-55]. Moreover, in Saehan Choi et al. studies, the generation of

ROS was reduced due to the combined effects of the mesoporous silica structure and chitosan coating [56]. These results confirmed reduced repressive effect behaviour performed by MNPs systems on H<sub>2</sub>O<sub>2</sub>- induced intracellular oxidative stress on Neo-dermal fibroblast, compared with engineered MNPs.

## 5. Conclusions and Future perspective

In this thesis, the already established extraction process for the recovery of antioxidant compounds from various biomasses using the ultrasound extraction method was verified with cocoa and coffee pod husks. These represent by-products of the cocoa and coffee industry, and it is generated in large quantities worldwide; thus, the use of biomass can have several benefits, including reducing waste, generating additional income for cocoa farmers, and providing a sustainable source of biomass for various industries. In addition, cocoa and coffee pod husks biomass can be a valuable source of natural antioxidants, and the extraction of these compounds can be achieved using different solvents resulting in a greener process.

The ultrasound assisted process was optimized resulting, both in cocoa and coffee, in a well-developed predictive extraction model with a very low error (2% and 8%, respectively) calculated on the total phenolic content (TPC) of final extracts. The best combination of input extraction parameters was for both case a temperature of 23°C, 58 min of time and 11 mL/mg of ratio, for coffee biowaste, while 17 min of time and 35 mL/mg of ratio for cocoa. TPC was higher in cocoa extracts (3.71 (mg/mL)) than coffee one (3.8 (mg/mL)) but in general the high values reached confirmed the good quality of the extracts. Cocoa extracts also performed higher antioxidant activity than coffee in the FRAP assay. Obtained cocoa and coffee extracts were then tested to DLS resulting in a strong negative charge, -20mV and -13 mV respectively.

Moreover, the extracted cocoa and coffee compounds were incorporated into the Layer-by-Layer technique for creating silica mesoporous nanoparticles with antioxidant behavior. According to extracts  $\zeta$ -potential value, cocoa and coffee solutions were incorporated into the pectin polyanion solution, which was combined with chitosan in the layer deposition. TEM images confirmed that initial spherical nanoparticle shape remained constant during the deposition process presenting a slight increase in functionalized nanoparticles diameter compared to silica one. Chitosan showed to be ideal material to reduce cytotoxicity behavior of silica nanoparticles which resulted in a general good cytocompatibility engineered system towards Neo-dermal fibroblasts, when tested with lower samples concentration (up to 250  $\mu\text{g/mL}$ ). Manufactured nanoparticles also showed a great repressive effect on H<sub>2</sub>O<sub>2</sub>- induced intracellular oxidative stress on Neo-dermal fibroblasts, ~50%, compared to the non-functionalized MNPs, confirming the antioxidant behaviour of engineered systems.

Further characterization studies of functionalized silica nanoparticles would be necessary. For example, in the context of PTSD, it would be interesting to study the manufactured nanoparticles with a neuronal cell line to establish

their behavior. To this aim, could be also interesting test MNPs obtained with cocoa and coffee with typical neuroinflammatory ROS.

Moreover, approaches to increase the biocompatibility of the final system could study the use of different nanoparticles as core, for example using pectin or coffee and cocoa by-product materials. Cytotoxicity could be also decrease optimizing the deposition process, considering for example a higher number of layers, or exploiting chitosan positive functional groups, evaluating for example different concentrations of polycation solution. Another future insight could be the evaluation of combined release of anti-inflammatory agents, such as drugs but also natural one, like curcumin, to enhance natural antioxidant activity in inflammation site.

## 6. References

- [1] Inflammation and post-traumatic stress disorder Hiroaki Hori. (2019)
- [2] Current Status of Neurofeedback for Post-traumatic Stress Disorder: A Systematic Review and the Possibility of Decoded Neurofeedback. Toshinori Chiba (2019)
- [3] Acute Posttraumatic Symptoms Are Associated With Multimodal Neuroimaging Structural Covariance Patterns: A Possible Role for the Neural Substrates of Visual Processing in Posttraumatic Stress Disorder. Nathaniel G. Harnett (2020)
- [4] The Relationship Between Inflammation and Post-traumatic Stress Disorder. Yajing Sun (2021)
- [5] PTSD, a Disorder with an Immunological Component Image. Zhewu Wang (2016)
- [6] A Systematic Review of Tumor Necrosis Factor- $\alpha$  in Post-Traumatic Stress Disorder: Evidence from Human and Animal Studies. Serkan Hussei (2017)
- [7] Systemic low-grade inflammation in post-traumatic stress disorder: a systematic review. Speer K (2018)
- [8] Heart rate variability (HRV) and posttraumatic stress disorder (PTSD): A pilot study. Applied Psychophysiology and Biofeedback. Tan, Dao, Farmer, Sutherland, & Gevirtz. (2011)
- [9] Dysregulation of inflammation, neurobiology, and cognitive function in PTSD: an integrative review Maria M. Quinones (2020)
- [10] COVID-19 pandemic and mental health consequences: Systematic review of the current evidence. Nina Vindegar (2020)
- [11] Antioxidant capacity of crude extracts and their solvent fractions of selected Algerian Lamiaceae, Nabyla Khled khoudjaa, Lila Boulekbache-Makhlouf b,\*, Khodir Madani (2014)
- [12] Reactive Oxygen Species in Metabolic and Inflammatory Signaling. Steven J. Forrester (2018)
- [13] Reactive oxygen species in cell signaling Victor J. Thannickal, and Barry L. Fanburg (2000)
- [14] Innovative approaches for cancer treatment: current perspectives and new challenges. Carlotta Pucci (2019)
- [15] A Review of Trauma Specific Treatments (TSTs) for Post-Traumatic Stress Disorder (PTSD). Eunjung Lee (2021)
- [16] Schemas and coping strategies in cognitive-behavioral therapy for PTSD: A systematic review. Delphine-Émilie Bourdon (2018)
- [17] Balancing the Risks and Benefits of Benzodiazepines. Matthew E. Hirschtritt (2021)
- [18] US Food and Drug Administration. FDA requiring Boxed Warning updated to improve safe use of benzodiazepine drug class. Published September 23, 2020. Accessed October 11, 2020.
- [19] The Relationship Between Anti-Anxiety and Anti-Depressant Medication on Therapy and Coping Mechanism. Kelsie Ballew (2021)

- [20] Increased Oxidative Stress in the Prefrontal Cortex as a Shared Feature of Depressive- and PTSD-Like Syndromes: Effects of a Standardized Herbal Antioxidant. Johannes de Munter (2021)
- [21] Withania somnifera root powder protects against post-traumatic stress disorder-induced memory impairment. Karem H. Alzoubi<sup>1</sup> (2019)
- [22] Evaluation of the antioxidant properties of fruits. Mari´a Garcı´a-Alonso (2002)
- [23] The Importance of Antioxidant Biomaterials in Human Health and Technological Innovation: A Review Alessandra Cristina Pedro (2022)
- [24] Procházková D, Bousová I, Wilhelmová N. Antioxidant and prooxidant properties of flavonoids. Fitoterapia. (2011)
- [25] Investigation of metal-flavonoid chelates and the determination of flavonoids via metal-flavonoid complexing reactions. J Serb Chem Soc. (2007)
- [26] Effects of Various Flavonoids on the -Synuclein Fibrillation Process. Xiaoyun Meng (2010)
- [27] Effect of Coffee and Cocoa-Based Confectionery Containing Coffee on Markers of DNA Damage and Lipid Peroxidation Products: Results from a Human Intervention Study Daniela Martini (2021)
- [28] Antioxidant and Antiradical Activity of Coffee Alexander Yashin (2013)
- [29] The Cardiovascular Effects of Cocoa Polyphenols—An Overview Ana Clara Aprotosoiaie (2016)
- [30] Novel trends in extraction and optimization methods of bioactives recovery from pomegranate fruit biowastes: Valorization purposes for industrial applications (2021)
- [31] Optimization of microwave-assisted extraction of cocoa bean shell waste and evaluation of its antioxidant, physicochemical and functional properties. A.C. Mellinas (2020)
- [32] Ultrasound-assisted extraction of active compounds from cocoa bean shell. Nika Pavlović (2021)
- [33] Optimization of ultrasound-assisted extraction (UAE) process for the recovery of bioactive compounds from bitter melon using response surface methodology (RSM). Sushma Chakraborty (2020)
- [34] Improving the efficiency of natural antioxidant compounds via different nanocarriers. Atefe Maqsoodlou (2020)
- [35] Novel Nanocarriers for Targeted Topical Skin Delivery of the Antioxidant Resveratrol. Christofori Nastiti
- [36] Antioxidants and Nanotechnology: Promises and Limits of Potentially Disruptive Approaches in the Treatment of Central Nervous System Diseases. Chiara Martinelli (2019)
- [37] PLGA-Based Nanoparticles for Neuroprotective Drug Delivery in Neurodegenerative Diseases. Anthony Cunha (2021)
- [38] Structure and Applications of Pectin in Food, Biomedical, and Pharmaceutical Industry: A Review. Cariny Maria Polesca Freitas (2021)
- [39] Pectin in biomedical and drug delivery applications: A review. De-qiang Li (2021)
- [40] Challenges in developing of chitosan – Based polyelectrolyte complexes as a platform for mucosal and skin drug delivery. Joanna Potaś (2020)

- [41] Pectin and Pectin-Based Composite Materials: Beyond Food Texture. Claudia Lara Espinoza(2018)
- [42] The Emulsifying and Emulsion-Stabilizing Properties of Pectin: A Review. Eugénie D. Ngouémazong (2015)
- [43] Extraction, Characterisation, and Application of Pectin from Tropical and Sub-Tropical Fruits: A Review. Marie Carene Nancy Picot-Allain (2020)
- [44] Combined Pulsed Electric Field and Microwave-Assisted Extraction as a Green Method for the Recovery of Antioxidant Compounds with Electroactive Potential from Coffee Agro-Waste. Rodrigo Macías-Garbett (2022)
- [45] Comparison of the antioxidant activity of coffee and cocoa extracts in human plasma: a randomized clinical trial. C. Martínez-Cano (2019)
- [46] Comparison of Antioxidant Activity of Coffee and Cocoa. T.P. Toung (2019)
- [47] A Rapid FTIR Spectroscopic Method for Estimation of Caffeine in Soft Drinks and Total Methylxanthines in Tea and Coffee. M.M. PARADKAR (2002)
- [48] In Vitro Antioxidant Activity and FTIR Characterization of High-Molecular Weight Melanoidin Fractions from Different Types of Cocoa Beans. Joanna Oracz (2019)
- [49] Interactions between Alginate and Chitosan Biopolymers Characterized Using FTIR and XPS. Gwen Lawrie (2007)
- [50] Extraction and characterization of pectin from apple pomace and its evaluation as lipase (steapsin) inhibitor. Amit Kumar (2010)
- [51] Dopamine functionalized tannic acid-templated mesoporous silica nanoparticles as a new sorbent for the efficient removal of Cu<sup>2+</sup> from aqueous solution Junkai Gao (2016)
- [52] Toxicity of silica nanoparticles depends on size, dose, and cell type. In-Yong Kim (2015)
- [53] In Vitro Cytotoxicity of Silica Nanoparticles at High Concentrations Strongly Depends on the Metabolic Activity Type of the Cell Line. to Jen Q-Shengchang (2007)
- [54] In vitro toxicity of silica nanoparticles in human lung cancer cells. Weisheng Lin (2006)
- [55] Silica Nanoparticles Induce Oxidative Stress and Autophagy but Not Apoptosis in the MRC-5 Cell Line. Sorina Nicoleta Petrache Voicu (2015)
- [56] Chitosan-coated mesoporous silica particles as a plastic-free platform for photochemical suppression and stabilization of organic ultraviolet filters. Saehan Choi (2022)

## Appendix

### 1. Ultrasound-assisted extraction process optimization for coffee

#### a. Response Surface Regression: TPC (mg/mL) versus Temp, Time, Ratio

##### Coded Coefficients

Term	Coef	SE Coef	T-Value	P-Value	VIF
Constant	1.9655	0.0193	101.98	0.000	
Temp	-0.0930	0.0182	-5.10	0.000	1.00
Time	0.0544	0.0182	2.98	0.010	1.00
Ratio	-0.1390	0.0182	-7.62	0.000	1.00
Ratio*Ratio	-0.1376	0.0176	-7.82	0.000	1.00
Time*Ratio	-0.1637	0.0238	-6.87	0.000	1.00

##### Model Summary

S	R-sq	R-sq(adj)	R-sq(pred)
0.0673983	93.50%	91.18%	84.57%

##### Analysis of Variance

Source	DF	Adj SS	Adj MS	F-Value	P-Value
Model	5	0.91470	0.182940	40.27	0.000
Linear	3	0.42236	0.140786	30.99	0.000
Temp	1	0.11812	0.118118	26.00	0.000
Time	1	0.04037	0.040372	8.89	0.010
Ratio	1	0.26387	0.263866	58.09	0.000
Square	1	0.27787	0.277870	61.17	0.000
Ratio*Ratio	1	0.27787	0.277870	61.17	0.000
2-Way	1	0.21447	0.214473	47.21	0.000
Interaction					
Time*Ratio	1	0.21447	0.214473	47.21	0.000
Error	14	0.06360	0.004543		
Lack-of-Fit	9	0.04698	0.005221	1.57	0.322
Pure Error	5	0.01661	0.003322		
Total	19	0.97830			

##### Regression Equation in Uncoded Units

$$\begin{aligned} \text{TPC (mg/mL)} &= -0.121 - 0.00930 \text{ Temp} + 0.04365 \text{ Time} + 0.1570 \text{ Ratio} \\ &\quad - 0.002446 \text{ Ratio*Ratio} \\ &\quad - 0.001747 \text{ Time*Ratio} \end{aligned}$$

## b. Response Optimization: TPC (mg/mL)

### Parameters

Response	Goal	Lower	Target	Upper	Weight	Importance
TPC (mg/mL)	Maximum	1.38875	2.25485		1	1

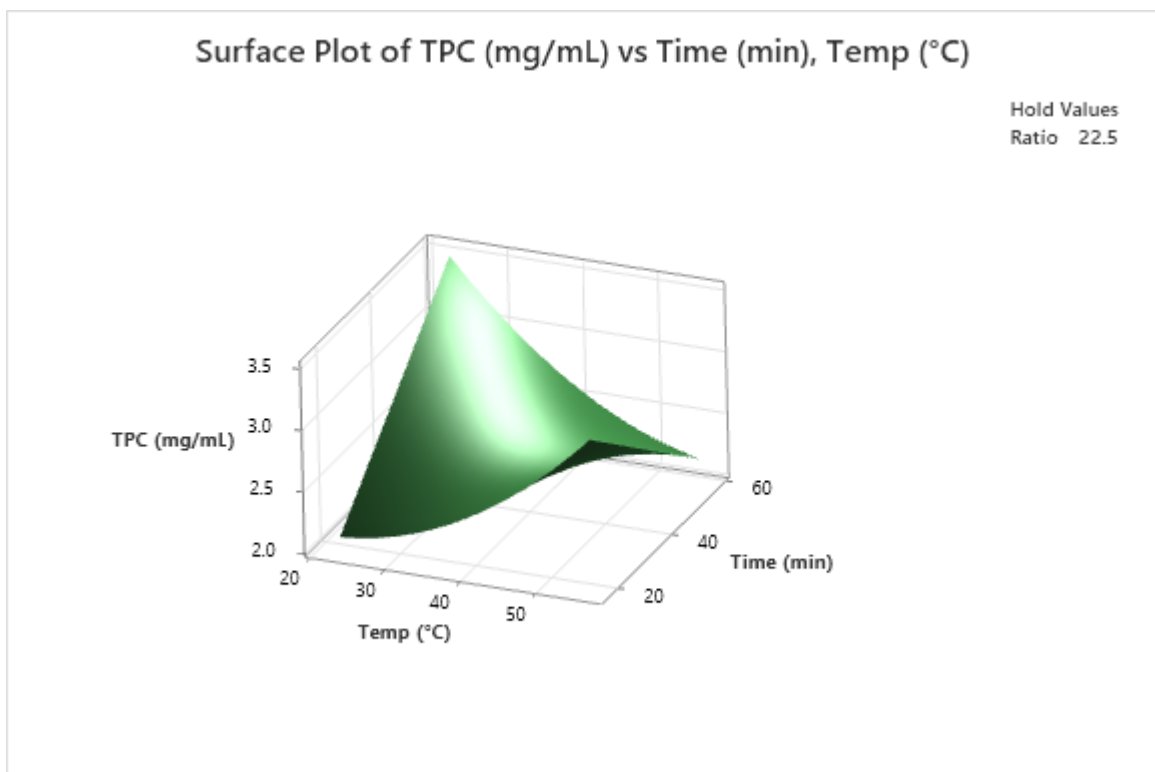
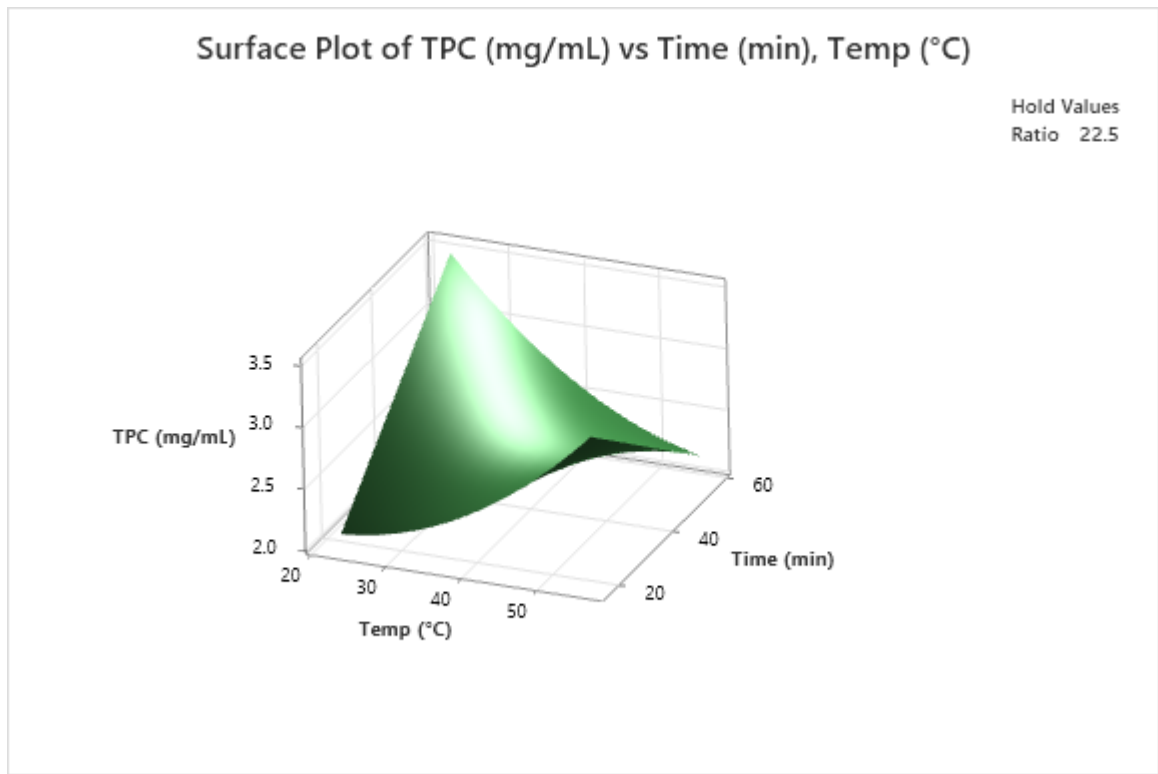
### Solution

Solution	Temp	Time	Ratio	TPC (mg/mL) Fit	Composite Desirability
1	23.1821	58.5224	11.1606	2.52532	1

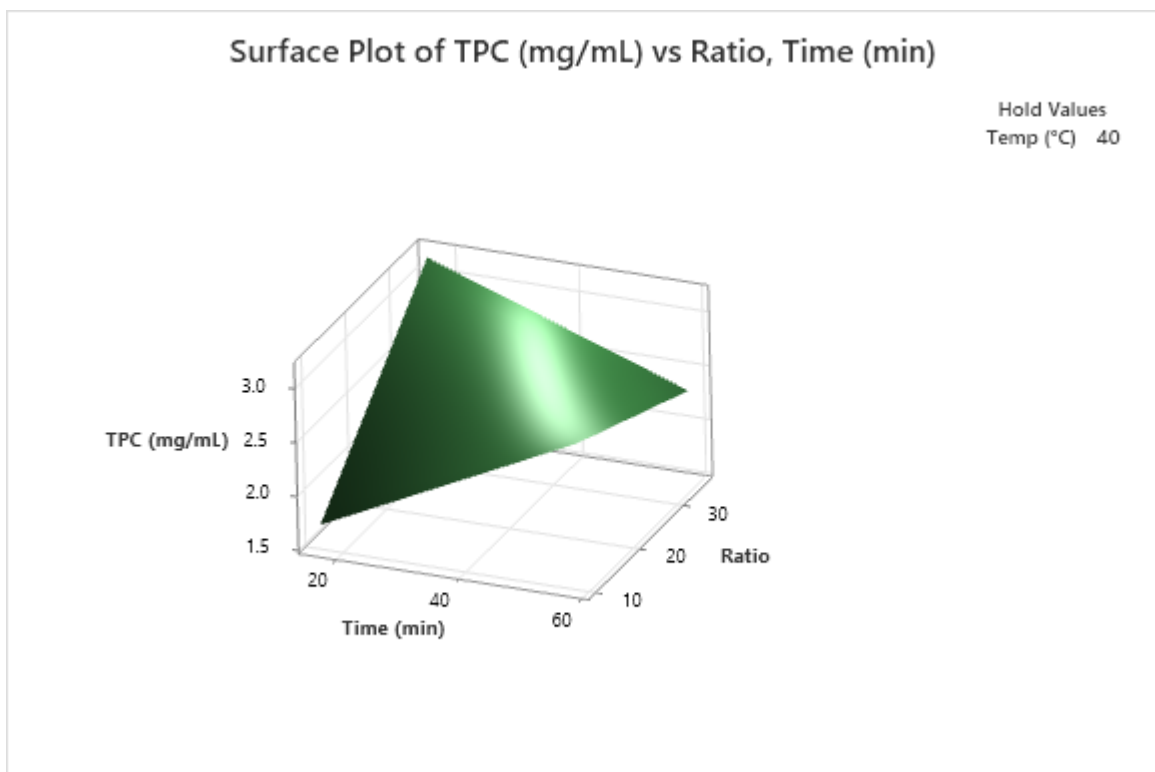
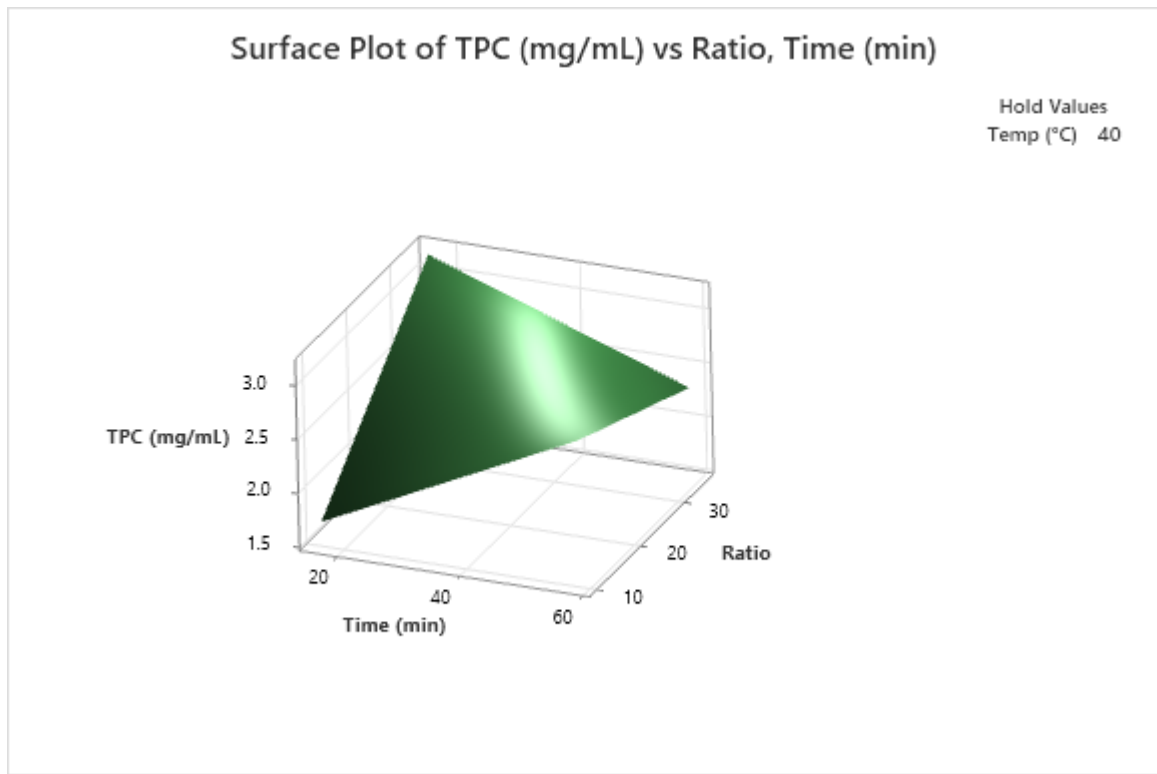
### Multiple Response Prediction

Variable	Setting			
Temp	23.1821			
Time	58.5224			
Ratio	11.1606			
Response	Fit	SE Fit	95% CI	95% PI
TPC (mg/mL)	2.5253	0.0856	(2.3416, 2.7090)	(2.2916, 2.7591)

# Surface Plot of TPC (mg/mL) vs Time (min), Temp (°C)



## Surface Plot of TPC (mg/mL) vs Ratio, Time (min)



## 2. Ultrasound-assisted extraction process optimization for cocoa

### a. Response Surface Regression: TPC (mg/mL) versus Temp, Time, Ratio

#### Coded Coefficients

Term	Coef	SE Coef	T-Value	P-Value	VIF
Constant	2.5010	0.0140	179.07	0.000	
Temp	-0.0326	0.0132	-2.47	0.028	1.00
Time	0.0418	0.0132	3.16	0.008	1.00
Ratio	0.1382	0.0132	10.45	0.000	1.00
Temp*Temp	0.0870	0.0127	6.83	0.000	1.00
Temp*Time	-0.2167	0.0173	-12.55	0.000	1.00
Time*Ratio	-0.1757	0.0173	-10.17	0.000	1.00

#### Model Summary

S	R-sq	R-sq(adj)	R-sq(pred)
0.0488400	97.09%	95.74%	94.20%

#### Analysis of Variance

Source	DF	Adj SS	Adj MS	F-Value	P-Value
Model	6	1.03282	0.172137	72.16	0.000
Linear	3	0.29902	0.099672	41.78	0.000
Temp	1	0.01451	0.014513	6.08	0.028
Time	1	0.02384	0.023837	9.99	0.008
Ratio	1	0.26067	0.260666	109.28	0.000
Square	1	0.11115	0.111146	46.60	0.000
Temp*Temp	1	0.11115	0.111146	46.60	0.000
2-Way	2	0.62266	0.311330	130.52	0.000
Interaction					
Temp*Time	1	0.37580	0.375801	157.55	0.000
Time*Ratio	1	0.24686	0.246859	103.49	0.000
Error	13	0.03101	0.002385		
Lack-of-Fit	8	0.01609	0.002011	0.67	0.705
Pure Error	5	0.01492	0.002984		
Total	19	1.06383			

#### Regression Equation in Uncoded Units

$$\begin{aligned} \text{TPC (mg/mL)} = & -0.698 - 0.0079 \text{ Temp} + 0.11486 \text{ Time} + 0.08869 \text{ Ratio} \\ & + 0.000870 \text{ Temp*Temp} \\ & - 0.001734 \text{ Temp*Time} - 0.001874 \text{ Time*Ratio} \end{aligned}$$

## b. Response Optimization: TPC (mg/mL)

### Parameters

Response	Goal	Lower	Target	Upper	Weight	Importance
TPC (mg/mL)	Maximum	2.0806	3.0413		1	1

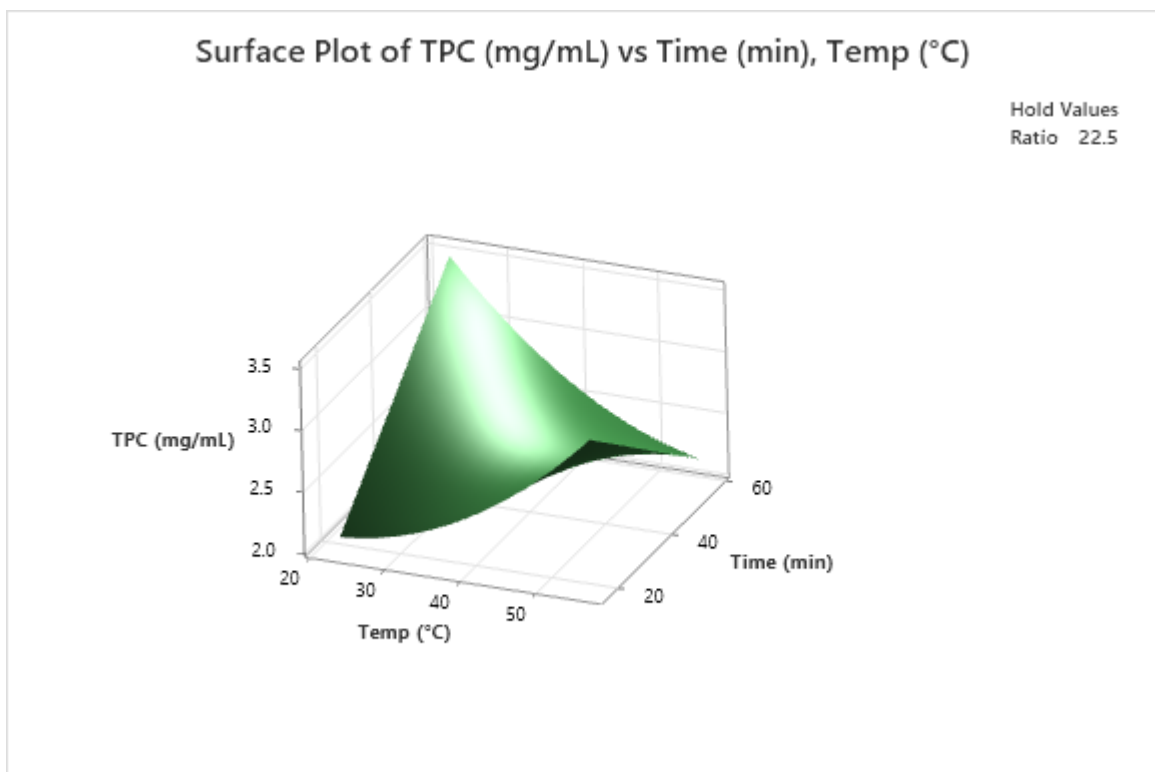
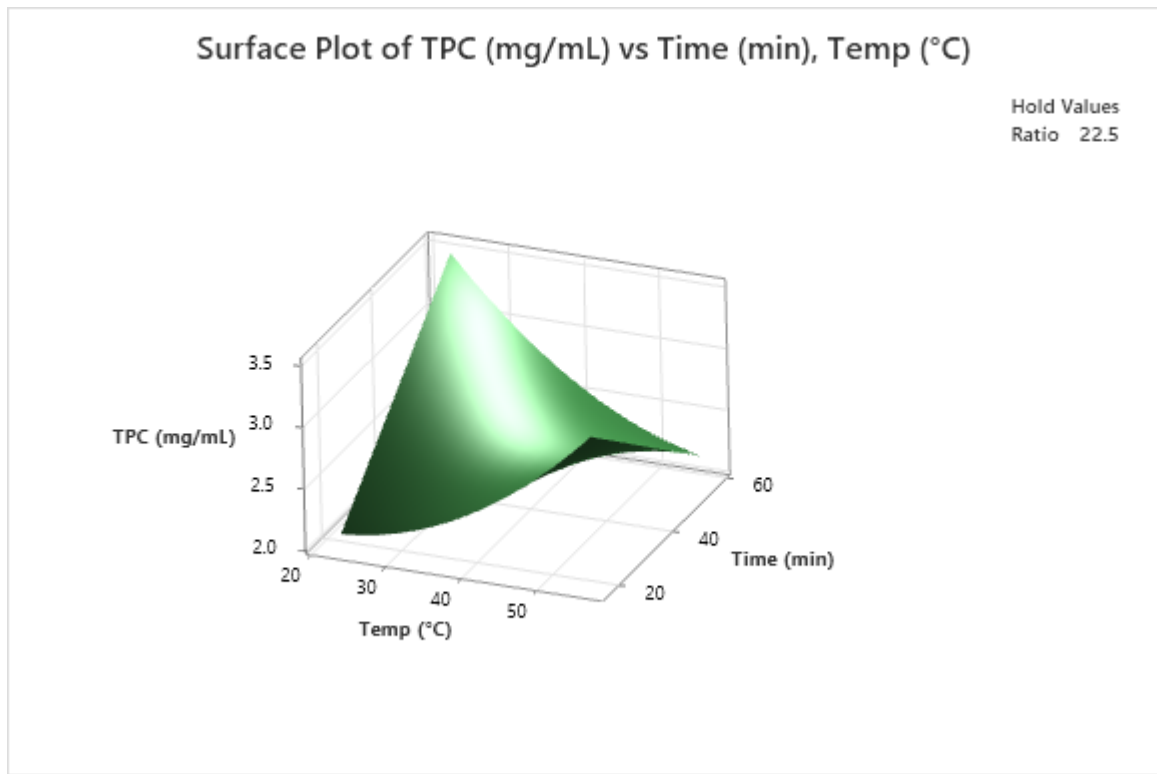
### Solution

Solution	Temp	Time	Ratio	TPC (mg/mL) Fit	Composite Desirability
1	56.8179	16.4776	35.1134	3.96430	1

### Multiple Response Prediction

Variable	Setting			
Temp	56.8179			
Time	16.4776			
Ratio	35.1134			
Response	Fit	SE Fit	95% CI	95% PI
TPC (mg/mL)	3.9643	0.0844	(3.7820, 4.1466)	(3.7537, 4.1749)

## Surface Plot of TPC (mg/mL) vs Time (min), Temp (°C)



## Surface Plot of TPC (mg/mL) vs Ratio, Time (min)

